Chapter 1

Theoretical Background

The chapter on the theoretical background serves to introduce the underlying methods required within the scope of the multiscale model for the simulation of charge transport in organic semiconducting materials. After introducing the Born-Oppenheimer approximation (Sec. 1.1), the focus is then on various electron structure methods and their approximation procedures (Sec. 1.2). This includes techniques for the ground state as well as for excited states. Both *ab initio*, as well as classical molecular dynamics simulations, allow the propagation of the atomic nuclei (Sec. 1.3). The methods for charge transfer reactions (Sec. 1.4) are then utilised in kinetic Monte Carlo simulations to determine charge transport (Sec. 1.5).

1.1 Born-Oppenheimer Approximation

The temporal evolution of a quantum mechanical system is obtained by solving the time-dependent non-relativistic Schrödinger equation [79]. In general, this equation is not solvable analytically for many-particle systems, hence approximations like the Born-Oppenheimer approximation [80,81] need to be applied for electron structure calculations or molecular dynamics simulations [82]. The total time-dependent Schrödinger equation,

$$\hat{H}\Psi(\mathbf{r},\mathbf{R};t) = i\hbar\frac{\partial}{\partial t}\Psi(\mathbf{r},\mathbf{R};t) \ , \tag{1}$$

contains the Hamilton operator $\hat{H}$ for a many particle system, which acts on the total wavefunction $\Psi(\mathbf{r},\mathbf{R};t)$. As a convention, we represent vectors and matrices by bold symbols. The equation 1 is a first-order differential equation in time t and describes the wave function of a quantum-mechanical system, which consists of N atoms and n electrons. Here, $\hbar$ denotes the Planck constant h divided by 2π and i is the imaginary unit.

The positions of all $3N$ nuclear coordinates $\mathbf{R} = (\mathbf{R}_1, \mathbf{R}_2, ..., \mathbf{R}_I, ..., \mathbf{R}_N)$ are denoted in a total vector $\mathbf{R}$, and the electrons are comprised as $\mathbf{r} = (\mathbf{r}_1, \mathbf{r}_2, ..., \mathbf{r}_i, ..., \mathbf{r}_n)$. The total Hamiltonian $\hat{H}(\mathbf{r},\mathbf{R})$ is composed of five terms

$$\hat{H}(\mathbf{r},\mathbf{R}) = \hat{T}_{\mathrm{nuc}}(\mathbf{R}) + \hat{T}_{\mathrm{e}}(\mathbf{r}) + \hat{V}_{\mathrm{nuc,nuc}}(\mathbf{R}) + \hat{V}_{\mathrm{e,e}}(\mathbf{r}) + \hat{V}_{\mathrm{nuc,e}}(\mathbf{r},\mathbf{R}). \tag{2}$$

The first term is the sum of kinetic energy of the atomic nuclei

$$\hat{T}_{\mathrm{nuc}}(\mathbf{R}) = -\sum_{I=1}^{N}\frac{\hbar^2}{2M_I}{\nabla_I}^2 \ , \tag{3}$$

where the nabla operator ∇_I acts only on the nuclear coordinates of atom I. The second term is the kinetic energy of the electrons,

$$\hat{T}_{\mathrm{e}}(\mathbf{r}) = -\sum_{i=1}^{n} \frac{\hbar^2}{2m_e} {\nabla_i}^2. \tag{4}$$

Here, the ∇_i operator acts only on the coordinates of electron i. This expression is followed by the internuclear repulsion,

$$\hat{V}_{\mathrm{nuc,nuc}}(\mathbf{R}) = \frac{e^2}{4\pi\epsilon_0} \sum_{I=1}^{N-1} \sum_{J>I}^{N} \frac{Z_I Z_J}{|\mathbf{R}_I - \mathbf{R}_J|} \ , \tag{5}$$

the electron-electron repulsion,

$$\hat{V}_{\mathrm{e,e}}(\mathbf{r}) = \frac{e^2}{4\pi\epsilon_0} \sum_{i=1}^{n-1} \sum_{j>i}^{n} \frac{1}{|\mathbf{r}_i - \mathbf{r}_j|} \ , \tag{6}$$

and the electron-nuclear attraction,

$$\hat{V}_{\mathrm{nuc,e}}(\mathbf{r}, \mathbf{R}) = -\frac{e^2}{4\pi\epsilon_0} \sum_{I=1}^{N} \sum_{i=1}^{n} \frac{Z_I}{|\mathbf{R}_I - \mathbf{r}_i|} \ . \tag{7}$$

In these equations m_e denotes the electron mass, e is the elementary charge, Z_I and M_I are the atomic number and mass of the nucleus I, and ϵ_0 denotes the vacuum permittivity. The total Hamilton operator,

$$\hat{H}(\mathbf{r}, \mathbf{R}) = \hat{T}_{\mathrm{nuc}}(\mathbf{R}) + \hat{H}_{\mathrm{el}}(\mathbf{r}, \mathbf{R}) \ , \tag{8}$$

is separated into the operator for the kinetic energy $\hat{T}_{\mathrm{nuc}}(\mathbf{R})$ of the atomic nuclei and the electronic Hamiltonian $\hat{H}_{\mathrm{el}}(\mathbf{r}, \mathbf{R})$. Here, the electronic Hamilton operator contains the four contributions, which are listed above

$$\hat{H}_{\mathrm{el}}(\mathbf{r}, \mathbf{R}) = \hat{T}_{\mathrm{e}}(\mathbf{r}) + \hat{V}_{\mathrm{nuc,nuc}}(\mathbf{R}) + \hat{V}_{\mathrm{e,e}}(\mathbf{r}) + \hat{V}_{\mathrm{nuc,e}}(\mathbf{r}, \mathbf{R}) \ . \tag{9}$$

The solution of the stationary, time-independent Schrödinger equation,

$$\hat{H}_{\mathrm{el}}(\mathbf{r}, \mathbf{R}) \Phi_k(\mathbf{r}, \mathbf{R}) = E_k(\mathbf{R}) \Phi_k(\mathbf{r}, \mathbf{R}) \ , \tag{10}$$

is assumed to be known for a set of fixed nuclear coordinates $\mathbf{R}$, yielding the energy eigenvalue $E_k(\mathbf{R})$ and the electron wave function $\Phi_k(\mathbf{r}, \mathbf{R})$. The spectrum of the Hamiltonian $\hat{H}_{\mathrm{el}}(\mathbf{r}, \mathbf{R})$ is assumed to be discrete and the electron wavefunctions have to satisfy the orthogonality relation $\langle \Phi_k | \Phi_l \rangle = \delta_{kl}$. In a next step, we insert the ansatz

$$\Psi(\mathbf{r}, \mathbf{R}; t) = \sum_l \Phi_l(\mathbf{r}, \mathbf{R}) \chi_l(\mathbf{R}, t) \tag{11}$$

for the total wavefunction $\Psi(\mathbf{r}, \mathbf{R}; t)$, consisting of the product of the electronic wavefunction $\Phi_l(\mathbf{r}, \mathbf{R})$ and the nuclear wavefunction $\chi_l(\mathbf{R}, t)$ into the time-dependent Schrödinger equation (Eq. 1). Multiplying from the left hand-side by $\langle \Phi_k |$ and integrating over all electron coordinates leads to a set of coupled differential equations,

$$\left[\hat{T}_{\mathrm{nuc}}(\mathbf{R}) + E_k(\mathbf{R})\right] \chi_k(\mathbf{R}, t) + \sum_l \hat{C}_{kl} \chi_l(\mathbf{R}, t) = i\hbar \frac{\partial}{\partial t} \chi_k(\mathbf{R}, t) \ . \tag{12}$$

Here, $\hat{C}_{kl}$ denote the non-adiabatic coupling elements

$$\hat{C}_{kl} = \left\langle \Phi_k \left| \hat{T}_{\text{nuc}}(\mathbf{R}) \right| \Phi_l \right\rangle - \sum_I \frac{\hbar^2}{M_I} \left\langle \Phi_k \left| \nabla_I \right| \Phi_l \right\rangle \nabla_I \ . \tag{13}$$

If the adiabatic approximation is applied, only the diagonal elements $\hat{C}_{kk}$ of the non-adiabatic coupling operator $\hat{C}_{kl}$ are evaluated to obtain a correction to the energy eigenvalue E_k of the electronic Schrödinger equation (Eq. 10). The coupling between various electronic states is neglected in the adiabatic approximation

$$\left[\hat{T}_{\text{nuc}}(\mathbf{R}) + E_k(\mathbf{R}) + \hat{C}_{kk}(\mathbf{R})\right] \chi_k(\mathbf{R}, t) = i\hbar \frac{\partial}{\partial t} \chi_k(\mathbf{R}, t) \ , \tag{14}$$

so the electrons adjust instantaneously to fluctuations in the nuclear positions without a change in the electronic state. If we also neglected the diagonal coupling terms in the Schrödinger equation, then the Born-Oppenheimer approximation is obtained

$$\left[\hat{T}_{\text{nuc}}(\mathbf{R}) + E_k(\mathbf{R})\right] \chi_k(\mathbf{R}, t) = i\hbar \frac{\partial}{\partial t} \chi_k(\mathbf{R}, t) \ . \tag{15}$$

This equation describes the temporal evolution of the nuclear wavefunction χ_k in a single electronic state.

If the stationary Schrödinger equation is applied for the electrons in this manner, the electron motion is completely decoupled from the nuclear motion. The approximation is justified if the electron wavefunction varies only slightly with a change in the nuclear positions. This requirement is fulfilled, for example, in the vicinity of the equilibrium geometry at the electronic ground state $k = 0$. The equation for the nuclear wavefunctions (Eq. 15) is replaced by Newton's equation of motion

$$M_I \ddot{\mathbf{R}}_I = -\nabla_I E_k \tag{16}$$

in the classical limit. The equation (Eq. 16) needs to be integrated to obtain the trajectory for the nuclear coordinates in conventional molecular dynamics. This undertaking is impeded by the fact that the time-independent Schrödinger equation (Eq. 10) cannot be solved exactly for a many-particle system using electronic structure methods. Therefore, the potential energy surface is approximated in *ab initio* molecular dynamics (AIMD) [83, 84] or force-field molecular dynamics [85].

1.2 Electronic Structure Calculations

The following chapter introduces several approaches in quantum chemistry to solve the stationary Schrödinger equation (Eq. 10). Hartree-Fock theory (Sec. 1.2.1) and density functional theory (Sec. 1.2.2), density functional tight binding (Sec. 1.2.3) and semiempirical methods (Sec. 1.2.4) give access to the electronic ground state. TDDFT (Sec. 1.2.2.7) and vibrationally resolved electronic spectra (Sec. 1.2.2.8) allow comparison of excited-state properties to experimental spectroscopic data. We use atomic units for simplicity.

1.2.1 Hartree-Fock Theory

The challenging task in electronic structure theory is finding the solution to the electrostatic problem for a quantum many-body system (Eq. 10). Following the Rayleigh-Ritz variational principle [86],

$$E_0 \leq \min_{\widetilde{\Phi}} \frac{\langle \widetilde{\Phi} | \hat{H}_{\mathrm{el}} | \widetilde{\Phi} \rangle}{\langle \widetilde{\Phi} | \widetilde{\Phi} \rangle} = \langle \Phi_0 | \hat{H}_{\mathrm{el}} | \Phi_0 \rangle \ , \tag{17}$$

one can minimise the ground state energy E_0 by selecting a trial wavefunction $\widetilde{\Phi}$ and alternating the parameters successively, till one finds a minimum in energy for the ground state wavefunction Φ_0. This minimum is the best approximation to the energy within a selected ansatz and the associated eigenfunctions. A suitable ansatz is the Slater determinant [87]

$$\Phi^{\mathrm{SD}} = \frac{1}{\sqrt{n!}} \begin{vmatrix} \phi_1(\mathbf{r}_1) & \cdots & \phi_n(\mathbf{r}_1) \\ \vdots & \ddots & \vdots \\ \phi_1(\mathbf{r}_n) & \cdots & \phi_n(\mathbf{r}_n) \end{vmatrix} \ , \tag{18}$$

which consists of a set with n one-electron orbitals $\{\phi_i\}$. The Slater determinant guarantees the antisymmetry of the wavefunction, as it switches sign upon exchange of two electrons and consequently satisfies the Pauli exclusion principle. Unless otherwise noted, the spin orbitals $\phi_i(\mathbf{r}_j) = \overline{\phi}_i(\mathbf{r}_j)\sigma(i)$ comprises the spatial component $\overline{\phi}_i(\mathbf{r}_j)$ and a spin component $\sigma(i)$.

The Hartree-Fock method [88, 89] employs a single Slater determinant Φ^{SD} and minimises, variationally the expectation value for the electronic Hamiltonian (Eq. 17) by means of the Lagrange operator method under the constraint of orthonormal orbitals $\langle \phi_i | \phi_j \rangle = \delta_{ij}$. As a result, one obtains the Hartree-Fock equations

$$\hat{F}\phi_i(\mathbf{r}) = \hat{h}_i + \sum_j \left[2\hat{J}_j - \hat{K}_j \right] \phi_i(\mathbf{r}) = \varepsilon_i \phi_i(\mathbf{r}) \ , \tag{19}$$

which are the eigenvalue equations for the one-electron wavefunctions ϕ_i with the Hartree-Fock eigenvalues $\{\varepsilon_i\}$ [83, 90]. The Fock operator $\hat{F}$ depends on all orbitals, as it includes the one-electron operator

$$\hat{h}_i = -\frac{1}{2}\nabla_i^2 - \sum_{I=1}^{N} \frac{Z_I}{|\mathbf{r}_i - \mathbf{R}_I|} \ , \tag{20}$$

and besides, the Coulomb operator and exchange operator

$$\hat{J}_j \phi_i(\mathbf{r}_1) = \int \frac{\phi_j^*(\mathbf{r}_2)\phi_j(\mathbf{r}_2)}{|\mathbf{r}_1 - \mathbf{r}_2|} \phi_i(\mathbf{r}_1)\, \mathrm{d}\mathbf{r}_2 \tag{21}$$

$$\hat{K}_j \phi_i(\mathbf{r}_1) = \int \frac{\phi_j^*(\mathbf{r}_2)\phi_i(\mathbf{r}_2)}{|\mathbf{r}_1 - \mathbf{r}_2|} \phi_j(\mathbf{r}_1)\, \mathrm{d}\mathbf{r}_2 \ . \tag{22}$$

The wavefunctions $\phi_i = \sum_k c_{ik}\varphi_k$ are developed in a selected basis $\{\varphi_k\}$ (see Sec. 1.2.5). As the development coefficients c_{ik} cannot be determined exactly, one selects an ansatz for all k, evaluates the integrals $\hat{J}_j$, and $\hat{K}_j$ and sets up the Fock operator $\hat{F}$. Solving the eigenvalue problem for $\hat{F}$ yields a new set of coefficients $\tilde{c}_{ik}$, which serve as a refined ansatz. The procedure is repeated iteratively until a self-consistent solution to the Hartree-Fock equations is found (self-consistent field method, SCF).

The nature of the Hartree-Fock approximation is determined by the Coulomb operator $\hat{J}_j$, which treats the electron-electron repulsion in a mean-field approximation. $\hat{J}_j$ describes a potential, which is integrated over the charge density $|\phi_j(\mathbf{r}_2)|^2$. As these electrostatic potentials are summed up for all other electrons j, an electron i is subject to the mean potential generated by all other electrons. So the instantaneous repulsion of two electrons is disregarded. The deviation of this approximation from the exact energy is called correlation. The exchange operator $\hat{K}_j$ is a consequence of the antisymmetry in the chosen ansatz for the wavefunction, and the resulting exchange interaction lacks a classical analogy.

1.2.2 Density Functional Theory

1.2.2.1 Time-independent Density Functional Theory (DFT)

The solution to the stationary Schrödinger equation for a system of n electrons is unknown in general and not solvable analytically. Therefore, further approximations are necessary. Density functional theory (DFT) offers a pathway to the electronic ground state energy with a convenient trade-off between computational costs and numeric accuracy. The theoretical basis for DFT are the Hohenberg-Kohn theorems. The first Hohenberg-Kohn theorem states that the external potential $\hat{v}_{\text{ext}}$ determines uniquely the electron density $\rho(\mathbf{r})$, and the statement holds vice versa [91,92]. The total energy of a system

$$E_0[\rho] = T_s[\rho] + \int v_{\text{ext}}(\mathbf{r})\rho(\mathbf{r})\ \mathrm{d}\mathbf{r} + J[\rho] + E_{\text{xc}}[\rho] \tag{23}$$

is a functional of the electron density $\rho(\mathbf{r})$ and depends explicitly on the external potential. Here, $T_s[\rho]$ is a term for the kinetic energy of the electrons and reads

$$T_s[\rho] = -\frac{1}{2}\sum_i^n p_i^{\text{occ}}\phi_i(\mathbf{r})\nabla^2\phi_i(\mathbf{r})\ . \tag{24}$$

It contains the occupation numbers p_i^{occ} for electrons in orbital ϕ_i. The external potential $v_{\text{ext}}(\mathbf{r})$ includes the attraction between the nuclei and the electron density as well as the nuclei-nuclei repulsion

$$v_{\text{ext}}(\mathbf{r}) = -\sum_{I=1}^{N}\frac{Z_I}{|\mathbf{R}_I - \mathbf{r}|} + \sum_{I=1}^{N-1}\sum_{J>I}^{N}\frac{Z_I Z_J}{|\mathbf{R}_I - \mathbf{R}_J|}\ . \tag{25}$$

The Coulomb term describes electron-electron repulsion as a mean-field approximation

$$J[\rho] = \frac{1}{2}\iint\frac{\rho(\mathbf{r})\rho(\mathbf{r}')}{|\mathbf{r} - \mathbf{r}'|}\ \mathrm{d}\mathbf{r}\,\mathrm{d}\mathbf{r}'\ , \tag{26}$$

and $E_{\text{xc}}[\rho]$ is the exchange-correlation energy (see Sec. 1.2.2.3).
The second Hohenberg-Kohn theorem provides a variational principle for the functional $E[\rho]$. If the ground state is not energetically degenerated, one obtains the ground state

electron density ρ_0 by varying a trial density $\widetilde{\rho}$ till one gets to the global minimum of the energy functional $E[\rho]$ with the ground state energy E_0. In other words, the optimised ground state electron density minimises the ground state energy of the system

$$E_0[\rho_0] \leq \widetilde{E}[\widetilde{\rho}] \ . \tag{27}$$

The trial density $\widetilde{\rho}$ needs to satisfy the secondary condition $\widetilde{\rho}(\mathbf{r}) \geq 0$ for all $\mathbf{r}$ and the constraint $n = \int \widetilde{\rho}(\mathbf{r}) \ \mathrm{d}\mathbf{r}$ must apply to the electron density in order to preserve the total number of electrons n.

1.2.2.2 Kohn-Sham Theory

The Kohn-Sham equations are the one-particle Schrödinger equations for a fictitious system of n non-interacting electrons, which generate the same electron density as a system of interacting electrons [93]. The Kohn-Sham ground state wavefunction Φ^{KS} of the system can be written as a Slater determinant (Eq. 18), consisting of one-electron Kohn-Sham orbitals ϕ_i and ensures the adherence to the Pauli exclusion principle. Solving the one-electron Kohn-Sham equations yields the Kohn-Sham orbitals ϕ_i, which minimise the total energy E_0 of the many-electron system

$$\left[-\frac{1}{2}\nabla^2 + v_{\mathrm{eff}}(\mathbf{r})\right] \phi_i(\mathbf{r}) = \varepsilon_i \phi_i(\mathbf{r}) \ . \tag{28}$$

Here, ε_i are the energy eigenvalues of the Kohn-Sham Hamilton operator. The total energy of a system, which contains n electrons, can be written in the form

$$E_0 \approx E_0^{\mathrm{KS}}[\rho] = -\frac{1}{2}\sum_{i=1}^{n} \int \phi_i^*(\mathbf{r}) \nabla^2 \phi_i(\mathbf{r}) \ \mathrm{d}\mathbf{r} - \int \rho(\mathbf{r}) v_{\mathrm{ext}}(\mathbf{r}) \ \mathrm{d}\mathbf{r} + J[\rho] + E_{\mathrm{xc}}[\rho]. \tag{29}$$

The electron density $\rho(\mathbf{r})$, which is made up of Kohn-Sham orbitals ϕ_i for non-interacting electrons,

$$\rho(\mathbf{r}) = \sum_{i=1}^{n} p_i^{\mathrm{occ}} |\phi_i(\mathbf{r})|^2 \tag{30}$$

corresponds to the same electron density, which is generated by a set of interacting electrons. The effective potential v_{eff} (Kohn-Sham potential)

$$v_{\mathrm{eff}}(\mathbf{r}) = v_{\mathrm{ext}}(\mathbf{r}) + \int \frac{\rho(\mathbf{r}')}{|\mathbf{r} - \mathbf{r}'|} \ \mathrm{d}\mathbf{r}' + v_{\mathrm{xc}}(\mathbf{r}) \tag{31}$$

depends on the electron density $\rho(\mathbf{r})$, which is created by the Kohn-Sham orbitals ϕ_i (Eq. 30), that in turn depend on the shape and magnitude of the effective potential v_{eff} (Eq. 28). Consequently, the Kohn-Sham equations need to be solved iteratively to obtain a self-consistent solution (Self-Consistent Field, SCF). The exchange-correlation potential $v_{\mathrm{xc}}(\mathbf{r})$ is the derivative of the stationary exchange-correlation ground state energy $E_{\mathrm{xc}}[\rho]$ with respect to the density ρ in the adiabatic approximation

$$v_{\mathrm{xc}}[\rho](\mathbf{r}) \approx \frac{\delta E_{\mathrm{xc}}[\rho]}{\delta \rho} \ . \tag{32}$$

Provided that the exact exchange-correlation energy E_{xc} is known, DFT is basically exact and the Kohn-Sham energy E_0^{KS} coincides with the exact ground state energy E_0. However, as the exact E_{xc} is unknown, (semiempirical) approximations are required instead (see 1.2.2.3 and 1.2.2.4).

1.2.2.3 Exchange-Correlation Functional

The exchange-correlation functional consists of a Hartree-Fock exchange energy term and a term for the correlation energy [79, 93]

$$E_{\mathrm{xc}}[\rho] = E_{\mathrm{x}}[\rho] + E_{\mathrm{c}}[\rho] \ . \tag{33}$$

As a first approach to the exchange-correlation functional the electron density ρ is treated as the electron density from the homogeneous electron gas. In this quantum mechanical model the interacting electrons cause a homogeneous electron density in front of a positive, uniformly distributed background charge generated by the nuclei.

$$E_{\mathrm{x}}^{\mathrm{LDA}}[\rho] = -\frac{3}{4}\left(\frac{3}{\pi}\right)^{\frac{1}{3}} \int \rho^{\frac{4}{3}}(\mathbf{r}) \ \mathrm{d}\mathbf{r} \tag{34}$$

In the local density approximation (LDA) the exact expression for the uniform electron gas is applied for the exchange energy $E_{\mathrm{x}}^{\mathrm{LDA}}$ [94] and Quantum Monte-Carlo calculations are used to determine correlation effects in $E_{\mathrm{c}}^{\mathrm{LDA}}$ [95]. LDA provides decent results for the description of systems in solid-state physics like metals with a homogeneous distribution of the electron density [96].

One can extend the LDA approach in the local spin density approximation (LSDA). As the number of α-spin electrons with a magnetic spin quantum number $m_s = +\frac{1}{2}$ can differ from the number of β-spin electrons with $m_s = -\frac{1}{2}$, one can also compose the total electron density $\rho = \rho_\alpha + \rho_\beta$ from of two distinct spin densities ρ_α and ρ_β and write the exchange functional as

$$E_{\mathrm{x}}^{\mathrm{LSDA}}[\rho_\alpha, \rho_\beta] = \frac{1}{2}\left(E_{\mathrm{x}}^{\mathrm{LDA}}[2\rho_\alpha] + E_{\mathrm{x}}^{\mathrm{LDA}}[2\rho_\beta]\right) . \tag{35}$$

Likewise, only approximative approaches exist for the corresponding correlation energy $E_{\mathrm{C}}^{\mathrm{LSDA}}$ for spin densities [97].

The generalised gradient approximation (GGA) yields clear improvements in the description of inhomogeneities in the electron density compared to LDA, as the method includes also the gradient of the electron density $\nabla\rho(\mathbf{r})$ in the exchange-correlation functional.

$$E_{\mathrm{xc}}[\rho] = \int F_{\mathrm{xc}}\left(\rho(\mathbf{r}), \nabla\rho(\mathbf{r})\right) \ \mathrm{d}\mathbf{r} \tag{36}$$

The Becke exchange functional

$$E_{\mathrm{x}} = E_{\mathrm{x}}^{\mathrm{LDA}}[\rho] - \int \rho^{\frac{4}{3}} F_{\mathrm{x}}(s) \ \mathrm{d}\mathbf{r} \tag{37}$$

is a widely used example for a GGA functional [98]. It contains a parameter $\beta_B = 0.0042$, which was obtained from optimisations of the Hartree-Fock exchange energy in noble gases.

$$F_{\mathrm{x}}(s) = \frac{2^{-\frac{1}{3}}\beta_B s^2}{1 + 6\beta_B \ s \ \mathrm{arcsinh}(s)} \tag{38}$$

The dimensionless parameter s takes local inhomogeneities in the electron density into account.

$$s = \frac{|\nabla\rho(\mathbf{r})|}{\rho^{\frac{4}{3}}(\mathbf{r})} \tag{39}$$

The BLYP functional combines the exchange functional B_{88} [98] and the GGA correlation functionals form Lee, Yang and Parr (LYP) [99]. Another GGA functional is the PBE by Perdew, Burke and Ernzerhof [100].

$$E_{\mathrm{c}}^{\mathrm{PBE}} = \int \rho(\mathbf{r})[\varepsilon_{\mathrm{C}} + H(r_s, t)]\ \mathrm{d}\mathbf{r} \tag{40}$$

This expression comprises the following abbreviations.

$$t = \frac{|\nabla\rho|}{2\rho k_s}, \quad k_s = \sqrt{\frac{4k_f}{\pi}}, \quad k_f = \left(\frac{9\pi}{4}\right)^{\frac{1}{3}} r_s, \quad r_s = \left(\frac{3}{4\pi\rho}\right)^{\frac{1}{3}} \tag{41}$$

In this expression ε_{C} is the correlation energy per electron in the homogeneous electron gas. The Thomas-Fermi screening wavenumber is denoted as k_s and r_s is the local Seitz radius.

$$H(r_s, t) = \gamma_{\mathrm{PBE}} \log\left(1 + \frac{\beta_{\mathrm{PBE}}}{\gamma_{\mathrm{PBE}}} t^2 \left[\frac{1 + At^2}{1 + At^2 + A^2t^4}\right]\right) \tag{42}$$

$$A = \frac{\beta_{\mathrm{PBE}}}{\gamma_{\mathrm{PBE}}} \frac{1}{\exp(\frac{-\varepsilon_{\mathrm{C}}}{\gamma_{\mathrm{PBE}}}) - 1} \tag{43}$$

The values for the parameters in PBE are $\gamma_{\mathrm{PBE}} \approx 0.03109$ and $\beta_{\mathrm{PBE}} \approx 0.06672$.

A further class of approximations to the exchange-correlation energy functional in DFT are hybrid functionals. They augment conventional GGA functionals with a portion of exact exchange from Hartree-Fock theory. An example is the PBE0 hyprid functional [101], which is based on the PBE functional [100]. The choice for the weighs for the contributions is based on theoretic considerations and does not contain any free empiric parameters.

$$E_{\mathrm{xc}}^{\mathrm{PBE0}} = E_{\mathrm{xc}}^{\mathrm{PBE}} + \frac{1}{4}(E_{\mathrm{x}}^{\mathrm{HF}} - E_{\mathrm{x}}^{\mathrm{PBE}}) \tag{44}$$

The most frequently used functional for the calculation of the exchange-correlation is the B3LYP functional. The B3LYP hybrid functional consists of the exchange functional from Becke (B_{88}) [98] and the GGA correlation functional LYP [83,99] and uses three weighting parameters $a = 0.20,\ b = 0.72$ and $c = 0.81$ [102]

$$E_{\mathrm{xc}}^{\mathrm{B3LYP}} = (1-a)E_{\mathrm{x}}^{\mathrm{LDA}} + aE_{\mathrm{x}}^{\mathrm{HF}} + bE_{\mathrm{x}}^{\mathrm{B_{88}}} + cE_{\mathrm{c}}^{\mathrm{LYP}} + (1-c)E_{\mathrm{c}}^{\mathrm{LDA}}\ . \tag{45}$$

Hybridisation with exact Hartree-Fock exchange yields improvements in the calculation of many molecular properties, such as binding energies, vibration frequencies, and bond lengths [102], which tend to exhibit weaknesses in pure GGA functionals.

Meta-GGA functionals [103–105] provide a further refinement by including the kinetic energy density

$$\tau(\mathbf{r}) = \sum_i |\nabla\phi_i(\mathbf{r})|^2\ , \tag{46}$$

which leads to an improved approximation for the exact correlation energy and by reducing errors due to the kinetic energy term.

Further deficiencies of GGA and hybrid functionals are known in the description of the polarisability in π-conjugated polyene chains, for the description of Rydberg states in TDDFT [106,107] and for charge-transfer states [108]. Therefore, long-range corrected functionals like LC-BLYP [109], CAM-B3LYP [110], LC-ωPBE [111,112] were developed to mitigate some insufficiencies.

1.2.2.4 Long-range Corrections in Density Functional Theory

Long-range-corrections (LC) in DFT partition the Coulomb potential into a short-rang and a long-range term, which are smoothly linked by an error function $\mathrm{erf}(x) = \frac{2}{\sqrt{\pi}} \int_0^x e^{-\tau^2}\, \mathrm{d}\tau$ and contain a parameter μ to discriminate both regimes [108].

$$\frac{1}{r_{12}} = \frac{1 - \mathrm{erf}(\mu r_{12})}{r_{12}} + \frac{\mathrm{erf}(\mu r_{12})}{r_{12}} \tag{47}$$

Here, the first term reflects the short-range interaction term with a DFT exchange contribution and the second term represents the long-range contribution, which possess a high portion of Hartree-Fock exchange between 0.65 and 0.8 $E_{\mathrm{x}}^{\mathrm{HF}}$. The parameter μ defines the extend in the contributions from short-range DFT exchange-energy and the exact long-range exchange energy. In the limit of $\mu \to 0$ the pure GGA is obtained and in the case of $\mu \to \infty$ one gets complete Hartree-Fock exchange for all distances.

The CAM-B3LYP is a range-separated functional and combines the B3LYP functional with a Coulomb-attenuating method (CAM) for long-range interactions. The introduction of additional parameters α, β yields a higher flexibility in the contribution of the exchange term [110].

$$\frac{1}{r_{12}} = \frac{1 - [\alpha + \beta \cdot \mathrm{erf}(\mu r_{12})]}{r_{12}} + \frac{\alpha + \beta \cdot \mathrm{erf}(\mu r_{12})}{r_{12}} \tag{48}$$

The CAM-B3LYP functional uses the parameters $\mu = 0.33\,\mathrm{a.u.}$, $\alpha = 0.19$ and $\beta = 0.46$. In the long range regime CAM-B3LYP utilises 0.65% HF und 0.35% $\mathrm{B_{88}}$ and for short distances 0.19% HF and 0.81% $\mathrm{B_{88}}$, respectively [110].

1.2.2.5 Constrained Density Functional Theory (CDFT)

The probability that an excess charge is transferred in a charge transfer reaction from one spatial region to another depends on the charge transfer integral,

$$|J_{\mathrm{ab}}| = |\langle \Phi_{\mathrm{a}} | H_{\mathrm{el}} | \Phi_{\mathrm{b}} \rangle| \ , \tag{49}$$

where the electronic Hamiltonian H_{el} links two diabatic states Φ_{a} are Φ_{b} [113]. $|J_{\mathrm{ab}}|$ is also referred to as electronic coupling or transition matrix element.

One runs into a problem using DFT for the description of a charge transfer process, as the electronic wavefunction is usually delocalised over all atoms. In order to remedy this problem, constrained density functional theory can be applied. The adiabatic ground state energy E_0 is obtained in standard DFT via minimisation of the energy functional $E_0[\rho]$ with respect to the electron density ρ, whereas TDDFT gives access to excited-state properties. The obtained adiabatic states are quite inaccurate owing to the electron delocalisation error in the exchange-correlation functional. Imposing a constraint on the excess charge in the course of minimising the energy functional mitigates this problem in constrained density functional theory (CDFT) [114–116]. The auxiliary condition for the charge difference constraint

$$N_c = \int w(\mathbf{r}) \rho(\mathbf{r})\, \mathrm{d}\mathbf{r}, \tag{50}$$

can be written as an integral over the electron density $\rho(\mathbf{r})$ and the weighting function $w(\mathbf{r})$, where N_c determines the charge difference between the donor and acceptor region.

The spatial localisation of the constrained excess charge is imposed by means of the weighting function

$$w(\mathbf{r}) = \frac{\sum_a \rho_a(\mathbf{r} - \mathbf{R}_a) - \sum_b \rho_b(\mathbf{r} - \mathbf{R}_b)}{\sum_{i=1}^{N} \rho_i(\mathbf{r} - \mathbf{R}_i)}. \tag{51}$$

The sums in the nominator run over all atoms a and b of the donor A and the acceptor B, respectively, whereas the denominator includes all atoms N. The unperturbed (or promolecular) electron density of atom i,

$$\rho_i(\mathbf{r} - \mathbf{R}_i) = \rho_i(r) = \sum_j p_j^{\mathrm{occ}} |\phi_i^j(r)|^2 \ , \tag{52}$$

is employed according to the Hirshfeld partitioning scheme [117], where the sum includes all orbitals $\phi_i^j(r)$ with occupation numbers p_j^{occ} and the distance $r = |\mathbf{r} - \mathbf{R}_i|$. Alternatively, Mulliken or Löwdin charges can be used.

The energy functional $E[\rho]$ is optimised under the condition of the additional constrain N_c (Eq. 50) with the help of the Lagrange multiplier technique. Therefore, the new functional $W[\rho, \eta]$ is written with density ρ and the Lagrange multiplier η as follows

$$W[\rho, \eta] = E[\rho] + \eta \left(\int w(\mathbf{r})\rho(\mathbf{r}) \ \mathrm{d}\mathbf{r} - N_c \right) \ . \tag{53}$$

The energy of the constrained selected state is found, as the stationary solution for W with respect to ρ and η, by means of minimising the density and maximizing the value of the Lagrange multiplier,

$$E = \min_{\rho} \max_{\eta} W[\rho, \eta] \ . \tag{54}$$

The expression $\eta w(\mathbf{r})$ acts as an external potential, which is added to the Kohn-Sham equation, as the constrain is applied. The magnitude of η determines the height of the potential since the condition $w(\mathbf{r}) \leq 1$ should be fulfilled for all $\mathbf{r}$.

Solving equation (54) for the values $N_c = N_{c,\mathrm{A}}$ and $N_c = N_{c,\mathrm{B}}$, one obtains the diabatic initial charge-transfer state Φ_{A} and the diabatic final acceptor state Φ_{B} for the studied charge transfer process. Assuming the charge transfer for only one excess charge $N_{c,\mathrm{A}} = -N_{c,\mathrm{B}} = 1$ in equation (54) one obtains a complete localisation of the electron at the donor in state Φ_{A} and the acceptor in state Φ_{B}, respectively.

This leads to two Kohn-Sham determinants for both diabatic states Φ_{A} and Φ_{B} with energy E_{A} and E_{B}, respectively. They minimise the functional W with the corresponding Lagrange multipliers η_{A} and η_{B}. Considering H_{ab} as the off-diagonal element of the exact Hamilton operator H_{el}, it is approximated by the state-dependent Kohn-Sham Hamilton operator $\mathcal{H}^{\mathrm{KS}}$ in CDFT. In general, Φ_{A} and Φ_{B} are not mutually orthogonal to each other. Therefore, they need to be distinguished from the orthogonal states Φ_a and Φ_b (Eq. 49), which is indicated by indices with lower case letters.

The coupling of both Kohn-Sham determinants can be expressed by means of the abbreviations $\mathcal{H}_{\mathrm{A}}^{\mathrm{KS}} = \mathcal{H}^{\mathrm{KS}}(\rho_{\mathrm{A}})$, $\mathcal{H}_{\mathrm{B}}^{\mathrm{KS}} = \mathcal{H}^{\mathrm{KS}}(\rho_{\mathrm{B}})$ with respect to the electron densities ρ_{A} and

ρ_{B} and the associated Φ_{A} and Φ_{B}.

$$H_{\mathrm{AB}} = \langle\Phi_{\mathrm{A}}|\mathcal{H}_{\mathrm{B}}^{\mathrm{KS}}|\Phi_{\mathrm{B}}\rangle \tag{55}$$

$$= \langle\Phi_{\mathrm{A}}|\mathcal{H}_{\mathrm{B}}^{\mathrm{KS}} + \eta_{\mathrm{B}}\sum_{i=1}^{n} w(\mathbf{r}_i)|\Phi_{\mathrm{B}}\rangle - \eta_{\mathrm{B}}\langle\Phi_{\mathrm{A}}|\sum_{i=1}^{n} w(\mathbf{r}_i)|\Phi_{\mathrm{B}}\rangle \tag{56}$$

$$= F_{\mathrm{B}}S_{\mathrm{AB}} - \eta_{\mathrm{B}}W_{\mathrm{AB}} \tag{57}$$

$$H_{\mathrm{BA}} = \langle\Phi_{\mathrm{B}}|\mathcal{H}_{\mathrm{A}}^{\mathrm{KS}}|\Phi_{\mathrm{A}}\rangle = F_{\mathrm{A}}S_{\mathrm{BA}} - \eta_{\mathrm{A}}W_{\mathrm{BA}} \tag{58}$$

Here, F_{A} and F_{B} are the potential energies including the interaction with the external potential and $S_{\mathrm{AB}} = \langle\Phi_{\mathrm{A}}|\Phi_{\mathrm{B}}\rangle$ are the off-diagonal elements of the overlap matrix $\mathbb{S}$ and $W_{\mathrm{AB}} = \langle\Phi_{\mathrm{A}}|\sum_{i=1}^{n} w(\mathbf{r}_i)|\Phi_{\mathrm{B}}\rangle$ are the off-diagonal elements of the weighting function matrix $\mathbb{W}$, including a sum over all electrons n.

$$F_{\mathrm{A}} = \langle\Phi_{\mathrm{A}}|\mathcal{H}_{\mathrm{A}}^{\mathrm{KS}} + \eta_{\mathrm{A}}\sum_{i=1}^{n} w(\mathbf{r}_i)|\Phi_{\mathrm{A}}\rangle \tag{59}$$

$$F_{\mathrm{B}} = \langle\Phi_{\mathrm{B}}|\mathcal{H}_{\mathrm{B}}^{\mathrm{KS}} + \eta_{\mathrm{B}}\sum_{i=1}^{n} w(\mathbf{r}_i)|\Phi_{\mathrm{B}}\rangle \tag{60}$$

The off-diagonal elements of the overlap matrix hold the relation $S_{\mathrm{AB}} = S_{\mathrm{BA}}^{*}$.

$$\mathbb{S} = \begin{pmatrix} 1 & S_{\mathrm{AB}} \\ S_{\mathrm{BA}} & 1 \end{pmatrix} \tag{61}$$

Analogously, $W_{\mathrm{AB}} = W_{\mathrm{BA}}^{*}$ is fulfilled for the off-diagonal elements in the weighting function matrix

$$\mathbb{W} = \begin{pmatrix} W_{\mathrm{AA}} & W_{\mathrm{AB}} \\ W_{\mathrm{BA}} & W_{\mathrm{BB}} \end{pmatrix}. \tag{62}$$

If we set N_c=1 and minimise $W[\rho,\eta]$ in equation 54, then we obtain the energy of the initial diabatic state E_{A} with the excess charge located on the donor. Similarly, optimisation with $N_c = -1$ yields the energy E_{B} of the final diabatic state where the excess charge is on the acceptor. With the help of two optimisations, we thus obtain the energy difference,

$$\Delta E(\mathbf{R}) = E_{\mathrm{B}}(\mathbf{R}) - E_{\mathrm{A}}(\mathbf{R}) \ , \tag{63}$$

which represents the vertical energy gap in the Marcus rate expression (Eq. 197) for a charge transfer reaction. The $3N$ dimensional vector $\mathbf{R}$ contains the nuclear coordinates at their fixed position.

If the diagonal elements are abbreviated with $H_{\mathrm{AA}} = \langle\Phi_{\mathrm{A}}|\mathcal{H}_{\mathrm{A}}^{\mathrm{KS}}|\Phi_{\mathrm{A}}\rangle = E_{\mathrm{A}}$ and $H_{\mathrm{BB}} = \langle\Phi_{\mathrm{B}}|\mathcal{H}_{\mathrm{B}}^{\mathrm{KS}}|\Phi_{\mathrm{B}}\rangle = E_{\mathrm{B}}$, one obtains the following matrix, which is not the final 2×2 matrix representation, as the wavefunctions Φ_{A} and Φ_{B} are in general not orthogonal.

$$\mathbb{H}'' = \begin{pmatrix} H_{\mathrm{AA}} & H_{\mathrm{AB}} \\ H_{\mathrm{BA}} & H_{\mathrm{BB}} \end{pmatrix}, \tag{64}$$

Hence, Φ_{A} and Φ_{B} need to be orthogonalised, which is achieved by a transformation on the eigenstates Φ_a and Φ_b of the 2×2 representation of matrix $\mathbb{W}$.

$$\mathbb{W}\mathbb{V} = \mathbb{S}\mathbb{V}\mathbb{L} \tag{65}$$

Here, $\mathbb{V}$ is the 2×2 matrix of the generalised eigenstates, and $\mathbb{L}$ is the diagonal matrix, which holds the eigenvalues. An additional transformation of the matrix $\mathbb{H}''$ is mandatory to receive the diabatic Hamilton matrix $\mathbb{H}$ in the basis of the orthogonal states Φ_a and Φ_b.

$$\mathbb{H} = \mathbb{V}^\dagger \mathbb{H}'' \mathbb{V}. \tag{66}$$

The off-diagonal element in this matrix $H_{ab} = \mathbb{H}_{ab}$ holds the desired electronic coupling matrix element. The matrix $\mathbb{H}$ is not hermitian in general. Therefore, the electronic coupling matrix element is selected as the average of both off-diagonal elements $H_{\mathrm{AB}} = \frac{1}{2}(H_{\mathrm{AB}} + H_{\mathrm{BA}})$ and $H_{\mathrm{BA}} = \frac{1}{2}(H_{\mathrm{AB}} + H_{\mathrm{BA}})^*$, which converts $\mathbb{H}''$ into a hermitian matrix.

Calculation of $\mathbb{S}$ and $\mathbb{W}$ in CDFT If two states Φ_{A} and Φ_{B} are minimised with a constrain for the excess charge, one obtains two Kohn-Sham determinants, which consist of Slater-determinants, that persist of n orthogonal spin orbitals each. They are denoted in the form $\Phi_{\mathrm{A}} = \frac{1}{\sqrt{n!}}\det(\phi_{\mathrm{A}}^1 \dots \phi_{\mathrm{A}}^n)$ and $\Phi_{\mathrm{B}} = \frac{1}{\sqrt{n!}}\det(\phi_{\mathrm{B}}^1 \dots \phi_{\mathrm{B}}^n)$. Considering two different orbitals possessing the indices $i \leq n$ and $j \leq n$, which do not originate from the same Slater determinant, they are not orthogonal to each other in general $\langle \phi_{\mathrm{A}}^i | \phi_{\mathrm{B}}^j \rangle \neq \delta_{ij}$. The orbitals,

$$\phi_{\mathrm{A(B)}}^k = \frac{1}{\Omega} \sum_{\mathbf{G}} c_{\mathrm{A(B)}}^k(\mathbf{G}) \exp(i\mathbf{G}\mathbf{r}) \ , \tag{67}$$

can be developed in a plane wave basis as a sum over all reciprocal lattice vectors $\mathbf{G}$. Here, $c_{\mathrm{A(B)}}^k(\mathbf{G})$ are the development coefficients in the reciprocal space, and Ω is the unit cell volume. The overlap of two Kohn-Sham wavefunctions S_{AB} can be calculated as the determinant of a matrix $\mathbb{O}$.

$$S_{\mathrm{AB}} = \langle \Phi_{\mathrm{A}} | \Phi_{\mathrm{B}} \rangle = \det(\mathbb{O}) \quad \text{with} \quad \mathbb{O}_{ij} = \langle \phi_{\mathrm{A}}^i | \phi_{\mathrm{B}}^j \rangle \tag{68}$$

Using a plain wave basis set in addition with the development coefficients $c_{\mathrm{A}}^i(\mathbf{G})$ the overlap matrix S_{AB} reads

$$S_{\mathrm{AB}} = \det \left[\sum_{\mathbf{G}} c_{\mathrm{A}}^i(\mathbf{G})^* c_{\mathrm{B}}^j(\mathbf{G}) \right]. \tag{69}$$

The elements of the weighting matrix W_{AB}

$$W_{\mathrm{AB}} = \langle \Phi_{\mathrm{A}} | \sum_{i=1}^{n} w(\mathbf{r}_i) | \Phi_{\mathrm{B}} \rangle = \sum_{i=1}^{n} \sum_{j=1}^{n} \langle \phi_{\mathrm{A}}^i | w | \phi_{\mathrm{B}}^j \rangle (-1)^{i+j} \det \mathbb{O}_{\overline{ij}}. = \sum_{i=1}^{n} \sum_{j=1}^{n} \langle \phi_{\mathrm{A}}^i | w | \phi_{\mathrm{B}}^j \rangle \left(\mathbb{O}^{-1} \cdot S_{\mathrm{AB}} \right)_{ji}. \tag{70}$$

An off-diagonal element in matrix $\mathbb{W}$ is represented by the i-th and j-th minor $\mathbb{O}_{\overline{ij}}$ referring to the matrix $\mathbb{O}$, where the i-th line and jth column are eliminated. The equation only yields a contribution if the orbitals ϕ_i and ϕ_j feature the same spin.

The Fourier transform of the weighting function $\tilde{w}(\mathbf{G} - \mathbf{G}')$ can now be employed to express the elements

$$\langle \phi_{\mathrm{B}}^i | w | \phi_{\mathrm{A}}^j \rangle = \sum_{\mathbf{G},\mathbf{G}'} c_{\mathrm{B}}^i(\mathbf{G}')^* c_{\mathrm{A}}^j(\mathbf{G}') \tilde{w}(\mathbf{G} - \mathbf{G}'). \tag{71}$$

Nevertheless, one can circumvent the double summation in reciprocal space, if w is calculated in real space and furthermore the computationally intensive calculation of the minor

determinates in (Eq. 70) is bypassed, if one uses the cofactor matrix $\mathbb{C}$ of matrix $\mathbb{O}$ with the elements

$$\mathbb{C}_{ij} = (-1)^{i+j} \det \mathbb{O}_{\overline{ij}}. \tag{72}$$

The transposed matrix $\mathbb{C}^T$ is determined with the Laplace expansion of the inverse of $\mathbb{O}$

$$\mathbb{C}^T = \mathbb{O}^{-1}[\det(\mathbb{O})\ \mathbb{1}] = \left(\mathbb{O}^{-1} \cdot S_{\mathrm{AB}}\right)_{ij}. \tag{73}$$

Instead of computing the determinants of all the minors of $\mathbb{O}$, we only need to compute the inverse and the determinant of $\mathbb{O}$. The diagonal elements of $\mathbb{W}$ are only the constraint values N_c for the two diabatic states.

1.2.2.6 Empirical Dispersion Corrections in DFT

As standard KS-DFT does not inherently account for London dispersion interactions [118], semi-classical methods were invented to compute long-range dispersion effects. Grimme's DFT-D dispersion corrections are widely applied for molecules and solids, and they come in different calculation schemes, e.g. D2 [119], D3 [120], D3(BJ) with Becke-Johnson damping [121], and D4 [122].
The total DFT-D3 energy is given as the KS-DFT energy with a dispersion correction

$$E^{\text{DFT-D3}} = E^{\mathrm{KS}} - E^{\mathrm{disp}} = E^{\mathrm{KS}} - (E^{\mathrm{disp(2)}} + E^{\mathrm{disp(3)}})\ . \tag{74}$$

The two-body dispersion energy term with the dispersion coefficients C_n^{ab} at n-th order reads

$$E^{\mathrm{disp(2)}} = \sum_{ab} \sum_{n=6,8} s_n \frac{C_n^{ab}}{R_{ab}^n} f_{d,n}(R_{ab})\ . \tag{75}$$

It is a sum over all pairs of atoms ab with a distance R_{ab} in the system. The sum is restricted to $n = 6$ and $n = 8$ as higher orders are neglected, as they neither improve the accuracy significantly nor the numeric stability. The factors s_n provoke a global scaling and are parametrised for the repulsion in different functionals individually. The damping function $f_{d,n}$ controls the short- and long-range behaviour of the dispersion correction, which reads for both D2 and D3

$$f_{d,n}(R_{ab}) = \frac{1}{1 + 6(\frac{R_{ab}}{s_{r,n} R_{ab}^0})^{-\alpha_n}}\ . \tag{76}$$

The expression includes an order-dependent scaling of the cutoff radius R_{ab}^0 with the factor $s_{r,n}$ and a steepness parameter α_n. R_{ab}^0 determines the distances for every pair of atoms, where the dispersion decreases and the DFT exchange-correlation energy comes in.

The C_6^{ab} coefficients can be pre-computed using TDDFT from the averaged dipole polarisability $\alpha(i\omega)$ at the imaginary frequency ω, and recursive formulas are employed to obtain coefficients with higher order

$$C_6^{ab} = \frac{3}{\pi} \int_0^\infty \alpha^a(i\omega)\alpha^b(i\omega)\, \mathrm{d}\omega\ . \tag{77}$$

In the D3 method, the coefficients C_n^{ab} are designed for interpolation purposes to exhibit a dependence on the fractional coordination numbers taking the structural, chemical environment into account. However, the D3 dispersion coefficients do not represent fluctuations in the underlying electron density.

In addition, the three-body terms for all triples of atoms $a,\ b,\ c$ are

$$E^{\mathrm{disp}(3)} = \sum_{abc} f_{d,3}(\overline{R}_{abc}) C_9^{abc} \frac{(1 + 3\cos\theta_A \cos\theta_B \cos\theta_C)}{(R_{ab} R_{bc} R_{ca})^3} \tag{78}$$

Here, the damping function uses $\alpha = 16$ and $s_r = \frac{4}{3}$. The atoms $a,\ b,\ c$ form a triangle with the distances R_{ab}, R_{bc} and R_{ca} and the internal angles are $\theta_A,\ \theta_B,\ \theta_C$. Also, the geometric average $\overline{R}_{abc}$ for the radii enters the damping function. One approximation for the triple-dipole constant is $C_9^{abc} = -\sqrt{C_6^{ab} C_6^{bc} C_6^{ca}}$, as the geometric mean. The negative sign in C_9^{abc} causes a repulsive effect in densely packed systems.

The D3 method yields shortcomings in the zero-damping functions $f_{d,n}$, which approach zero in the asymptotic limit for $R_{ab} \to 0$. Therefore, also the dispersion energy E^{disp} turns equal to zero. In contrast, it should instead reach a finite, constant value as stated by an expansion of the dispersion energy in multipoles [123].

The introduction of the Becke-Johnson (BJ) damping [124] extenuates the problem, as it forces the dispersion correction to a constant contribution at small interatomic distances R_{ab} [121]. The D3(BJ) expression for the two-body term reads

$$E_{\mathrm{disp}}^{\mathrm{D3(BJ)}} = -\frac{1}{2} \sum_{\substack{ab \\ a \neq b}} s_6 \frac{C_6^{ab}}{R_{ab}^6 + [f(R_{ab}^0)]^6} + s_8 \frac{C_8^{ab}}{R_{ab}^8 + [f(R_{ab}^0)]^8} \tag{79}$$

and includes a linear function $f(R_{ab}^0) = a_1 R_{ab}^0 + a_2$, with the free fit parameters a_1 and a_2. The choice of $R_{ab}^0 = \sqrt{\frac{C_8^{ab}}{C_6^{ab}}}$ in the BJ-damping gives an enhanced performance. D3(BJ) does not need pair-specific cutoff radii and avoids artificial repulsive forces at small interatomic distances.

The D4 dispersion model refines atomic dispersion coefficients in the D3 approach via the introduction of charge-dependent local polarisabilities calculated using a self-consistent tight-binding approach [122]. All presented DFT-D methods exhibit straightforward expressions for analytical gradients, and hence the atomic forces are applied in, e.g. geometry optimisations or MD-simulations.

1.2.2.7 Time-Dependent Density Functional Theory (TDDFT)

So far, we have discussed only electronic structure methods for the ground state. Time-dependent density functional theory is a computational method, which is applicable for the description of excited states and absorption spectra of molecules [79,125]. The Hohenberg-Kohn-Sham formulation [91] of density functional theory needs to be generalised in order to describe the evolution of time-dependent properties.

The Runge-Gross theorem is the theoretical basis of time-dependent density functional theory. The theorem states, if the initial state of a multi-particle system is given by the wavefunction $\phi(t)$ at the initial time $t = t_0$, then there exists a mapping between the time-dependent electron density $\rho(\mathbf{r}, t)$ and the time-dependent external potential $v_{\mathrm{ext}}(\mathbf{r}, t)$ for every instance of time $t > t_0$. This mapping is unique, apart from an additional term with a single time-dependent shift, and makes it possible to calculate the dynamic of a quantum mechanical multi-particle problem on the basis of the ground state electron density [93,126].

The Kohn-Sham ansatz permits the computation of the density of an interacting electron system by means of the density generated by non-interacting electrons, as it is the case

in time-independent DFT. The time-dependent density $\rho(\mathbf{r},t)$ is attained from the time-dependent Kohn-Sham orbitals $\phi_i(\mathbf{r},t)$.

$$\rho(\mathbf{r},t) = \sum_i p_i^{\mathrm{occ}} |\phi_i(\mathbf{r},t)|^2 \tag{80}$$

In analogy to time-independent DFT the time-dependent Kohn-Sham equations need to be solved iteratively in a self-consistent manner till convergence to deduce the time-dependent density $\rho(\mathbf{r},t)$ from the effective potential $v_{\mathrm{eff}}(\mathbf{r},t)$.

$$i\frac{\partial}{\partial t}\phi_i(\mathbf{r},t) = \left(-\frac{\nabla^2}{2} + v_{\mathrm{eff}}[\rho](\mathbf{r},t)\right)\phi_i(\mathbf{r},t) \tag{81}$$

The effective potential $v_{\mathrm{eff}}(\mathbf{r},t)$ and the exchange-correlation potential $v_{\mathrm{xc}}(\mathbf{r},t)$ are both time-dependent in the Kohn-Sham equations.

$$v_{\mathrm{eff}}[\rho](\mathbf{r},t) = v_{\mathrm{ext}}(\mathbf{r},t) + \int \frac{\rho(\mathbf{r}',t)}{|\mathbf{r}-\mathbf{r}'|}\,\mathrm{d}\mathbf{r}' + v_{\mathrm{xc}}[\rho](\mathbf{r},t) \tag{82}$$

As the time-dependent Kohn-Sham equations determine the dynamic propagation of orbitals and the electron density, one can use the direct solution to describe the dynamics of nuclei and electrons. However, the main focus of applications on TDDFT is the description of systems under the influence of weak, electromagnetic fields by means of linear response theory (LR-TDDFT), e.g. for the calculation of molecular absorption spectra.

Linear Response Theory Linear response theory can describe the behaviour of a system, which is affected by a small time-dependent external perturbation $v_1(\mathbf{r},t) = E_z \cos\omega t$. As the external electric field oscillates with a frequency ω and an amplitude E_z in z direction, it induces a perturbation in the system, after it is switched on at time $t = t_0$ [79,125,127]. One obtains the response of the electron density to the external perturbing potential v_1, taking the unperturbed ground state density $\rho_0(\mathbf{r})$ as a starting point in the equation

$$\rho(\mathbf{r},t) - \rho_0(\mathbf{r}) \approx \rho_1(\mathbf{r},t) = \int \mathrm{d}t' \int \mathrm{d}\mathbf{r}'\ \chi(\mathbf{r},t,\mathbf{r}',t')v_1(\mathbf{r},t) \tag{83}$$

and calculating the interacting response function

$$\chi(\mathbf{r},t,\mathbf{r}',t') = \left.\frac{\delta\rho(\mathbf{r},t)}{\delta v_{\mathrm{ext}}(\mathbf{r}',t')}\right|_{v_0} . \tag{84}$$

The Fourier transform yields the frequency-dependent linear response density

$$\begin{aligned}\rho_1(\mathbf{r},\omega) = \int \mathrm{d}\mathbf{r}'\chi(\mathbf{r},\mathbf{r}';\omega)v_1(\mathbf{r}',\omega) + \int \mathrm{d}\mathbf{r}' \int \mathrm{d}\mathbf{r}''\chi(\mathbf{r},\mathbf{r}';\omega)\times \\ \times\left(\frac{1}{|\mathbf{r}'-\mathbf{r}''|} + f_{\mathrm{xc}}[\rho_0](\mathbf{r}',\mathbf{r}'';\omega)\right)\rho(\mathbf{r}'',\omega)\ ,\end{aligned} \tag{85}$$

and with the response function

$$\chi(\mathbf{r},\mathbf{r}';\omega) = \sum_{ph}\left(\frac{\phi_p(\mathbf{r})\phi_h^*(\mathbf{r})\phi_p^*(\mathbf{r}')\phi_h(\mathbf{r}')}{\omega-(\varepsilon_p-\varepsilon_h)} - \frac{\phi_p^*(\mathbf{r})\phi_h(\mathbf{r})\phi_p(\mathbf{r}')\phi_h^*(\mathbf{r}')}{\omega+(\varepsilon_p-\varepsilon_h)}\right) . \tag{86}$$

The one-particle Kohn-Sham orbital ϕ_p corresponds to an orbital, which is occupied by an electron and the Kohn-Sham orbital ϕ_h represents an unoccupied orbital for a hole. The energy of the single-particle excitations $\varepsilon_{ph} = \varepsilon_p - \varepsilon_h$ is given by the particle Kohn-Sham energy ε_p and the hole Kohn-Sham energy ε_h. The exchange-correlation kernel reads

$$f_{\mathrm{xc}}[\rho_0](\mathbf{r}, t, \mathbf{r}', t') = \frac{\delta v_{\mathrm{xc}}[\rho](\mathbf{r}, t)}{\delta \rho(\mathbf{r}', t')} \ . \tag{87}$$

The equation 85 needs to be solved self-consistently for the density in first order approximation.
Solving the following time-independent eigenvalue problem yields the sought-after excitation energies [125].

$$\Omega |\mathbf{F}_n\rangle = \omega_n^2 |\mathbf{F}_n\rangle \tag{88}$$

The eigenvector $|\mathbf{F}\rangle$ consists of the response amplitudes $\mathbf{X}$ and $\mathbf{Y}$. The contributions of involved transitions, which contribute to a selected excited state n, from an initial orbital to a target orbital are weighted by the coefficients in $\mathbf{X}$ and $\mathbf{Y}$ [125]. The response matrix Ω reads:

$$\Omega_{p,h,p',h'} = \delta_{pp'}\delta_{hh'}(\epsilon_p - \epsilon_h)^2 + \sqrt{\epsilon_p - \epsilon_h} K_{p,h,p',h'} \sqrt{\epsilon_{p'} - \epsilon_{h'}} \ . \tag{89}$$

Here, $K_{p,h,p',h'}$ is the coupling matrix

$$K_{p,h,p',h'} = \iint \mathrm{d}\mathbf{r}\, \mathrm{d}\mathbf{r}' \ \phi_p(\mathbf{r})\phi_h(\mathbf{r}) f_{\mathrm{H,xc}}(\mathbf{r}, \mathbf{r}')\phi_{p'}(\mathbf{r}')\phi_{h'}(\mathbf{r}') \ . \tag{90}$$

The exchange-correlation kernel is $f_{\mathrm{H,xc}}$ and comprises a Hartree term as well as an exchange-correlation term in adiabatic approximation.

$$f_{\mathrm{H,xc}} = \frac{1}{|\mathbf{r} - \mathbf{r}'|} + \delta(\mathbf{r} - \mathbf{r}') \frac{\delta^2 E_{\mathrm{xc}}}{\delta^2 \rho(\mathbf{r})} \tag{91}$$

TDDFT commonly exhibits a systematic error for excited state energies about $0.2 - 0.4$ eV [107, 128]. Furthermore, TDDFT turns out to provide unsatisfactory results for the description of charge-transfer states [129]. Linear response time-dependent density functional theory (LR-TDDFT) is a widely-used method for the calculation of vertical excitation energies, as it is a good trade-off between computational accuracy and computing time.

Electronic Circular Dichroism Spectra (ECD) The absolute configurations of chiral molecules can be identified via comparison of experimental chiroptical properties like optical rotatory dispersion (ORD) or circular dichroism (CD) spectra to *ab-initio* calculations of electronic circular dichroism (ECD) [130, 131]. These methods enable the clear differentiation of stereoisomers of a substance. A substance possesses CD, if it exhibits a difference in the absorption coefficient ε for left- and right-handed circularly polarized light.

$$\Delta\varepsilon = \varepsilon_L - \varepsilon_R \tag{92}$$

The measurement of $\Delta\varepsilon$ as a function of the frequency ω of the incident, visible or ultraviolet light gives a CD spectrum.

$$\Delta\varepsilon(\omega) = \frac{cN_A}{3\ln 10} 16\pi^2\omega^2 \sum_n \frac{1}{\omega_{0n}} (R_{0n}\delta(\omega - \omega_{0n}) - R_{0n}\delta(\omega + \omega_{0n})) \tag{93}$$

Here, N_A is Avogadro's constant, c is the velocity of light and the sum accounts the excitation from the ground state 0 to an excited state n with an excitation energy E_{0n} and a corresponding frequency ω_{0n}. A characteristic parameter for a certain transition is the rotatory strength R_{0n}, which is the integrated intensity of a single ECD band [131].

$$R_{0n} = \frac{3\ln 10}{16\pi^2 c N_A} \int_{\omega_{0n}-\varepsilon}^{\omega_{0n}+\varepsilon} \frac{\Delta\varepsilon(\omega)}{\omega}\,\mathrm{d}\omega \tag{94}$$

The rotatory strength is usually expressed in 10^{-40} c.g.s units and $64604.8 \times 10^{-40}\mathrm{erg\,cm}^3$ is associated with 1 a.u..

The Cotton effect [132, 133] describes the characteristic alternation the circular dichroism (CD) in the proximity of an absorption band of a material. If the optical rotation first increases as the wavelength decreases, the effect is called positive, and negative if the rotation first decreases. For corresponding enantiomers, the Cotton effect is reversed.

The dissymmetry factor g describes the chiroptical response of an absorber as a function of the intensities in the absorption of right-handed circular polarised light I_R and left-handed I_L respectively.

$$g = \frac{I_L - I_R}{0.5(I_L + I_R)} \tag{95}$$

An approach to calculate the optical rotation parameter is to use perturbation theory for an external perturbation field with frequency ω on the electric moment $\boldsymbol{\mu}$ and the magnetic moment $\boldsymbol{m}$ [134, 135].

$$\mu'_u = \sum_v \alpha_{uv} E_v - \sum_v \frac{\beta_{uv}}{c} \frac{\partial B_v}{\partial t} + \ldots \quad \text{with} \quad u, v \in \{x, y, z\} \tag{96}$$

$$m'_u = \sum_v \kappa_{uv} B_v - \sum_v \frac{\beta_{uv}}{c} \frac{\partial E_v}{\partial t} + \ldots \quad \text{with} \quad u, v \in \{x, y, z\} \tag{97}$$

In these expressions enter three tensor quantities, which are all frequency dependent, like the electric polarisability tensor $\boldsymbol{\alpha}_{uv}$, the magnetic susceptibility tensor $\boldsymbol{\kappa}_{uv}$ and the optical rotation tensor $\boldsymbol{\beta}_{uv}$. The experimental accessible observable are their rotational averages like $\overline{\alpha}$, $\overline{\kappa}$ and the optical rotation parameter $\overline{\beta}$, which reads $\overline{\beta} = \frac{(\beta_{xx}+\beta_{yy}+\beta_{zz})}{3}$.

With the help of a sum-over-states expressions one can write $\overline{\beta}$ as a function of the electric $\boldsymbol{\mu}_{0n}$ and magnetic dipole moment $\boldsymbol{m}_{n0}$ or expressed by the rotatory strength R_{0n} for a single excitation.

$$\overline{\beta} = \frac{2c}{3} \sum_n \frac{\mathrm{Im}(\boldsymbol{\mu}_{0n}\boldsymbol{m}_{n0})}{\omega_{0n}^2 - \omega^2} = \frac{2c}{3} \sum_n \frac{R_{0n}}{\omega_{0n}^2 - \omega^2} \tag{98}$$

Analogous expressions for $\overline{\alpha}$ and $\overline{\kappa}$ hold.

$$\overline{\alpha} = \frac{2}{3} \sum_n \frac{\omega_{0n}\mathrm{Re}(\boldsymbol{\mu}_{0n}\boldsymbol{\mu}_{n0})}{\omega_{0n}^2 - \omega^2} = \sum_n \frac{f_{0n}}{\omega_{0n}^2 - \omega^2} \quad \text{and} \quad \overline{\kappa} = \frac{2}{3} \sum_n \frac{\omega_{0n}\mathrm{Re}(\boldsymbol{m}_{0n}\boldsymbol{m}_{n0})}{\omega_{0n}^2 - \omega^2} \tag{99}$$

It involves the definition of the oscillator strengths f_{0n} for the $0 \rightarrow n$ excitation. If no absorption takes place $\overline{\alpha}$, $\overline{\kappa}$ and $\overline{\beta}$ are real quantities. If the ground state wavefunction Φ_0 and excited state wavefunctions Φ_n are accessible, e.g. from configuration interaction (CI)

methods, the electric transition dipole moment $\boldsymbol{\mu}_{0n} = \langle\Phi_0|\hat{\boldsymbol{\mu}}|\Phi_n\rangle$ can be determined by means of the electric dipole moment operator $\hat{\boldsymbol{\mu}} = -e\hat{\mathbf{r}}$ and in the same way the magnetic transition dipole moment $\boldsymbol{m}_{0n} = \langle\Phi_0|\hat{\boldsymbol{m}}|\Phi_n\rangle$ is obtained form the magnetic dipole moment operator $\hat{\boldsymbol{m}} = -\frac{e}{2c}\hat{\mathbf{r}} \times \hat{\mathbf{p}}$.

In the following, the expression for β_{uv} is derived in the TDDFT framework [134, 135]. Assuming $\phi_{i\sigma}$ are Kohn-Sham spin orbitals with occupation numbers $n_{i\sigma} \in \{0, 1\}$ and spin σ for the unperturbed system, one can write the first-order density perturbation as a function of the frequency ω by means of the first-order response P' of the KS-density matrix

$$\varrho'_\sigma(\mathbf{r}, \omega) = \sum_i \sum_a P'_{ai\sigma}(\omega)\phi_{i\sigma}(\mathbf{r})\phi_{a\sigma}(\mathbf{r}) \tag{100}$$

If we exploit the matrix notation with composite indices $(ai\sigma)$, for spin orbital pairs that fulfill $n_{a\sigma}<n_{i\sigma}$, for the density matrix P' and for the vectors $\mathbf{V}, \mathbf{W}, \mathbf{X}, \mathbf{Y}$, then the definitions of $X_{ai\sigma} = P'_{ai\sigma}(\omega)$ and $Y_{ai\sigma} = P'_{ai\sigma}(\omega)$ allow to write the first-order electric dipole moment perturbation as

$$\mu'_u(\omega) = \sum_{ai\sigma} D_{u,ai\sigma}(X_{ai\sigma} + Y_{ai\sigma}) = \mathbf{D}_u(\mathbf{X} + \mathbf{Y}), \tag{101}$$

where the matrix elements obey the relation $D_{u,ai\sigma} = D_{u,ia\sigma}$ and the magnetic moment exploits $M_{u,ai\sigma} = -M_{u,ia\sigma}$ in

$$m'_u(\omega) = \sum_{ai\sigma} M_{u,ai\sigma}(X_{ai\sigma} - Y_{ai\sigma}) = \mathbf{M}_u(\mathbf{X} - \mathbf{Y}). \tag{102}$$

Here, $\mathbf{D}_u$ and $\mathbf{M}_u$ represent the u-th component of the matrices from the electric and magnetic dipole moment operators $\hat{\mu}_u$ and $-\hat{m}_u$ based on unperturbed KS-orbitals [68]. As only the symmetric $(\mathbf{X}+\mathbf{Y})$ or asymmetric $(\mathbf{X}-\mathbf{Y})$ ingredients of P' are required to determine $\boldsymbol{\mu}_{0n}$ and $\boldsymbol{m}_{0n}$, one can solve for these quantities and save computational coasts, compared to an individual treatment of $\mathbf{X}$ and $\mathbf{Y}$. If the impact on the unperturbed KS-orbitals of an external frequency-dependent perturbation, represented by the Hamiltonian $\mathcal{H}'(\omega)$ from an external electric or magnetic field with a component v, is written in the notation above like $V_{v,ai\sigma}$ and $W_{v,ai\sigma} = V_{v,ai\sigma}$, then one can get to a random phase approximation-like equation system for the aspired solutions [68].

$$(\boldsymbol{\mathcal{A}} + \boldsymbol{\mathcal{B}})(\mathbf{X} + \mathbf{Y}) + \omega\boldsymbol{\mathcal{C}}(\mathbf{Y} - \mathbf{X}) = \mathbf{V}_v + \mathbf{W}_v \tag{103}$$

$$(\boldsymbol{\mathcal{A}} - \boldsymbol{\mathcal{B}})(\mathbf{X} - \mathbf{Y}) + \omega\boldsymbol{\mathcal{C}}(\mathbf{X} + \mathbf{Y}) = \mathbf{V}_v - \mathbf{W}_v \tag{104}$$

In this expression $\boldsymbol{\mathcal{A}}, \boldsymbol{\mathcal{B}}$ and $\boldsymbol{\mathcal{C}}$ are the matrices with two composed indices $(ai\sigma)$ and $(bj\tau)$ and they are determined by formulas

$$\mathcal{A}_{ai\sigma,bj\tau} = \delta_{\sigma\tau}\delta_{ab}\delta_{ij}\frac{\varepsilon_{b\tau} - \varepsilon_{j\tau}}{n_{b\tau} - n_{j\tau}} - K_{ai\sigma,bj\tau} \tag{105}$$

$$\mathcal{B}_{ai\sigma,bj\tau} = -K_{ai\sigma,jb\tau} \tag{106}$$

$$\mathcal{C}_{ai\sigma,bj\tau} = \frac{\delta_{\sigma\tau}\delta_{ab}\delta_{ij}}{n_{b\tau} - n_{j\tau}}\ . \tag{107}$$

The matrix $\boldsymbol{\mathcal{C}}$ reduces to the negative unit matrix, if all orbitals possesses only the occupation numbers 0 and 1. The coupling matrix $\mathbf{K}$ possesses a Coulomb and an exchange-correlation contribution (XC) and it specifies the response at first-order of the molecular KS-potential.

$$K_{ai\sigma,bj\tau} = K^{\mathrm{c}}_{ai\sigma,bj\tau} + K^{\mathrm{xc}}_{ai\sigma,bj\tau} \tag{108}$$

$$K^{\mathrm{c}}_{ai\sigma,bj\tau} = \int \mathrm{d}\mathbf{r} \int \mathrm{d}\mathbf{r}' \frac{\phi^*_{a\sigma}(\mathbf{r})\phi_{i\sigma}(\mathbf{r})\phi_{b\tau}(\mathbf{r}')\phi^*_{j\tau}(\mathbf{r}')}{|\mathbf{r}-\mathbf{r}'|}$$

$$K^{\mathrm{xc}}_{ai\sigma,bj\tau} = \int \mathrm{d}\mathbf{r} \int \mathrm{d}\mathbf{r}' \phi^*_{a\sigma}(\mathbf{r})\phi_{i\sigma}(\mathbf{r}) f^{\mathrm{xc}}_{\sigma\tau}(\mathbf{r},\mathbf{r}',\omega)\phi_{b\tau}(\mathbf{r}')\phi^*_{j\tau}(\mathbf{r}')$$

The expression includes the exchange-correlation kernel $f^{\mathrm{xc}}_{\sigma\tau}(\mathbf{r},\mathbf{r}',\omega)$, which is obtained by Fourier transform of the exchange potential from the time to the frequency domain.

$$f^{\mathrm{xc}}_{\sigma\tau}(\mathbf{r},\mathbf{r}',t-t') = \frac{\delta V^{\mathrm{xc}}_{\sigma}(\mathbf{r},t)}{\delta\rho_{\tau}(\mathbf{r}',t')} \tag{109}$$

If one uses the terms $(\mathbf{X}-\mathbf{Y})$ for the perturbation of the external electric field, one can derive an expression (Eq. 102) to retrieve an equation for the rotatory strength β_{uv} (see [135]).

$$\beta_{uv} = 2c\ \mathrm{Im}\left(\mathbf{D}_u\mathbf{S}^{-1/2}[\omega^2-\boldsymbol{\Omega}]^{-1}\mathbf{S}^{1/2}\boldsymbol{\mathcal{C}}^{-1}\mathbf{M}_v\right) \tag{110}$$

Similar expressions hold for κ_{uv} and α_{uv} [135]. Here, the diagonal matrix $\mathbf{S}$ and the Hermitian matrix $\boldsymbol{\Omega}$ can be expressed in terms of the matrices $\boldsymbol{\mathcal{A}}$, $\boldsymbol{\mathcal{B}}$, $\boldsymbol{\mathcal{C}}$ with

$$\mathbf{S} = -\boldsymbol{\mathcal{C}}(\boldsymbol{\mathcal{A}}-\boldsymbol{\mathcal{B}})^{-1}\boldsymbol{\mathcal{C}} \quad \text{and} \quad \boldsymbol{\Omega} = -\mathbf{S}^{-1/2}(\boldsymbol{\mathcal{A}}+\boldsymbol{\mathcal{B}})\mathbf{S}^{-1/2}\ . \tag{111}$$

As stated in [68] the inverse of the term $[\omega^2-\boldsymbol{\Omega}]$ can be written in terms of the eigenvectors $\boldsymbol{F}_{0n}$ to the matrix $\boldsymbol{\Omega}$.

$$[\omega^2-\boldsymbol{\Omega}]^{-1} = -\sum_n \frac{\boldsymbol{F}_{0n}\otimes\boldsymbol{F}_{0n}}{\omega^2_{0n}-\omega^2} \tag{112}$$

This expression includes the squared frequencies ω^2_{n0} that correspond to excitation energies form the ground state to an excited state n and can be obtained as the solution to the following eigenvalue problem

$$\boldsymbol{\Omega}\boldsymbol{F}_{0n} = \omega^2_{0n}\boldsymbol{F}_{0n} \tag{113}$$

With the excitations ω_{n0} at hand and insertion of (Eq. 112) in (Eq. 110) one can detail the sum over states expression for β_{uv} in (Eq. 98) and hence determine the rotatory strength associated with a single transition as

$$R_{0n} = \mathrm{Im}\left(\sum_u \mathbf{D}_u\mathbf{S}^{-1/2}\boldsymbol{F}_{0n}\cdot\boldsymbol{F}_{0n}\mathbf{S}^{-1/2}\boldsymbol{\mathcal{C}}^{-1}\mathbf{M}_u\right) \tag{114}$$

Therefore, a single component u of the electric transition dipole moment $\boldsymbol{\mu}_{0n}$ reads

$$\mu_{u,0n} = \omega^{-1/2}_{0n}\mathbf{D}_u\mathbf{S}^{-1/2}\boldsymbol{F}_{0n} \tag{115}$$

and one can get similarly to the expression for the magnetic transition dipole moment $\mathbf{m}_{0n}$

$$m_{u,0n} = -\omega^{-1/2}_{0n}\mathbf{M}_u\boldsymbol{\mathcal{C}}^{-1}\mathbf{S}^{-1/2}\boldsymbol{F}_{0n} \tag{116}$$

In order to achieve adequate origin-independence in the results, even if no gauge-independent atomic orbitals (GIAO)s are applied, one can replace the expression (Eq. 115) by

$$\mu^{\nabla}_{u,0n} = \omega^{-1/2}_{0n}\nabla_u\mathbf{D}_u\mathbf{S}^{-1/2}\boldsymbol{F}_{0n}, \tag{117}$$

which is the dipole-velocity of the electric transition dipole moment. The operator $\nabla_u = -\frac{\partial}{\partial u}$ is the derivative to the matrix elements with index (a,i,σ).

All in all, the R_{0n} are accessible in TDDFT and represent a discrete line spectrum, that can be broadened by Gaussian functions, to obtain a theoretical ECD spectrum $\Delta\varepsilon(\omega)$.

1.2.2.8 Vibronic Absorption and Emission Spectra

In a first approach, ultraviolet-visible (UV-Vis) absorption spectra can be calculated by vertical excitations at the optimised ground state geometry of a molecule. The obtained line spectra (e.g. using TDDFT) are usually convoluted with Lorentzian or Gaussian functions. Following this procedure for the broadening of the lines spectrum neglects dynamic effects, which can be incorporated applying vibrationally-resolved electronic spectra or molecular dynamics simulations (Sec. 1.3.1 [136])

In the following, we will introduce a method to simulate intensities of transitions between pairs of vibronic states [137]. The absorption or emission of electromagnetic radiation can be treated in first-order perturbation theory with the Hamilton operator $H' = \boldsymbol{\mu}\mathbf{E}$ for the dipole moment $\boldsymbol{\mu}$ and an external perturbing electromagnetic field $\mathbf{E}$.

A transition from an initial state Ψ_i to a final state Ψ_f is associated with a transition rate per molecule k. The transition rate is proportional to the transition probability, which depends on both the transition matrix element $\langle\Psi_i|\boldsymbol{\mu}|\Psi_f\rangle$ and the Boltzmann distributed occupation of the initial state p_i and the wavelength ω of the absorbed or emitted photon, respectively.

The transition rate for photon absorption is

$$k_{\mathrm{abs}}(\omega) = \frac{4\pi^2\omega}{3}\sum_i p_i \sum_f |\langle\Psi_i|\boldsymbol{\mu}|\Psi_f\rangle|^2 \delta(E_f - E_i - \hbar\omega) \tag{118}$$

and the rate for photon emission

$$k_{\mathrm{em}}(\omega) = \frac{4\omega^3}{3\hbar c^3}\sum_i p_i \sum_f |\langle\Psi_i|\boldsymbol{\mu}|\Psi_f\rangle|^2 \delta(E_f - E_i + \hbar\omega)\ . \tag{119}$$

In a subsequent step the dipole moment is separated into an expression for the nuclear dipole moment $\boldsymbol{\mu}_n$ and the electronic dipole moment $\boldsymbol{\mu}_e$.

$$\langle\Psi_i|\boldsymbol{\mu}|\Psi_f\rangle = \langle\Phi_i\chi_i|\boldsymbol{\mu}_n|\Phi_f\chi_f\rangle + \langle\Phi_i\chi_i|\boldsymbol{\mu}_e|\Phi_f\chi_f\rangle \tag{120}$$

According to Born-Oppenheimer approximation the wavefunction can be written as a product of the nuclear wavefunction and the electronic wavefunction. As the nuclear dipole moment acts only on the nuclear wavefunction and the electronic wavefunctions in the ground state and in the excited state are orthogonal on each other, all terms with $\boldsymbol{\mu}_n$ are omitted when calculating the transition matrix element. So the transition dipole moment only depends on the nuclear wavefuntions and the electronic transition dipole moment $\boldsymbol{\mu}_{if} = \langle\Phi_i|\boldsymbol{\mu}_e|\Phi_f\rangle$.

$$\langle\Psi_i|\boldsymbol{\mu}|\Psi_f\rangle \approx \langle\chi_{i,\nu}|\boldsymbol{\mu}_{if}|\chi_{f,\nu}\rangle \tag{121}$$

As the integral is not solvable analytically, further approximations like the harmonic approximation needs to be applied. This implies the transcription of the multi-dimensional vibrational wavefunction χ_ν as a product of one dimensional wavefunctions $\chi_{\nu_j}(\boldsymbol{Q}_j)$. Here, $\boldsymbol{Q}_j$ denotes one of the normal coordinates of the j-th oscillation in a molecule with N coordinates. Expanding $\boldsymbol{\mu}_{if}$ in a Taylor series with respect to the normal coordinates, one obtains a description of the vibrational modes in the final state in the harmonic approximation.

$$\boldsymbol{\mu}_{if}(\boldsymbol{Q}_f) \approx \boldsymbol{\mu}_{if}(\boldsymbol{Q}_{f,0}) + \sum_{k=1}^{N}\left(\frac{\partial\boldsymbol{\mu}_{if}}{\partial\boldsymbol{Q}_{f,k}}\right)_0 \boldsymbol{Q}_{f,k} + \frac{1}{2}\sum_{k=1}^{N}\sum_{l=1}^{N}\left(\frac{\partial^2\boldsymbol{\mu}_{if}}{\partial\boldsymbol{Q}_{f,k}\partial\boldsymbol{Q}_{f,l}}\right)_0 \boldsymbol{Q}_{f,k}\boldsymbol{Q}_{f,l} + \ldots \tag{122}$$

In the Franck-Condon Approximation one assumes that the transition dipole moment remains constant and only the first term in the Taylor series is taken into account [138,139]. The change of the electrons from the initial to the final state occurs much faster than the vibrational motion of the nuclei, so the nuclear positions remain unchanged during an electronic transition. The transition with the highest intensity is a vertical transition from the minimum of the initial state to an excited vibrational final state with the highest value in the overlap integral $\langle\chi_{i,\nu}|\chi_{f,\nu}\rangle$. The overlap integral is also called Frank-Condon integral.

The Herzberg-Teller Approximation allows small changes in the nuclear coordinates in the course of a transition, which allows dipole forbidden transitions, e.g. symmetry-forbidden transitions (T_1-S_0 phosphorescence transitions) if also second-order terms are taken into account. The total transition dipole moment is

$$\begin{aligned}\langle\Psi_i|\boldsymbol{\mu}|\Psi_f\rangle \approx \boldsymbol{\mu}_{if}(\boldsymbol{Q}_{f,0})\langle\chi_{i,\nu}|\chi_{f,\nu}\rangle + \sum_{k=1}^{N}\left(\frac{\partial\boldsymbol{\mu}_{if}}{\partial\boldsymbol{Q}_{f,k}}\right)_0\langle\chi_{i,\nu}|\boldsymbol{Q}_{f,k}|\chi_{f,\nu}\rangle \\ + \frac{1}{2}\sum_{k=1}^{N}\sum_{l=1}^{N}\left(\frac{\partial^2\boldsymbol{\mu}_{if}}{\partial\boldsymbol{Q}_{f,k}\partial\boldsymbol{Q}_{f,l}}\right)_0\langle\chi_{i,\nu}|\boldsymbol{Q}_{f,k}\boldsymbol{Q}_{f,l}|\chi_{f,\nu}\rangle + \ldots\end{aligned} \tag{123}$$

A transformation is applied if second or higher order terms are calculated, which possess a dependency on the normal coordinates. This allows the calculation of overlap integrals like $\langle\chi_{i,\nu}|\chi_{f,\nu}\rangle$ in a recursive way, starting with the exact result of the $\langle\chi_{i,0}|\chi_{f,0}\rangle$ transition [140].

As in general, an infinite number of quantum numbers ν_i, ν_f exist, a preselection for transitions is applied to only calculate transitions with a high intensity explicitly. The selected transitions are categorised due to the number of simultaneously excited modes i into classes C_j of a specific electronic final state. The overlap integrals for the classes 1 and 2 are the initial points for the calculation of higher classes in a recursive scheme. The accuracy of a spectrum is determined by the number of overlap integrals $N^{\max}$.

1.2.3 Density-Functional Tight-Binding (DFTB)

A further approximative quantum chemical method is density-functional tight-binding (DFTB) [141], which can be derived from density functional theory as an approximation by means of a Taylor expansion series to the second or higher order [142] of the total DFT energy functional with respects to fluctuations in the charge density $\Delta\rho$ around a reference density ρ^0 [143]. The Taylor expansion series for the total ground state energy reads:

$$\begin{aligned}E[\rho^0+\Delta\rho] = \sum_i p_i\left\langle\varphi_i\left|-\frac{\nabla^2}{2} + V_{\text{nuc,e}} + \int'\frac{\rho^{0\prime}}{|\mathbf{r}-\mathbf{r}'|}\,\mathrm{d}\mathbf{r}' + V_{\text{xc}}[\rho^0]\right|\varphi_i\right\rangle \\ - \frac{1}{2}\int'\int\frac{\rho^0\rho^{0\prime}}{|\mathbf{r}-\mathbf{r}'|}\,\mathrm{d}\mathbf{r}\,\mathrm{d}\mathbf{r}' - \int V_{\text{xc}}[\rho^0]\rho^0\,\mathrm{d}\mathbf{r} + E_{\text{xc}}[\rho^0] + E_{\text{nuc,nuc}} \\ + \frac{1}{2}\int'\int\left(\frac{1}{|\mathbf{r}-\mathbf{r}'|} + \left.\frac{\delta^2E_{\text{xc}}[\rho]}{\delta\rho\delta\rho'}\right|_{\rho^0\rho^{0\prime}}\right)\Delta\rho\Delta\rho'\,\mathrm{d}\mathbf{r}\,\mathrm{d}\mathbf{r}' \\ + \frac{1}{6}\int''\int'\int\left.\frac{\delta^3E_{\text{xc}}[\rho]}{\delta\rho\delta\rho'\delta\rho''}\right|_{\rho^0\rho^{0\prime}\rho^{0\prime\prime}}\Delta\rho\Delta\rho'\Delta\rho''\,\mathrm{d}\mathbf{r}\,\mathrm{d}\mathbf{r}'\,\mathrm{d}\mathbf{r}'' + \cdots\end{aligned} \tag{124}$$

The zeroth-order formulation of DFTB is equivalent to a common non-selfconsistent tight-binding (TB) formalism [141], while at the second order one can obtain a transparent,

parameter-free, and readily calculable expression for generalised Hamiltonian matrix elements, which are altered by a self-consistent redistribution of Mulliken charges (SCC). The total energy in self-consistent-charge density-functional tight-binding method (SCC-DFTB) [142] reads

$$E^{\text{SCC-DFTB}} = E^{H^0} + E^{\gamma} + E^{\text{rep}} = \sum_{iab} \sum_{\mu \in a} \sum_{\nu \in b} p_i c_{\mu i} c_{\nu i} H^0_{\mu\nu} + \frac{1}{2} \sum_{ab} \Delta q_a \Delta q_b \gamma_{ab} + \frac{1}{2} \sum_{ab} V^{\text{rep}}_{ab} \tag{125}$$

and approximates the total energy to the second order in the density fluctuations. The first term E^{H^0} in (Eq. 125) comprises the matrix element $H^0_{\mu\nu} = \langle \varphi_\mu | H^0 | \varphi_\nu \rangle$ and is also regarded as the band-structure energy in tight-binding formalism. $p_i \in [0, 2]$ is the occupation number of the single-particle states φ, that are expressed in a linear combination of atomic orbital (LCAO) as a minimal basis set for the valence electrons $\varphi_\mu = \sum_i c_{\mu i} \phi_\mu$ with the expansion coefficients $c_{\mu i}$. This implies the application of the frozen-core approximation. The Hamilton matrix elements $H^0_{\mu\nu}$ and the overlap matrix elements $S_{\mu\nu}$ are parametrised and tabulated in advance of a DFTB calculation in Slater-Koster-files [144, 145] for every pair of atoms that occurs in the system. In other words, the distance dependence of $H^0_{\mu\nu}$ and $S_{\mu\nu}$ is computed beforehand, and a two-centre approximation for a neutral atomic reference density is applied.

The second expression E^{γ} is the charge fluctuation term and contains the net charge $\Delta q_a = q_a - q^0_a$ of the atoms a or b, respectively. Furthermore, the function γ describes the electron-electron interaction and is determined as an integral of two spherically symmetric Slater-type charge densities. The function γ_{ab} is fitted to represent a R^{-1}_{ab} dependence in the long-range limit to describe the Coulomb interaction of the charges Δq_a and Δq_b. The on-site term with $a = b$ contains the Hubbard constant U_a, which is twice the absolute chemical hardness η_a of an atom and can be approximated as the difference of the ionisation energy and the electron affinity.

$$U_a = 2\eta_a = \frac{\partial^2 E_a}{\partial^2 q_a} \approx E^{\text{IE}} - E^{\text{EA}} \tag{126}$$

Especially in SCC-DFTB, the Hubbard constant U_a is calculated as the first derivative of the HOMO energy with respect to the occupation number according to Janak's theorem [146]. On the other hand the terms γ_{ab} with $a \neq b$ also estimate the atomic size, as the Hubbard constant is proportional to the exponent $\tau_a = \frac{16}{5} U_a$ of the spherical Slater-type charge density and τ_a is inversely proportional to the covalent radius R^{cov}.

The third term E^{rep} in (Eq. 125) holds the repulsive energy contribution for each pair of atoms ab with a repulsive function V^{rep}_{ab}, which is obtained from fits to high-level theoretical calculations and possesses an interatomic distance dependence R_{ab}. The on-site energy contributions to this term for $a = b$ are usually neglected, as they only result in a constant energy shift in the total energy. The parametrisation of V^{rep}_{ab} is a tedious and laborious task in DFTB, since one aims to minimise the average in the force $|\mathbf{F}^{\text{DFT}} - \mathbf{F}^{\text{DFTB}}|$, energy differences $|E^{\text{DFT}} - E^{\text{DFTB}}|$ or similar quantities to fit repulsion derivatives for a given set of DFT structures [143].

In DFTB3 [142] the SCC-DFTB expression for the total energy is extended to third order for the exchange-correlation energy. Whereas in SCC-DFTB the Hubbard parameter is constant and independent from the atomic charge state, in DFTB3 the inclusion of the term E^{Γ}, which contains the derivative of the function γ with respect to the charge, results

in a charge dependence of U_a.

$$E^{\text{DFTB3}} = E^{\text{SCC-DFTB}} + \frac{1}{3}\sum_{ab} \Delta q_a^2 \Delta q_b \Gamma_{ab} \quad \text{with} \quad \Gamma_{ab} = \left.\frac{\partial \gamma_{ab}}{\partial q_a}\right|_{q_a^0} \tag{127}$$

One can obtain the approximate Kohn-Sham equations via application of the variational principle, and solve the equations iteratively to obtain the expansion coefficients $c_{\mu i}$.

$$\sum_b \sum_{\nu \in b} c_{\nu i}(H_{\mu\nu} - \varepsilon_i S_{\mu\nu}) = 0 \quad \forall a, \mu \in a, i \tag{128}$$

This expression implies the third order matrix elements:

$$H_{\mu\nu} = H^0_{\mu\nu} + S_{\mu\nu}\sum_c \Delta q_c \left(\frac{1}{2}(\gamma_{ac} + \gamma_{bc}) + \frac{1}{3}(\Delta q_a \Gamma_{ac} + \Delta q_b \Gamma_{bc}) + \frac{\Delta q_c}{6}(\Gamma_{ca} + \Gamma_{cb})\right) \quad \forall a, b, \mu \in a, \nu \in b \tag{129}$$

DFTB is a useful method for large systems, simulations on long time-scales, or for the application as a pre-screening method in structural search as the applied approximations lead to a reduction of computational costs while maintaining reasonable accuracy. Nevertheless, DFTB exhibits deficiencies for the description of systems with intermediate charge transfer and the inherent absence of dispersion corrections, that can be extenuated via incorporation of empirical corrections in analogy to DFT [120, 147].

Furthermore, there are extensions to a spin-polarised DFTB (S-DFTB) [148] or formalisms that give access to excited-state properties in a time-dependent (TD-DFTB) [149] or linear response framework [150]. The long-range corrected density functional based tight-binding method (LC-DFTB) [151] is reported to exhibit in general the same trends and similar accuracy as range-separated DFT methods at a significantly reduced computational cost.

1.2.4 Semi-empirical Methods

Semi-empirical quantum chemistry methods are Hartree-Fock based methods (Sec. 1.2.1) in computational chemistry and reduce computational costs by decreasing the number of evaluated two-electron integrals. The compensation for the approximations is included in the parametrisation of the semiempirical methods inside a theoretical framework, as a set of parameters is fitted to reproduce experimental results or to achieve an agreement with *ab initio* data [152]. One applied simplification is the *frozen-core* approximation, and the description of valence electrons using a minimal basis set (STO-3G) [153].

Several semiempirical methods exploit the zero differential overlap approximation (ZDO), which disregards all *products* of basis functions $\phi_{\mu_A}\phi_{\nu_B} = 0$, which are a function of the same electron coordinates but are localised on distinct atoms A, B. This approximation results in (i) the substitution of the overlap matrix $S_{\mu\nu} = \delta_{\mu\nu}\delta_{AB}$ with a unity matrix, (ii) the disregard of one-electron integrals with three centres (including centres in both basis functions and one in the operator) (iii) the neglect of all two-electron integrals involving three and four-centres. A Fock matrix element contains a one-electron part $h_{\mu\nu} = \langle\phi_\mu|\hat{h}_i|\phi_\nu\rangle$ with the one-electron operator $\hat{h}_i$ (Eq. 20) and the functions $\phi_\mu, \phi_\nu, \phi_\lambda, \phi_\sigma$ in the two-electron integrals.

$$F_{\mu\nu} = h_{\mu\nu} + \sum_{\lambda\sigma}^{N_{\text{basis}}} D_{\lambda\sigma}\left(\langle\phi_\mu\phi_\nu|\phi_\lambda\phi_\sigma\rangle - \langle\phi_\mu\phi_\lambda|\phi_\nu\phi_\sigma\rangle\right) \tag{130}$$

In this expression, Z'_a is the number of nuclear charges extenuated by the number of core electrons. In the neglect of diatomic differential overlap approximation (NDDO) two-electron integrals, which are localised on distinct atoms, are set to zero. Further approximations are the intermediate neglect of differential overlap approximation (INDO) or the complete neglect of differential overlap approximation (CNDO).

The methods modified neglect of diatomic overlap (MNDO) [154], the Austin Model 1 (AM1) [155] and the Parametric Method number 3 (PM3) [156] are different parametrisations of the NDDO approximation using only atomic variables. They differ in the parameter assignment and in the treatment of the core-core repulsion term, which is given as a reduced Coulomb repulsion between nuclear charges due to the presence of core-electrons.

The PM3 method uses 11 parameters for the hydrogen atom, and 18 parameters for every other element: $U_s, U_p, \beta_s, \beta_p, \zeta_s, \zeta_p, \alpha, G_{ss}, G_{sp}, G_{pp}, G_{p2}, H_{sp}, a_1, b_1, c_1, a_2, b_2, c_2$. The indices s and p refer to the s-type and p-type basis functions. The parameters U_s and U_p give the values for the one-centre one-electron integrals and represent the one-electron atomic orbital energies for the remaining ion if all valence electrons are removed. ζ_s and ζ_p represent the exponents in the STO functions. The atomic resonance parameters β_s and β_p are used to parametrise the two-centre one-electron integrals, calculating the overlap matrix element $S_{\mu\nu}$ explicitly.

$$\langle \phi_{\mu_A} | \mathbf{h} | \phi_{\nu_B} \rangle = \frac{1}{2} S_{\mu\nu} (\beta_\mu + \beta_\nu) \tag{131}$$

The NDDO approximation includes five types of one-centre two-electron integrals in a basis with s- and p-type functions.

$$H_{sp} = \langle ss|pp\rangle \ ; \ G_{ss} = \langle ss|ss\rangle \ ; \ G_{sp} = \langle sp|sp\rangle \ ; \ G_{pp} = \langle pp|pp\rangle \ ; \ G_{p2} = \langle pp'|pp'\rangle \tag{132}$$

The parameter H_{sp} represents an exchange integral, whereas the Coulomb terms are summarised in the G parameters, where $p, p' \in [p_x, p_y, p_z]$ take two separate wavefunctions into account. The parameters H and G come from atomic spectra.

The core-core repulsion energy in AM1 and PM3 includes an extension on the MNDO model and uses the fitting parameters α, a_k, b_k and c_k to molecular data.

$$\begin{aligned} V_{nn}(AB) &= Z'_A Z'_B \langle s_A s_A | s_B s_B \rangle (1 + e^{-\alpha_A R_{AB}} + e^{-\alpha_B R_{AB}}) \\ &= \frac{Z'_A Z'_B}{R_{AB}} \sum_k \left(a_{kA} e^{-b_{kA}(R_{AB} - c_{kA})^2} + a_{kB} e^{-b_{kB}(R_{AB} - c_{kB})^2} \right) \end{aligned} \tag{133}$$

With these approximations for the elements of the Fock matrix $F_{\mu\nu}$ at hand, one has to solve the secular equation

$$\sum_\nu (F_{\mu\nu} - \varepsilon_i \delta_{\mu\nu}) C_{\nu,i} = 0 \tag{134}$$

Another semiempirical quantum chemistry method is Zerner's Intermediate Neglect of Differential Overlap (ZINDO) [157] in conjugation with a revised method ZINDO/S [158]. It is optimised for accessing spectroscopic properties using configuration interaction (CI) calculations with a small active space for excited state construction in terms of single-electron excitations. It provides decent results for $\pi \rightarrow \pi^*$ excitations in small molecules or for molecular ionisation potentials.

1.2.5 Basis Sets

It is common to develop the molecular orbitals (MOs) $\phi_i(\mathbf{r})$ in a basis of localised atomic orbitals (AOs) $\psi(\mathbf{r})$ in electronic structure calculations:

$$\phi_i(\mathbf{r}) = \sum_j C_{ij}\psi_j(\mathbf{r}) \ . \tag{135}$$

This approach is called linear combination of atomic orbitals (LCAO) [79, 152]. The use of fixed MOs with explicit r dependence alone, allows the determination of the development coefficients C_{ij} by solving the matrix equation

$$\mathbf{H}\mathbf{C}_i = \varepsilon_i \mathbf{S}\mathbf{C}_i \tag{136}$$

with

$$\begin{aligned} H_{ij} &= \langle\psi_i| \left[-\frac{1}{2}\nabla^2 + v_{\text{eff}}(\mathbf{r})\right] |\psi_i\rangle \\ S_{ij} &= \langle\psi_i|\psi_j\rangle \ . \end{aligned}$$

This is easier to implement and less computationally demanding than solving the Kohn-Sham equations (Eq. 28) on a real space grid.

The wavefunctions ψ_i are represented by means of atom centred functions, which are located at the nuclei positions $\mathbf{R}_I$ and posses an exponential decay $e^{-\zeta\mathbf{r}}$ behaviour. The Slater Type Orbitals (STO),

$$\psi^{\text{STO}}_{Inlm} = N_n Y_{lm}(\phi,\theta)|\mathbf{r}-\mathbf{R}_I|^{n-1}e^{-\zeta_n|\mathbf{r}-\mathbf{R}_I|} \ , \tag{137}$$

contain a normalisation factor N_n, spherical harmonics $Y_{lm}(\phi,\theta)$, which depend on polar angle ϕ and azimuthal angle θ, and a Slater exponent ζ_n [159]. The STOs are approximated as a linear combination of Gaussian Type Orbitals (GTO),

$$\psi^{\text{GTO}}_{Inlm} = N_n Y_{lm}(\phi,\theta)|\mathbf{r}-\mathbf{R}_I|^{(2n-2-l)}e^{-\alpha|\mathbf{r}-\mathbf{R}_I|^2} \ , \tag{138}$$

for practical purposes, as their $e^{-\alpha\mathbf{r}^2}$ dependence facilitates numeric integration. The indices n, l and m are used to denote the shell ($n = 1, 2, 3, \dots$), the angular momentum $l = s, p, d$, etc. and the magnetic quantum number m. Further improvement is achieved with Contracted Gaussian Functions (CGF),

$$\psi^{\text{CGF}}_i(\mathbf{r}-\mathbf{R}_I) = \sum_{j=1}^{L} d_{ij}\psi^{\text{GTO}}_j(\alpha_{ij}, \mathbf{r}-\mathbf{R}_I) \ , \tag{139}$$

which form a linear combination of Gaussian functions ψ^{GTO}. The STO-nG basis set is a minimal basis set with a contraction length n for the number of primitive Gaussian functions, d_{ij} are the contraction coefficients and the α_{ij} are in the contraction exponent [153, 160].

Dunning and Huzinaga introduced full 'double zeta' functions, where ζ displays the number of contracted Gaussian function for each atomic orbital [161]. Double Zeta functions (DZ) utilise two basis functions with distinct factors ζ in the exponent for each atomic orbital. A higher number of ζ functions improves the flexibility in the radial direction (double DZ, triple TZ, quadruple QZ). The split-valence or Valence Double-Zeta functions (VDZ)

use double ζ functions only for the valence electrons. The incorporation of polarisation functions abets flexibility in the angular dependence (e.g. in DZP, PVDZ, *). In the 'cc-p' correlation-consistent polarised basis set cc-pVDZ the V stands for valence-only double-zeta basis sets. Diffuse functions are extended Gaussian basis functions with a small factor in the exponent, which ensures flexibility of the atomic orbitals far away from the nucleus. Furthermore, the addition of diffuse functions is common [162]. These are Gaussian basis functions with a small exponent that make the end of the atomic orbital that is located far from the nucleus more flexible. Diffuse basis functions are important for describing dipole moments, but they also play a crucial role in the accurate modelling of intra- and intermolecular bonds.

The Pople basis sets [153,160,163] are split-valence basis sets in the form $X-YZ$G. The X indicates the number of primitive Gaussian functions (G) for each atomic orbital. The labels YZ note that valence orbitals consist of two basis functions, which are made up of a linear combination of Y and Z primitive Gaussian functions, respectively. For instance, the 6-31G* basis set consists of six CGF-functions for orbitals, which are localised close to the nuclei. Moreover, it contains three CGF-functions, one non-contracted Gaussian function and one polarisation function for each valence orbital.

Plane Wave Basis Set Kohn-Sham orbitals can be developed in a plane wave basis set [83] and are applied especially for periodic systems in a DFT framework, as they satisfy the Bloch theorem [164].

If $\mathbf{T} = N_1\mathbf{a}_1 + N_2\mathbf{a}_2 + N_3\mathbf{a}_3$ is a linear combination of lattice vectors $\mathbf{a}_1, \mathbf{a}_2, \mathbf{a}_3$ and $\mathbf{G}$ is a linear combination of reciprocal lattice vectors $\mathbf{b}_1, \mathbf{b}_2, \mathbf{b}_3$, which fulfill the relation $\delta_{i,j} = \mathbf{a}_i \cdot \mathbf{b}_j$, then the volume of the unit cell is given by the determinant of the matrix $\Omega = \det|\mathbf{a}_1, \mathbf{a}_2, \mathbf{a}_3|$, which consists of the individual lattice vectors. The plane waves possess the following form

$$f_{\mathbf{G}}(\mathbf{r}) = \frac{1}{\sqrt{\Omega}} e^{i\mathbf{G}\mathbf{r}} \tag{140}$$

and can be used as basis functions, which satisfy the Bloch theorem for Bloch's wavefunctions

$$\phi_j(\mathbf{r}, \mathbf{k}) = u_j(\mathbf{r}, \mathbf{k}) e^{i\mathbf{k}\mathbf{r}} \tag{141}$$

in a periodic potential with lattice periodicity. Here, the plane wave vector $\mathbf{k}$ is localised in the first Brillouin zone [165].

$$u_j(\mathbf{r}, \mathbf{k}) = u_j(\mathbf{r} + \mathbf{T}, \mathbf{k}) = \frac{1}{\sqrt{\Omega}} \sum_{\mathbf{G}} c_j(\mathbf{G}, \mathbf{k}) e^{i\mathbf{G}\mathbf{r}} \tag{142}$$

The electron density reads with occupation numbers $p^{\mathrm{occ}}_{\mathbf{k},j}$

$$\rho(\mathbf{r}) = \frac{1}{\Omega} \sum_{\mathbf{k},j} \sum_{\mathbf{G},\mathbf{G}'} p^{\mathrm{occ}}_{\mathbf{k},j} c^*_j(\mathbf{G}', \mathbf{k}) c_j(\mathbf{G}, \mathbf{k}) e^{i(\mathbf{G}-\mathbf{G}')\mathbf{r}} \ . \tag{143}$$

The sum is carried until an energy limit E_{cut} is reached, which is a cutoff for the kinetic energy. E_{cut} is utilised to control convergence.

$$\frac{\hbar^2}{2m} |\mathbf{k} + \mathbf{G}|^2 \leq E_{\mathrm{cut}} \tag{144}$$

Also non-periodic, isolated molecular systems can be treated in this framework, if the simulation box is chosen large enough to avoid artifacts due to self-interaction errors.

Pseudopotentials for a Plane Wave Basis Set Many properties of chemical compounds are determined by the valence electrons rather than by inert core electrons. Hence, an explicit treatment of the inner electrons is not mandatory [152]. Pseudopotentials (PP) or effective core potentials are applied in quantum chemical calculations to approximate the effects of core (non-valence) electrons in an atom by an effective potential.

The valence electrons are orthogonal to all core electrons, that is why their wavefunction shows strong oscillations close to the core. Therefore, the explicit description of core electrons requires the application of a large basis set and is computationally demanding. In contrast, the PP combines the effects of all nuclear states into a nuclear Coulomb potential, which allows the valence electrons to be represented by knotless pseudo-wavefunctions. The PP is generated such that the all-electron valence wavefunction and the pseudo-wavefunction are the same for a radial distance r higher than the cutoff radius R_{cut}. Furthermore, the pseudopotential must meet the requirement of orbital energy conservation [83].

A further requirement holds for norm-conserving pseudopotentials

$$\int_0^{R_{\mathrm{cut}}} r^2 |\phi_i^{\mathrm{pseudo}}(r)|^2 \, \mathrm{d}r = \int_0^{R_{\mathrm{cut}}} r^2 |\phi_i^{\mathrm{total}}(r)|^2 \, \mathrm{d}r, \tag{145}$$

which states that the norm for the exact wavefunction ϕ_i^{total} – taking all electrons into account – and the pseudo-wavefunction ϕ_i^{pseudo} are identical within R_{cut}. In contrast, ultrasoft pseudopotentials do not meet this condition and allow more smoothness of the wavefunction close to the nucleus, which enables the use of a reduced basis. However, this requires the incorporation of augmentation charges to cope with the deficit in the resulting charge. These additional point charges are localised at the nuclear positions in Vanderbilt ultrasoft pseudopotentials [166, 167]. Nonetheless, there are many different schemes to obtain a pseudopotential from all-electron wavefunctions. Following one schema this can require a different pseudopotential for every angular momentum to obtain a total pseudopotential

$$V^{\mathrm{PP}}(\mathbf{r}) = \sum_l \sum_l^{m=-l} V_l^{\mathrm{PP}}(r) \mathbf{P}_{lm}(\phi, \theta). \tag{146}$$

Here, $\mathbf{P}_{lm}(\phi, \theta)$ denotes a projector on the angular momentum state $|l, m\rangle$. The Troulier-Martins schema uses the following form for the pseudo-wavefunctions inside the radius R_{cut} with a polynomial function $p(r)$ of 12th order and even exponents [168].

$$\phi_l^{\mathrm{pseudo}}(r) = r^{l+1} \exp\left[p(r)\right] \ . \tag{147}$$

The polynomial coefficients are determined with the constraint to ensure the continuity of the orbitals and the continuity of the derivatives at R_{cut}. If the pseudo-wavefunction ϕ_l^{pseudo} is determined completely by a selected construction scheme, then one employs the inversion of the radial Schrödinger equation

$$V_l^{\mathrm{PP}}(r) = \frac{1}{\phi_l^{\mathrm{pseudo}}(r)} \frac{\partial^2}{\partial r^2} \phi_l^{\mathrm{pseudo}}(r) + \frac{l(l+1)}{r^2} + \epsilon_l - v_H[\rho] - v_{\mathrm{xc}}[\rho] \tag{148}$$

to obtain the desired pseudopotential (see [83]).

1.3 Molecular Dynamics

1.3.1 Ab Initio Molecular Dynamics

The temporal evolution of a many-body system can be computed by solving the time-dependent Schrödinger equation in an approximate fashion using *ab initio* molecular dynamics simulations [79]. In the so-called *on the fly* simulations the energies and all forces acting on the atomic nuclei are not defined by predetermined, given potentials, but by means of solving the stationary Schrödinger equation for a given molecular configuration at every timestep along the trajectory. Born-Oppenheimer molecular dynamics (BOMD) and Car-Parrinello molecular dynamics are the most frequently used *ab initio* methods to simulate the dynamics of molecules, clusters, crystal structures or biomolecules [83]. The CDFT method can also be employed for a charge transfer reaction in molecular dynamics simulation (MD-CDFT) [169].

1.3.1.1 Born-Oppenheimer Molecular Dynamics

Born-Oppenheimer molecular dynamics is based on the Born-Oppenheimer approximation (Sec. 1.1). The nuclei are propagated in time by integrating Newton's equations of motion (Eq. 16) and solving the static electron problem i.e. the stationary Schrödinger equation at every instance of time [83]

$$H_{\mathrm{el}}^{\mathrm{KS}}\Psi_0 = E_0^{\mathrm{KS}}\Psi_0 \ . \tag{149}$$

The electronic ground-state energy E_0^{KS} for a multi-electron wavefunction Ψ_0 is determined using Kohn-Sham DFT. The nuclei are propagated in the ground state potential of all electrons similar to classical molecular dynamics according to

$$M_I\ddot{\mathbf{R}}_I = -\nabla_I\langle\Psi_0|\hat{H}^{\mathrm{KS}}|\Psi_0\rangle = -\nabla_I \mathrm{min}_{\{\widetilde{\phi}_i\}}E^{\mathrm{KS}}[\varrho(\{\widetilde{\phi}_i\})] \ . \tag{150}$$

Here, $\hat{H}^{\mathrm{KS}}$ is the Kohn-Sham Hamilton operator for all electrons and Ψ_0 is the associated ground-state wavefunction. The Kohn-Sham energy E^{KS} has to be minimised for every nuclear configuration. The minimisation is computationally demanding, as the Kohn-Sham energy E^{KS} depends on the electron density ϱ, which has to be determined for a set of one-electron Kohn-Sham orbitals $\{\widetilde{\phi}_i\}$. The orbitals $\widetilde{\phi}_i$ have to be converged iteratively till a self-consisted solution is found. The timestep Δt in Born-Oppenheimer molecular dynamics is restricted due to the highest vibrational frequency of the nuclei $\omega_{\mathrm{max}}^{\mathrm{nuc}}$ in the system

$$\Delta t = \frac{2\pi}{\omega_{\mathrm{max}}^{\mathrm{nuc}}}. \tag{151}$$

Since the numerical integration of the nuclear dynamics does not directly depend on the electron dynamics here, the new nuclear coordinates can be determined by means of the Verlet algorithm [170] using this time step Δt (see Sec. 1.3.3).

1.3.1.2 Car-Parrinello Molecular Dynamics

Car-Parrinello molecular dynamics (CPMD) was developed in 1985 by Michele Parrinello and Roberto Car [171]. In CPMD one circumvents the computationally intensive optimisation of the wavefunction at every timestep by calculating the time-dependent changes in the

electron structure utilising a combination of DFT and classical Newton mechanics for the nuclear motion [79,83]. The quantum mechanical problem to describe the adiabatic motion of rapid electrons and slow nuclei, which occur on different time scales, is transcribed to a purely classical problem of two different components on distinct energy scales.

An electronic degree of freedom is introduced as a fictitious dynamic variable to take the dynamics of electron structure into account. In this approximation one exploits the fact that the electronic energy $\langle\widetilde{\Psi}_0|\hat{\widetilde{H}}^{\mathrm{KS}}|\widetilde{\Psi}_0\rangle$ is a function of the nuclear positions $\mathbf{R}_I$ and it is likewise a functional of the wavefunction $\widetilde{\Psi}_0$. The Car-Parrinello Lagrangian function reads

$$\mathcal{L}_{\mathrm{CP}} = \sum_{I=1}^{\text{nuclei}} \frac{1}{2} M_I \dot{\mathbf{R}}_I^2 + \sum_{i=1}^{\text{orbitals}} \frac{1}{2}\mu\langle\dot{\phi}_i|\dot{\phi}_i\rangle - \langle\widetilde{\Psi}_0|\hat{\widetilde{H}}^{\mathrm{KS}}|\widetilde{\Psi}_0\rangle + \sum_{ij}\Lambda_{ij}(\langle\phi_i|\phi_j\rangle - \delta_{ij}) \ , \quad (152)$$

where the first term is the kinetic energy of the nuclei. The second term in equation (152) gives the kinetic energy of the fictitious electronic degrees of freedom. Here, the μ_i are the fictitious masses of the electronic degrees of freedom and ϕ_i are the one-electron Kohn-Sham orbitals. The ground state wavefunction Ψ_0 is composed of a set of one-electron orbitals $\{\phi_i\}$. For instance, this can be a Slater determinant $\Psi_0 = \det\{\phi_i\}$. The Lagrange multiplier matrix Λ_{ij} ensures the conservation of orthonormal orbitals. Starting with the Lagrange function the Euler-Lagrange equations yield the equations of motion

$$\frac{\mathrm{d}}{\mathrm{d}t}\frac{\partial\mathcal{L}}{\partial\dot{\mathbf{R}}_I} = \frac{\partial\mathcal{L}}{\partial\mathbf{R}_I} \quad \text{and} \quad \frac{\mathrm{d}}{\mathrm{d}t}\frac{\partial\mathcal{L}}{\partial\langle\dot{\phi}_i|} = \frac{\partial\mathcal{L}}{\partial\langle\phi_i|} \ . \quad (153)$$

On the one hand we obtain the nuclear equations of motion,

$$M_I\ddot{\mathbf{R}}_I = -\nabla_I\langle\widetilde{\Psi}_0|\hat{\widetilde{H}}^{\mathrm{KS}}|\widetilde{\Psi}_0\rangle \ , \quad (154)$$

and on the other hand the equations of motion for the orbitals as a set of coupled differential equations

$$\mu\ddot{\phi}_i = -\frac{\partial}{\partial\langle\phi_i|}\langle\widetilde{\Psi}_0|\hat{\widetilde{H}}^{\mathrm{KS}}|\widetilde{\Psi}_0\rangle + \sum_j \Lambda_{ij}\,|\phi_j\rangle \ . \quad (155)$$

Hence, nuclei and orbitals need to be propagated simultaneously in time t. A CPMD calculation commences by minimising the multi-electron configuration in analogy to BOMD. The dynamics of the fictitious mass μ maintains the electrons at the electronic ground state throughout the entire simulation. Different temperatures are assigned to both nuclei and the fictitious electronic degrees of freedom. The temperature of the electrons can fluctuate around a value but is supposed to remain at a preferred low level. Therefore, the system remains close to the ground state energy to guarantee a motion in proximity to the minimal Born-Oppenheimer potential energy surface.

The fictitious mass $\mu = (300 - 800)$ a.u. is selected in a way, which makes sure that an adiabatic separation of electron and nuclear motion is guaranteed. This ensures that the frequency spectrum of the nuclei does not overlap the spectrum for the fictitious, electronic degrees of freedom $\omega_{\mathrm{min}}^{\mathrm{el}} > \omega_{\mathrm{max}}^{\mathrm{nuc}}$ [172]. The maximum timestep Δt is determined by the highest vibrational frequency mode in the system $\omega_{\mathrm{max}}^{\mathrm{el}}$ so that the energy cutoff for the plane-wave basis E_{cut} is marked (see Sec. 1.2.5).

$$\Delta t = \frac{2\pi}{\omega_{\mathrm{max}}^{\mathrm{el}}} = 2\pi\sqrt{\frac{\mu}{2E_{\mathrm{cut}}}} \quad (156)$$

The energy difference $\Delta E = \varepsilon_{\mathrm{HOMO}} - \varepsilon_{\mathrm{LUMO}}$ between highest occupied molecular orbital (HOMO) and lowest unoccupied molecular orbital (LUMO) and the choice of μ give a limit to the lowest electronic frequency

$$\omega_{\mathrm{min}}^{\mathrm{el}} = \sqrt{\frac{2(\varepsilon_{\mathrm{HOMO}} - \varepsilon_{\mathrm{LUMO}})}{\mu}}. \tag{157}$$

Thus, a large fictitious mass μ is desirable to maximise the time step Δt. In turn, the value of Δt must not be chosen too large in order to prevent a transfer of energy between nuclear and orbital degrees of freedom.

1.3.2 Classical Molecular Dynamics

The goal of classical molecular dynamics simulation is to determine the time evolution of a given set of interacting particles. Therefore one has to solve the Newtonian equations of motion at an initial configuration [173]. In a molecular dynamics simulation, the atoms are treated as classical, point-shaped particles, with a constant charge that interact via *a priori* defined particle-particle potentials. Their chosen functional form with associated parameter sets for calculating the potential energy of a system of atoms or coarse-grained particles is called a force field (FF). Since these classical methods scale with particle number squared, $\mathcal{O}(N^2)$, they allow simulations of systems with up to millions of atoms, enabling time scales of microseconds and reaching the micrometre-scale lengths [79].

With an initial set of particle positions $\mathbf{R}$, their initial velocities $\mathbf{V}^{(0)}$, and the interaction potentials $V(\mathbf{R})$ at hand, the forces on every particle i are given as the negative derivative of the interaction potential with respect to the coordinates

$$\mathbf{F}_i = -\frac{\partial V}{\partial \mathbf{R}} \ . \tag{158}$$

As the interaction potential $V(\mathbf{R})$ is a function of the positions, the total force $\mathbf{F}_i$ on a particle i can be expressed as the sum of all bonded and non-bonded interactions between particle pairs $\mathbf{F}_i = \sum_j \mathbf{F}_{ij}$. The latter have electrostatic or Van der Waals character for atoms that are more than four bond lengths apart. These interactions are approximated by parametrised potentials, which depend on particle-specific constants. However, these constants cannot be derived classically but can be determined from *ab-initio* electronic structure methods or empirical methods [85].

Bonded Interactions In the following, we describe the bonded interactions used in a classical force field. The stretching of an atomic bond is described as a two-particle interaction, the alternations of a bond angle are treated as a three-particle interaction and changes in a dihedral angle as a four-particle interaction. The characteristic bond types are visualised in Fig. 1.1.

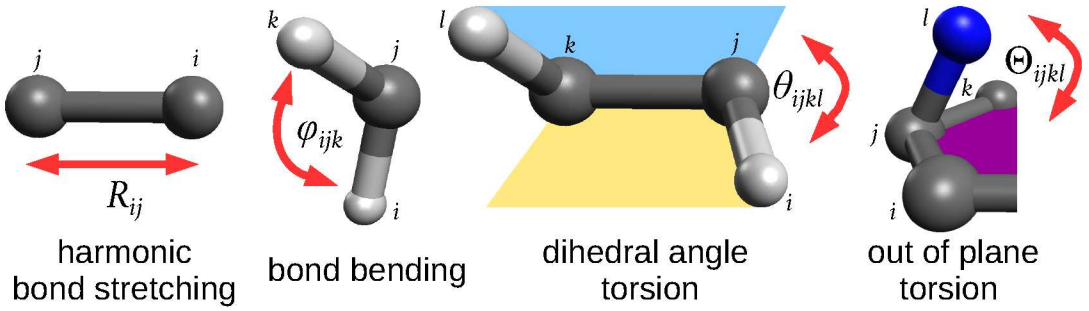

Figure 1.1: Bonded interactions in molecular mechanic force fields, harmonic bond stretching along the interatomic distance R_{ij}, bond bending with bond angle φ_{ijk}, dihedral angle torsion θ_{ijkl} between the planes (ijk) and (jkl) and out of plane torsion along the improper dihedral angle Θ_{ijkl}.

The simplest way to describe a covalent bond is the use of a **harmonic bond stretching** potential

$$V(R_{ij}) = \frac{1}{2}k_{ij}(R_{ij} - R_{ij}^0)^2, \tag{159}$$

which models the oscillation of the instantaneous bond distance $R_{ij} = |\mathbf{R}_i - \mathbf{R}_j|$ between two atoms i and j around the equilibrium bond R_{ij}^0 as a spring. The spring constant k_{ij} and R_{ij}^0 can be determined for ab-initio simulations.

In the same way, a **bond bending** can be assigned by a harmonic potential with respect of the bond angle φ_{ijk} between three atoms i, j and k. The spring constant k_{ijk} describes the stiffness of the potential to model the motion around an associated equilibrium bond angle φ_{ijk}^0,

$$V(\varphi_{ijk}) = \frac{1}{2}k_{ijk}(\varphi_{ijk} - \varphi_{ijk}^0)^2 \ . \tag{160}$$

Also, potentials for **proper dihedral** angles describe the torsion rotation around a n-fold symmetric bound with a torsion barrier hight V_n. The angle θ_{ijkl} is a dihedral angle, which enters the cosine-shaped potential,

$$V(\theta_{ijkl}) = \frac{V_n}{2}\left(1 + \cos(n\theta_{ijkl} - \theta_{ijkl}^0)\right) \ , \tag{161}$$

Furthermore, one can introduce potentials for **improper dihedral** angles Θ_{ijkl}, which essentially serve to ensure the planarity of aromatic ring systems,

$$V(\Theta_{ijkl}) = \frac{1}{2}k_{ijkl}\left(\Theta_{ijkl} - \Theta_{ijkl}^0\right)^2 \ . \tag{162}$$

Here, Θ_{ijkl} is the dihedral angle between the planes with indices (ijk) and (jkl). The angles Θ_{ijkl}^0, θ_{ijkl}^0 and φ_{ijk}^0 determine the respective equilibrium orientation.

Non-bonded Interactions The **Lennard-Jones potential** [174,175] approximates the force between two uncharged atoms, that do not possess a direct chemical bond. Van der Waals forces and dipole-dipole interactions dominate the interplay of atoms at long distances. They are summed up in the attractive R^{-6}-term in the Lennard-Jones potential. The repulsive R^{-12}-term reflects the Pauli repulsion, which emerges if two atoms approach

each other, then the electron orbital overlap increases and as a consequence, some electrons have to shift to orbitals with higher energy. This (12,6)-combination of the Lennard-Jones potential is chosen for numerical simplicity

$$V^{\mathrm{LJ}}(R_{ij}) = 4\varepsilon \left[\frac{\sigma_{ij}^{(12)}}{R_{ij}^{12}} - \frac{\sigma_{ij}^{(6)}}{R_{ij}^{6}} \right] . \tag{163}$$

Here, R_{ij} describes the distance between two atoms i and j. σ_{ij} is a substance-specific parameter and refers to the particle distance at which the Lennard-Jones potential is zero. ε is the depth of the potential at a distance $R_{ij}^{(0)} = 2^{1/6}\sigma_{ij}$.

Another non-bonded interaction is mediated by the **Coulomb potential** between the atoms with partial charges q_i. Presuming the use of periodic boundary conditions for the force field simulations, the Coulomb potential for a simulation box with edge length L has the form

$$U^{\mathrm{Coul}}(\mathbf{R}) = \frac{1}{2} \sum_{\mathbf{n}} \sum_{ij} \frac{q_i q_j}{|\mathbf{R}_i - \mathbf{R}_j + \mathbf{n}L|} . \tag{164}$$

The calculation is computationally demanding due to the long-range nature of the interaction, as all atoms within the simulation box as well as those of all periodic images ($\mathbf{n} \in \mathbb{N}^3$) must be considered. Note that the cases for $i = j$ and $\mathbf{n} = 0$ are excluded in the summations. The Ewald summation technique [176] helps to significantly reduce the computational effort by splitting the summation and calculating the short-range part of the interaction in real space, while calculating the long-range part in reciprocal space using fast Fourier transform (FFT) [177].

1.3.3 Verlet Algorithm

A standard numerical integrator for the Newtonian equations of motion is the Verlet algorithm [170]. It is applied to compute the particle trajectories in molecular dynamics simulations. The Verlet algorithm can be derived by a Taylor expansion series of the position $\mathbf{R}_i$ of particle i at time $t + \Delta t$,

$$\mathbf{R}_i(t + \Delta t) = \mathbf{R}_i(t) + \dot{\mathbf{R}}_i(t)\Delta t + \frac{1}{2}\ddot{\mathbf{R}}_i(t)\Delta t^2 + \frac{1}{6}\dddot{\mathbf{R}}_i(t)\Delta t^3 + \mathcal{O}(\Delta t^4) . \tag{165}$$

The analogous expression holds for the Taylor expansion of the position at time $t - \Delta t$.

$$\mathbf{R}_i(t - \Delta t) = \mathbf{R}_i(t) - \dot{\mathbf{R}}_i(t)\Delta t + \frac{1}{2}\ddot{\mathbf{R}}_i(t)\Delta t^2 - \frac{1}{6}\dddot{\mathbf{R}}_i(t)\Delta t^3 + \mathcal{O}(\Delta t^4) \tag{166}$$

The addition of the expression Eq. 165 to Eq. 166 and the insertion of Newton's equation of motion for the acceleration $\ddot{\mathbf{R}}_i$ yields the position Verlet algorithm.

$$\mathbf{R}_i(t - \Delta t) = 2\mathbf{R}_i(t) - \mathbf{R}_i(t - \Delta t) + \frac{\mathbf{F}_i(t)}{M_i}\Delta t^2 + \mathcal{O}(\Delta t^4) \tag{167}$$

Here, $\mathbf{F}_i$ is the force on particle i with mass M_i. Note the small error of the order $\mathcal{O}(\Delta t^4)$. The time step Δt is selected to be small, so the acceleration is considered as constant within the time interval. Furthermore, one can obtain the velocity by subtracting the expression Eq. 165 from Eq. 166,

$$\mathbf{V}_i(t) = \frac{\mathbf{R}_i(t + \Delta t) - \mathbf{R}_i(t - \Delta t)}{2\Delta t} + \mathcal{O}(\Delta t^3) . \tag{168}$$

A deficiency in this method is the delayed evaluation of the velocity about an entire time step Δt after the determination of the particle position. This aspect can be overcome by employing the velocity Verlet or leapfrog Verlet algorithm. In the leapfrog algorithm, the particle positions and the velocities are propagated with Δt, but they feature a relative offset of $\Delta t/2$. So, one evaluates the particle velocity $\mathbf{V}_i$ at time $t + \frac{1}{2}\Delta t$ for half a step,

$$\mathbf{V}_i(t + \frac{1}{2}\Delta t) = \mathbf{V}_i(t - \frac{1}{2}\Delta t) + \frac{\mathbf{F}_i(t)}{M_i}\Delta t \ , \tag{169}$$

and afterwards one promotes the particle position for an entire step to $t + \Delta t$

$$\mathbf{R}_i(t + \Delta t) = \mathbf{R}_i(t) + \mathbf{V}_i(t - \frac{1}{2}\Delta t)\Delta t \ . \tag{170}$$

The leapfrog algorithm is invariant for time inversion symmetry and conserves the total momentum of the system, which is mandatory in classical physics [178].

1.3.4 Temperature and Pressure Control

There are several techniques to control temperature [179] in molecular dynamic simulations as velocity rescaling [180], the Andersen thermostat [181], the Nosé-Hoover thermostat [182, 183], Nosé-Hoover chains, the Berendsen thermostat [184] and Langevin dynamics [79].

Velocity Rescale Thermostat The solution of the Newtonian equations of motion yields the behaviour of the microcanonical ensemble (NVE). The application of temperature control is mandatory to reproduce the usual experimental condition of a canonical ensemble (NVT), which conserves the particle number N, the volume V and the temperature T. For a set of N atoms with initial velocities $\mathbf{V}^{(0)}$, one can rescale the velocities $\mathbf{V}$ of the nuclei at an instance of time t by a scaling factor λ to maintain the system at a selected target temperature T_0 [180].

$$T(t) = \frac{1}{3Nk_\mathrm{B}} \sum_I M_I \mathbf{V}_I^2 \tag{171}$$

If the instantaneous temperature $T(t)$ in the system differs from the target temperature T_0 to a certain extend, then the velocities $\mathbf{V}^{(0)} = \lambda \mathbf{V}$ are adapted by the scaling factor $\lambda = \sqrt{\frac{T_0}{T(t)}}$ to reproduce

$$T_0 = \frac{1}{3Nk_\mathrm{B}} \sum_I M_I \mathbf{V}_I^{(0)^2} = \frac{1}{3Nk_\mathrm{B}} \sum_I M_I (\lambda \mathbf{V}_I)^2 = \lambda T(t) \tag{172}$$

Even though the temperature and the average kinetic energy are kept constant, the instantaneous kinetic energy is prone to fluctuations.

Nosé Hoover Thermostate Instead of rescaling the velocities, one can apply the Nosé-Hoover approach [182, 183] and include a friction term in Newton's equations of motion to reproduce a canonical ensemble in a constant-temperature molecular dynamics simulations [79].

$$\ddot{\mathbf{R}}_I = \frac{\mathbf{F}}{M_I} - \zeta \dot{\mathbf{R}}_I \tag{173}$$

Fluctuating changes in the friction coefficient ζ are determined by the equation

$$\dot{\zeta} = \frac{1}{Q}\left[\sum_{I}^{N} M_I \dot{\mathbf{R}}_I^2 - 3Nk_\mathrm{B}T\right] . \tag{174}$$

If the instantaneous kinetic energy term (first term on the right-hand side) falls below the term for the canonical average (second term), then the friction coefficient decreases and can turn to a negative sign, which leads to heating and an acceleration of the nuclear motion. In contrast, if the first term for the kinetic energy exceeds the canonical average, then the friction coefficient ζ rises, and once its sign turns to a positive value, the system is cooled down by a deceleration of the nuclei. The speed of the temperature adaption is adjusted by the magnitude of the fictitious mass parameter Q. The inclusion of the Nosé-Hoover friction term entails that the Hamiltonian H is no longer a conserved quantity. Nevertheless, one can adapt the schema to obtain a time-conserved quantity as an extended quasi-Hamiltonian

$$\overline{H} = H + \frac{Q}{2}\zeta^2 + 3Nk_\mathrm{B}T\int \zeta \,\mathrm{d}t. \tag{175}$$

In order to obtain a canonical ensemble, one has to ensure that the time average of an observable over the trajectory yields the same result as the ensemble average (ergodicity) [185]. Therefore, one can extend the approach and apply a chain of l thermostats and couple a given thermostat ζ_k to an additional thermostat ζ_{k+1}. This Nosé-Hoover chains lead to a more chaotic nuclear motion and one has to solve a set of coupled equations.

$$\ddot{\mathbf{R}}_I = \frac{\mathbf{F}}{M_I} - \zeta_1 \dot{\mathbf{R}}_I \tag{176}$$

$$\dot{\zeta}_1 = \frac{1}{Q_1}\left[\sum_{I}^{N} M_I \dot{\mathbf{R}}_I^2 - 3Nk_\mathrm{B}T\right] - \zeta_1\zeta_2 \tag{177}$$

$$\dot{\zeta}_k = \frac{1}{Q_k}\left[Q_{k-1}\zeta_{k-1} - k_\mathrm{B}T\right] - \zeta_k\zeta_{k+1} \tag{178}$$

$$\dot{\zeta}_l = \frac{1}{Q_l}\left[Q_{l-1}\zeta_{l-1} - k_\mathrm{B}T\right] \tag{179}$$

The resulting conserved quasi Hamiltonian reads

$$\overline{H} = H + \sum_{k=1}^{l}\frac{Q_k}{2}\zeta_k^2 + 3Nk_\mathrm{B}T\int \zeta_1 \,\mathrm{d}t + \sum_{k=2}^{l} k_\mathrm{B}T\int \zeta_k \,\mathrm{d}t \tag{180}$$

The coupling of the system to a thermal reservoir with a Nosé-Hoover thermostat results in an oscillatory relaxation, whereas a Berendsen weak coupling scheme yields a damped exponential relaxation [184].

Pressure Control The simulation in the isothermal-isobaric ensemble (NPT) requires the conservation of the temperature T and the pressure P, which can be achieved by alternating the volume V of the simulation box. Hence, the coordinates and the simulation box size are scaled to a reference pressure value $\mathbf{P}^0$ in Berendsen pressure coupling. The Berendsen barostat [184] couples the pressure $\mathbf{P}$ weakly to an external, hypothetical heat bath via a time constant τ_P to maintain a reference pressure $\mathbf{P}^0$.

$$\frac{\mathrm{d}\mathbf{P}}{\mathrm{d}t} = \frac{\mathbf{P}^0 - \mathbf{P}}{\tau_P} \tag{181}$$

Here, $\mathbf{P}$ is a matrix, which contains the pressure for a given direction in space, and the matrix $\mathbf{P}^0$ is made up of the values for the reference pressure P_{ij}^0. The pressure $\mathbf{P}$ is adjusted by means of the scaling matrix $\boldsymbol{\mu}$ with the elements

$$\mu_{ij} = \delta_{ij} - \frac{\Delta t}{3\tau_P}\beta_{ij}\left[P_{ij}^0 - P_{ij}(t)\right], \tag{182}$$

which depend on the isothermal compressibility $\boldsymbol{\beta}$ of the system.

The ratio of the simulation box vectors are conserved in isotropic pressure coupling, so a diagonal matrix with elements of size trace($\mathbf{P}$)/3 is applied. Whereas in anisotropic pressure coupling, the scaling factors are evaluated independently for each of the three orthogonal box axes.

1.4 Charge Transfer in Molecular Systems

In the subsequent section, we give a derivation for the central physical quantity of this thesis, the Marcus rate (Eq. 197) to describe charge transfer between a pair of neighbouring molecules (Sec. 1.4.1). Some alternative rate types are presented (Sec. 1.4.2), as well as methods for calculating the charge transfer integral (Sec. 1.4.3) and the outer-sphere contributions (Sec. 1.4.4).

1.4.1 Marcus Theory

The charge transfer of an excess charge carrier from a donor molecule A to an acceptor molecule B in a charge-transfer complex can be characterised by a charge transfer rate k_{AB} [186, 187]. We consider charge transfer processes,

$$A^{\pm} + B^0 \underset{k_{\mathrm{BA}}}{\overset{k_{\mathrm{AB}}}{\rightleftharpoons}} A^0 + B^{\pm}, \tag{183}$$

in which either the transfer of a negative excess charge occurs (electron transfer) or a positive vacancy is transferred (hole transfer). In the spirit of Fermi's Golden Rule, we can write a rate expression for the charge transfer process (see eq. 118) with a perturbation operator $\hat{H}'$ and the wavefunction Ψ_i for the initial state localised at the molecule A and the wavefunction Ψ_f for the final state at the second molecule B. The rate expression

$$k_{if}^{\nu} = \frac{2\pi}{\hbar}\sum_{\mu}|\langle\Psi_{i\nu}|\hat{H}'|\Psi_{f\mu}\rangle|^2\delta(E_{f\mu} - E_{i\nu}) \tag{184}$$

$$= \frac{2\pi}{\hbar}|H'_{if}|^2\sum_{\mu}|\langle\chi_{i\nu}|\chi_{f\mu}\rangle|^2\delta(E_{f\mu} - E_{i\nu}) \tag{185}$$

can be approximated using the Born-Oppenheimer approximation with a product ansatz for the total wavefunction $\Psi_{i\nu} = \Phi_{i\nu}\chi_{i\nu}$ and $\Psi_{f\mu} = \Phi_{f\mu}\chi_{f\mu}$, respectively. Different vibrational states are denoted by ν in the initial state and μ in the final state, respectively. The Condon approximation $\langle\Psi_i|\hat{H}'|\Psi_f\rangle = \langle\chi_{i\nu}|\chi_{f\mu}\rangle\langle\Phi_i|\hat{H}'|\Phi_f\rangle$ is applied to obtain electronic transition matrix element $|H'_{if}| = |\langle\Phi_i|\hat{H}'|\Phi_f\rangle|$, which is only parametrically dependent on the nuclear coordinates. Moreover, we introduce a Boltzmann factor for weighting in combination with the partition function Z for all vibrational states and write the rate as

$$k_{if} = \frac{2\pi}{\hbar}|H'_{if}|^2\sum_{\nu}\sum_{\mu}|\langle\chi_{i\nu}|\chi_{f\mu}\rangle|^2\delta(E_{f\mu} - E_{i\nu})\frac{\exp(\frac{-E_{i\nu}}{k_{\mathrm{B}}T})}{Z}. \tag{186}$$

In this way, we average over all vibrational states ν. Furthermore, the potential energy surfaces are approximated as a product of harmonic oscillators $\Theta\ (\boldsymbol{Q}_j)$ with the nuclear coordinates $\boldsymbol{Q}_j$:

$$\chi_{i\nu} = \prod_j \Theta_{i\nu_j}(\boldsymbol{Q}_j)\ . \tag{187}$$

If we rewrite the energy difference

$$\hbar\omega_{f\mu,i\nu} = E_{f\mu} - E_{i\nu} = E_f - E_i + (\mu + \frac{1}{2})\omega_{f\mu} - (\nu + \frac{1}{2})\omega_{i\nu} \tag{188}$$

and use the definition of the Dirac delta function

$$\delta(\omega_{f\mu,i\nu}) = \frac{1}{2\pi}\int_{-\infty}^{\infty} \exp(i\omega_{f\mu,i\nu}t)\ \mathrm{d}t \tag{189}$$

we get a rate expression k_{if} with the nuclear correlation function $G_j(t)$

$$k_{if} = \frac{|H'_{if}|^2}{\hbar^2}\int_{-\infty}^{\infty} \exp(i\omega_{f,i}t)\prod_j G_j(t)\ \mathrm{d}t \tag{190}$$

The nuclear correlation function $G_j(t)$ has the following form:

$$G_j(t) = \sum_\nu \sum_\mu |\langle\chi_{i\nu}|\chi_{f\mu}\rangle|^2 \frac{\exp(\frac{-E_{i\nu}}{k_\mathrm{B}T})}{Z} \exp\left[i(\mu + \frac{1}{2})\omega_{f\mu}t - i(\nu + \frac{1}{2})\omega_{i\nu}t\right] \tag{191}$$

Here, we have simplified the index notation by merging the indices $\nu \equiv \nu_j$ and $\mu \equiv \mu_j$ due to Eq. 187. Assuming shifted oscillators with identical frequencies ($\omega_j = \omega_{f\mu} = \omega_{i\nu}$), we can rewrite the expression as

$$G_j(t) = \exp\Big[- S_j\big((2\overline{n}_j + 1) - \overline{n}_j\exp(-i\omega_j t) - (\overline{n}_j + 1)\exp(i\omega_j t)\big)\Big]\ . \tag{192}$$

Here we involve the factors $S_j = \frac{\omega_j}{2\hbar}\Delta\boldsymbol{Q}_j^2$, the Planck distribution for the vibrational modes (phonons) $\overline{n}_j = \exp(\frac{\hbar\omega_j}{k_\mathrm{B}T} - 1)^{-1}$, and the oscillator displacement $\Delta\boldsymbol{Q}_j = \boldsymbol{Q}_{j\nu} - \boldsymbol{Q}_{j\mu}$. If we insert Eq. (192) into Eq. (190) and rewrite the sum of exponential functions as a product in the exponent, we get the expression:

$$k_{if} = \frac{|H'_{if}|^2}{\hbar^2}\int_{-\infty}^{\infty} \exp\left[i\omega_{f,i}t - \sum_j S_j\Big((2\overline{n}_j + 1) - \overline{n}_j\exp(-i\omega_j t) - (\overline{n}_j + 1)\exp(i\omega_j t)\Big)\right]\ \mathrm{d}t\ . \tag{193}$$

In the next step, we approximate the exponential term for short times $t \ll \omega_j^{-1}$ by means of the Taylor series $\exp(-i\omega_j t) \approx 1 + i\omega_j t + \frac{(i\omega_j t)^2}{2}$ using the three leading terms. After completing the square in the integrand, the expression can be simplified to

$$k_{if} = \frac{|H'_{if}|^2}{\hbar^2}\int_{-\infty}^{\infty} \exp\left[it(\omega_{f,i} - \sum_j S_j\omega_j) - \frac{t^2}{2}\sum_j S_j\omega_j(2\overline{n}_j + 1)\right]\ \mathrm{d}t\ . \tag{194}$$

If we carry out the integration over time t, we obtain the Marcus-Levich equation:

$$k_{if} = \frac{|H'_{if}|^2}{\hbar^2}\sqrt{\frac{2\pi}{\sum_j S_j\omega_j^2(2\overline{n}_j+1)}}\exp\left[-\frac{(\omega_{f,i}+\sum_j S_j\omega_j)^2}{2\sum_j S_j\omega_j^2(2\overline{n}_j+1)}\right] . \tag{195}$$

In the next step, we obtain the classical limiting case if the conditions $\frac{\hbar\omega_j}{k_\mathrm{B}T} \ll 1$ and $\overline{n}_j \approx \frac{k_\mathrm{B}T}{\hbar\omega_j} \gg 1$ are satisfied, yielding a reduced expression

$$k_{if} = \frac{|H'_{if}|^2}{\hbar^2}\sqrt{\frac{\pi\hbar}{k_\mathrm{B}T\sum_j S_j\omega_j}}\exp\left[-\frac{(\omega_{f,i}+\sum_j S_j\omega_j)^2}{\frac{4k_\mathrm{B}T}{\hbar}\sum_j S_j\omega_j}\right] . \tag{196}$$

If we identify $|H'_{if}|$ with the charge transfer integral $|J_\mathrm{AB}|$ (see Sec. 1.4.3), the sum $\sum_j \hbar S_j\omega_j$ with the reorganization energy λ_AB, and $\hbar\omega_{f,i} = E_f - E_i$ with the site-energy difference ΔE_AB, we arrive at the Marcus rate expression k_AB for a charge transfer reaction in the high temperature regime [188, 189].

$$k_\mathrm{AB} = \frac{|J_\mathrm{AB}|^2}{\hbar}\sqrt{\frac{\pi}{k_\mathrm{B}T\lambda_\mathrm{AB}}}\exp\left[-\frac{(\Delta E_\mathrm{AB}+\lambda_\mathrm{AB})^2}{4k_\mathrm{B}T\lambda_\mathrm{AB}}\right] \tag{197}$$

In the Marcus rate[1] enter the temperature T, Boltzmann constant k_B, the reduced Planck constant $\hbar$, the reorganization energy λ_AB, the site-energy difference ΔE_AB, and the charge transfer integral $|J_\mathrm{AB}|$.

As a summary, the following approximations are carried out to obtain the Marcus rate expression. First, the Born-Oppenheimer approximation guarantees the independence of the electronic coupling matrix elements from the nuclear coordinates. Second, the hyper potential energy surfaces are approximated as shifted harmonic oscillators. Third, the short time approximation $t \ll \omega^{-1}$ and the classical approximation $\frac{\hbar\omega_j}{k_\mathrm{B}T} \ll 1$ are used in the derivation. Hence, the Marcus theory is restricted to the high-temperature regime, where molecular vibrations can be treated as classical oscillations, and tunnelling processes are neglected.

The change in the nuclear coordinates in the relaxation process, as the excess charge is transferred inside the charge-transfer complex, is taken into account by the reorganization energy λ_AB. The reorganization energy $\lambda = \lambda^\mathrm{in} + \lambda^\mathrm{out}$ is split into an internal λ^in and an outer-sphere contribution λ^out, referring to a relaxation process of nuclear coordinates within the charge transfer complex and the environment upon charge transfer, respectively [57].

The internal contribution is evaluated in a four point scheme using the internal energies on the diabatic potential energy surface (PES) of molecules A and B in the charged c and neutral n states in the optimised neutral N or charged C geometry [57, 191]:

$$\lambda^\mathrm{in}_\mathrm{AB} = \underbrace{(U^{nC}_\mathrm{A} - U^{nN}_\mathrm{A})}_{\lambda^{cn}_\mathrm{A}} + \underbrace{(U^{cN}_\mathrm{B} - U^{cC}_\mathrm{B})}_{\lambda^{nc}_\mathrm{B}} \tag{198}$$

Figure 1.2 sketches the potential energy surface in harmonic approximation to visualise the energy levels for a charge transfer reaction in the framework of Marcus Theory. Here $\mathbf{q}^c_\mathrm{A}$

[1] In some references [57,190] one can find the Marcus rate expression $(\Delta E_\mathrm{AB} - \lambda)^2$ in the exponent. Note that this implies a convention for the distance definition $\mathbf{r}_\mathrm{AB} = \mathbf{r}_\mathrm{A} - \mathbf{r}_\mathrm{B}$ and $\Delta E_\mathrm{AB} = E_\mathrm{A} - E_\mathrm{B}$, whereas here we use $\Delta E_\mathrm{AB} = E_\mathrm{B} - E_\mathrm{A}$.

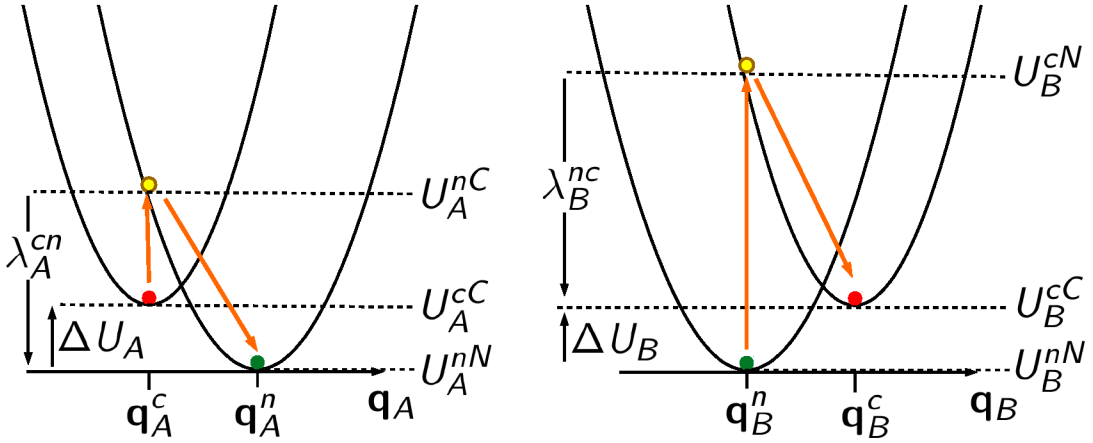

Figure 1.2: Potential energy surface in a harmonic approximation for the charge transfer process from molecule A to B in the framework of Marcus theory. The donor A and acceptor B are presented in the charged state c and neutral state n. Definition of the internal reorganization energy $\lambda_{\mathrm{AB}}^{\mathrm{in}} = \lambda_{\mathrm{A}}^{cn} + \lambda_{\mathrm{B}}^{nc}$ and the internal site-energy difference $\Delta E_{\mathrm{AB}}^{\mathrm{in}} = \Delta U_{\mathrm{B}} - \Delta U_{\mathrm{A}}$.

and $\mathbf{q}_{\mathrm{A}}^n$ represent the collective vibrational coordinate vector for molecule A in the charged c and neutral state n, whereas $\mathbf{q}_{\mathrm{B}}^c$ and $\mathbf{q}_{\mathrm{B}}^n$ represent the same with respect to molecule B. In this notation, U_{A}^{nC} is the internal energy of molecule A in the neutral state n in the geometry of the charged state C. Similarly, U_{B}^{cN} is the internal energy of molecule B with an excess charge in the neutral state geometry.

The site energy difference $\Delta E_{\mathrm{AB}} = E_{\mathrm{B}} - E_{\mathrm{A}}$ is the driving quantity for a charge transfer reaction and consists of three contributions.

$$\Delta E_{\mathrm{AB}} = \Delta E_{\mathrm{AB}}^{\mathrm{in}} + \Delta E_{\mathrm{AB}}^{\mathrm{ext}} + \Delta E_{\mathrm{AB}}^{\mathrm{out}} \tag{199}$$

The outer-sphere contribution to the site-energy difference ΔE^{out} can be subdivided into electrostatic E^{el} and polarisation E^{pol} effects accounting for environmental perturbations. They are discussed in detail in chapter 1.4.4.1.

The internal site-energy difference $\Delta E_{\mathrm{AB}}^{\mathrm{in}}$ between two hopping sites is determined by the difference between the minima of the diabatic potential energy surface (Fig. 1.2).

$$\Delta E_{\mathrm{AB}}^{\mathrm{in}} = \Delta U_{\mathrm{B}} - \Delta U_{\mathrm{A}} = \underbrace{(U_{\mathrm{B}}^{cC} - U_{\mathrm{B}}^{nN})}_{\Delta U_{\mathrm{B}}} - \underbrace{(U_{\mathrm{A}}^{cC} - U_{\mathrm{A}}^{nN})}_{\Delta U_{\mathrm{A}}} \tag{200}$$

The contributions to the site-energy difference that arise due to the internal energies can be extracted from the energy U_{A}^{cC} of the charged molecule in the optimised charged geometry and the energy in the optimised neutral ground state U_{A}^{nN} for the molecules A and B. $\Delta U_{\mathrm{A(B)}}$ corresponds to the adiabatic ionisation potential for hole transfer or the electron affinity for electron transfer, respectively. If A and B are similar chemical compounds, and the charge transfer process does not give rise to conformational changes, the internal site-energy difference is negligible $\Delta E_{\mathrm{AB}}^{\mathrm{in}} \approx 0$.

An external electric field $\mathbf{F}^{\mathrm{ext}}$ leads to the external contribution of the site-energy difference ΔE^{ext} with the elementary electric charge $q = \pm e$ and the distance of the centres of mass between the hopping sites $\mathbf{r}_{\mathrm{AB}} = \mathbf{r}_{\mathrm{B}} - \mathbf{r}_{\mathrm{A}}$

$$\Delta E_{\mathrm{AB}}^{\mathrm{ext}} = -q(\mathbf{r}_{\mathrm{AB}} \cdot \mathbf{F}^{\mathrm{ext}}) \tag{201}$$

Marcus theory was initially derived for outer-sphere electron transfer in solvents [188,189]. Therefore, the entire donor-acceptor complex is represented by only a single collective coordinate. However, in the presented approach, the donor and the acceptor are treated by different collective coordinates.

1.4.2 Alternative Rate Expressions

In the following section, we introduce alternatives to the Marcus rate for charge transfer. We start with the basic Miller-Abrahams approach (Eq. 202) and compare with Weiss-Dorsey rates (Eq. 203) and Levich-Jortner rates (Eq. 204).

Miller-Abrahams Rate An alternative approach to charge transfer yield Miller-Abrahams (MA) rates k^{MA} for phonon-assisted tunnelling processes [192], which are primarily employed in Gaussian disorder models (GDM) [193–196]. They relay on fits of the distribution of site-energy difference ΔE_{ij} to experimental data.

$$k^{\mathrm{MA}} = \begin{cases} k_0 \exp\left(-\gamma R_{ij}\right) \exp\left(-\frac{\Delta E_{ij}}{k_{\mathrm{B}} T}\right) & \text{for } \Delta E_{ij} > 0 \\ k_0 \exp\left(-\gamma R_{ij}\right) & \text{for } \Delta E_{ij} < 0 \end{cases} \tag{202}$$

Here, k_0 is the maximum hopping rate or the attempt-to-escape frequency, the factor γ is the inverse localisation radius that approximates the decay of transfer integrals, and R_{ij} is the hopping distance between two sites i and j. The first term denotes the tunnelling contribution. The second expression is a Boltzmann term for thermal activation with temperature T and treats an uphill hopping in energy $\Delta E_{ij} > 0$ with an exponential penalty. The downhill direction is favoured by setting the Boltzmann term equal to one in the opposite case $\Delta E_{ij} < 0$. Miller-Abrahams rates do not yield an inverted region in contrast to Marcus rate. The major limitation of Miller-Abrahams rates is the need for experimental reference data in the parametrisation. Hence, they cannot be applied to determine charge carrier mobilities from an *ab initio* perspective.

Weiss-Dorsey Rate Both semi-classical approaches from Marcus and Miller-Abrahams predict vanishing charge transport in the low-temperature limit $T \to 0$. However, many experimental findings detail the presence of a finite conductivity at the low-temperature regime [197–200]. As these semi-classical models break down at low-temperatures, some approaches divide charge transport into a thermally activated high-energy regime and an activation-less low-energy regime [197]. The breakdown of these semi-classical models originates from the missing treatment of quantum mechanical zero-point vibrations, which can drive nuclear tunnelling processes [201]. In a quantum mechanical treatment of the nuclear motion, the kinetic energy of the nuclei can be regarded as a heat bath that couples to the transferred charge, where the nuclear tunnelling assists the charge carrier to overcome the energy barrier.

The main factor why the quantum mechanical description is essential in semiconducting polymers is that the characteristic frequency of the heat bath is relatively high. In a non-polar semiconducting polymer, the charge moves mainly due to changes in bond length. The relevant stretching vibrations are at high frequency, and most of the states are still in the vibrational ground state at room temperature, which is entirely different for a classical oscillator.

The rate expression k^{WD} from Weiss [202,203], Dorsey [204] and coworkers includes the nuclear tunnelling in the charge transfer process as it involves the coupling between charge

and nuclear bath [201]. It was derived based on the spin-boson model [205], which is a dissipative two-level system [206], where both states are coupled to an environmental heat bath of bosons. Both spin-up and spin-down states of a spin-$^1/_2$ system in the spin-boson model are replaced by donor and acceptor state to model charge transfer.

In the non-adiabatic limit the transfer rate reads:

$$k^{\mathrm{WD}} = \frac{|J_{\mathrm{AB}}|^2}{\hbar^2\omega_c}\left(\frac{\hbar\omega_c}{2\pi k_{\mathrm{B}}T}\right)^{1-2\alpha'}\left|\Gamma\left(\alpha' + i\frac{\Delta E_{\mathrm{AB}}}{2\pi k_{\mathrm{B}}T}\right)\right|^2\Gamma(2\alpha')^{-1}\exp\left(\frac{\Delta E_{\mathrm{AB}}}{2k_{\mathrm{B}}T}\right)\exp\left(-\frac{|\Delta E_{\mathrm{AB}}|}{\hbar\omega_c}\right) \tag{203}$$

The charge transfer integral is denoted by $|J_{\mathrm{AB}}|$ in the Weiss-Dorsey rate expression, the energy difference between donor and acceptor state is ΔE_{AB}, the coupling strength between charge and the bath is given by the Kondo parameter $\alpha' = \alpha/2 + 1$, the characteristic frequency of the bath is ω_c, and the gamma function is denoted by Γ. The classical reorganization energy is linked to the characteristic frequency by $\lambda = 2\alpha'\omega_c$ [201,205].

In the high-temperature limit ($k_{\mathrm{B}}T \gg \hbar\omega_c$) the expression (Eq. 203) reduces to the semi-classical Marcus rate (Eq. 197), whereas k^{WD} reduces to a finite, non-zero value at low temperatures.

Levich-Jortner Rate The Levich-Jortner [207] rate expression yields a mixed quantum-classical multi-channel generalisation of the Marcus rate. It treats the high-frequency intramolecular vibrational modes of molecules A and B on a quantum level but in a common set of vibrational coordinates, whereas low-frequency vibrational coordinates from outer-sphere contributions remain classical.

$$k_{\mathrm{AB}}^{\mathrm{LJ}} = \frac{2\pi}{\hbar}\frac{|J_{\mathrm{AB}}|^2}{\sqrt{4\pi\lambda_{\mathrm{AB}}^{\mathrm{out}}k_{\mathrm{B}}T}}\sum_{N=0}^{\infty}\frac{1}{N!}\left(\frac{\lambda_{\mathrm{AB}}^{\mathrm{in}}}{\hbar\omega^{\mathrm{int}}}\right)^N\exp\left(-\frac{\lambda_{\mathrm{AB}}^{\mathrm{in}}}{\hbar\omega^{\mathrm{int}}}\right)\exp\left(-\frac{(\Delta E_{\mathrm{AB}} + N\hbar\omega^{\mathrm{int}} + \lambda_{\mathrm{AB}}^{\mathrm{out}})^2}{4\lambda_{\mathrm{AB}}^{\mathrm{out}}k_{\mathrm{B}}T}\right) \tag{204}$$

All quantum mechanically treated intramolecular vibrations of the donor-acceptor complex are averaged to an effective, internal frequency ω^{int}. It is also assumed that the effective frequencies give similar results for the neutral ground state and the charged excited state. The Levich-Jortner rate is transformed into the Marcus rate for high temperatures.

1.4.3 Charge Transfer Integral

The charge transfer integral, electronic coupling or transition matrix element $|J_{\mathrm{AB}}|$ for charge transfer between two hopping sites A and B is given as the off-diagonal Hamiltonian matrix element

$$|J_{\mathrm{AB}}| = \langle\Phi_{\mathrm{A}}|\hat{H}|\Phi_{\mathrm{B}}\rangle \tag{205}$$

in the diabatic basis Φ_{A} and Φ_{B} describing the charge being localised on A and B, respectively [208]. It is one of the critical components that enter the Marcus rate expression (Eq. 197). As squared prefactor of the rate, the charge transfer integral selects sites for charge transfer with a significant orbital overlap. The charge transfer integral does not provide information concerning the predominant direction for charge transfer.

Several numerical methods are available to calculate the charge transfer integral $|J_{\mathrm{AB}}|$ at different levels of theory applying distinct approximations. Among these methods are block-diagonalisation methods, the generalised Mulliken-Hush method [209,210], fragment

charge difference method, fragment energy difference method [211], fragment orbital DFT (Sec. 1.4.3.3), constrained DFT (Sec. 1.2.2.5) and projection methods like the dimer projection method (DIPRO) (Sec. 1.4.3.1). Furthermore, one can employ an effective Hamiltonian approach on DFT level or fragment orbital DFTB [212]. In the VOTCA programme package [57,213] an approximate semiempirical method [214], using the molecular orbital overlap (MOO) based on the ZINDO Hamiltonian [158] (Sec. 1.4.3.2), can be employed to evaluate the charge transfer integral rapidly for a large number of hopping sites in the morphology. Another method to calculate electronic couplings is the Projection-Operator Diabatisation (POD) method [215], which is applied on molecule/metal and molecule/semiconductor interfaces [216] or used to model charge transport in proteins [217].

1.4.3.1 DIPRO Method

The charge transfer integral $|J_{\mathrm{AB}}|$ can be determined utilising the dimer projection method (DIPRO) [218]. As a simplification, the charge transfer reaction (Eq. 183) for hole transport occurs between the highest occupied molecular orbitals HOMOs of both molecules A and B in the charge-transfer complex and electron transport occurs between the lowest unoccupied molecular orbitals LUMOs, respectively. So only the frontier orbitals are applied in this frozen-core approximation. The system is described by an effective tight-binding Hamiltonian.

$$H^{\mathrm{eff}} = \sum_m \varepsilon_m a_m^\dagger a_m + \sum_{m \neq n} (J'_{mn} a_m^\dagger a_n + c.c.) \tag{206}$$

Here, ε_m is the site-energy, J'_{mn} is the transition matrix element, $a_M^\dagger$, is a charge creation operator, and a_m is a charge annihilation operator. The off-diagonal element J'_{mn} of the effective Hamiltonian in (Eq. 206) can be identified with the element J_{AB} in (Eq. 205), if polarisation effects of one frontier orbital upon an orbital in a neighbour molecule can be neglected. With the help of these approximations one can reduce the problem to a (2x2) matrix eigenvalue problem.

$$\mathbf{H} = \begin{pmatrix} H_{\mathrm{AA}} & J_{\mathrm{AB}} \\ J_{\mathrm{BA}} & H_{\mathrm{BB}} \end{pmatrix} = \begin{pmatrix} e_{\mathrm{A}} & J_{\mathrm{AB}} \\ J_{\mathrm{BA}} & e_{\mathrm{B}} \end{pmatrix} \tag{207}$$

The dimer Hamilton operator is a self-adjungated operator and the associated normalised eigenfunctions build a complete orthonormal system for the corresponding Hilbert space. Introducing an identity element $\mathbf{1} = \sum_i |\psi_i\rangle\langle\psi_i|$ into the transition matrix element $|J_{\mathrm{AB}}|$ yields the following expression with the help of the eigenfunctions ψ_i of the dimer Hamiltonian:

$$|J_{\mathrm{AB}}| = |\langle\phi_{\mathrm{A}}|\hat{H}|\phi_{\mathrm{B}}\rangle| = \sum_{ij} |\langle\phi_{\mathrm{A}}|\psi_i\rangle\langle\psi_i|\hat{H}|\psi_j\rangle\langle\psi_j|\phi_{\mathrm{B}}\rangle| \tag{208}$$

As the Hamiltonian is diagonal with respect to the basis of the eigenfunctions ψ_i, we use $\langle\psi_i|\hat{H}|\psi_j\rangle = \delta_{ij}\epsilon_i$ with the eigenvalues ϵ_i for the dimer molecular orbitals, and obtain

$$|J_{\mathrm{AB}}| = \sum_i |\langle\phi_{\mathrm{A}}|\psi_i\rangle\ \epsilon_i\ \langle\psi_i|\phi_{\mathrm{B}}\rangle| \ . \tag{209}$$

In the following, the projections $\gamma^i_{\mathrm{A(B)}} = \langle\phi_{\mathrm{A(B)}}|\psi_i\rangle$ are calculated, which describe the orbital projections from the monomer $\phi_{\mathrm{A(B)}}$ on the dimer ψ_i basis functions. Therefore, the

wavefunctions $\psi_i = \sum_k c_k^{(i)} |\varphi_k\rangle$ and $\phi_i = \sum_l c_l^{(i)} |\varphi_l\rangle$ are represented in a basis of localised atomic orbitals $\{\varphi_k\}$ or a plane wave basis (eq. 142). The projections read

$$\gamma^i_{A(B)} = \sum_l c_l^{(A(B))^*} \langle\varphi_l| \sum_k c_k^{(i)} |\varphi_k\rangle \quad = \sum_{k,l} c_l^{(A(B))^*} \langle\varphi_l|\varphi_k\rangle c_k^{(i)} = \mathbf{c}^{\dagger(A(B))} \mathbf{O} \mathbf{c}^{(i)} \ . \tag{210}$$

Here, $\mathbf{O}$ is the overlap matrix of the atomic orbitals and $\mathbf{c}^{\dagger(A(B))}$ is a vector, which contains the development coefficients for the monomer wavefunctions and $\mathbf{c}^{(i)}$ those for the dimer wavefunctions of a given frontier orbital with index i. The DIPRO approach assumes that the dimer frontier orbitals only depend on the interaction of the monomer frontier orbitals, which includes that the dimer wavefunctions can be expressed in the monomer basis with the wavefunctions ϕ_A and ϕ_B by means of the development coefficients $\mathbf{C}$. Solving the generalised secular equations gives the coefficients $\mathbf{C}$. In these equations enter the matrices for the Hamilton operator $\mathbf{H}$ and the overlap $\mathbf{S}$.

$$(\mathbf{H} - E\mathbf{S})\mathbf{C} = \mathbf{0} \tag{211}$$

The elements read,

$$\begin{aligned} e_\mathrm{A} &= \langle\phi_\mathrm{A}|\hat{H}|\phi_\mathrm{A}\rangle \\ e_\mathrm{B} &= \langle\phi_\mathrm{B}|\hat{H}|\phi_\mathrm{B}\rangle \\ J_\mathrm{AB} &= \langle\phi_\mathrm{A}|\hat{H}|\phi_\mathrm{B}\rangle \\ S_\mathrm{AB} &= \langle\phi_\mathrm{A}|\phi_\mathrm{B}\rangle \ , \end{aligned} \tag{212}$$

in the (2x2) matrix representation for the Hamiltonian (Eq. 207), and the overlap matrix for the frontier orbital wavefunctions is

$$\mathbf{S} = \begin{pmatrix} 1 & S_\mathrm{AB} \\ S_\mathrm{BA} & 1 \end{pmatrix}. \tag{213}$$

As the orbitals ϕ_A and ϕ_B are not orthogonal in general one applies a Löwdin transformation [219] by making use of the inverse square-root of the overlap matrix $\mathbf{S}^{-\frac{1}{2}}$ with $\mathbf{S} = \boldsymbol{\gamma}_\mathrm{A}^\dagger \boldsymbol{\gamma}_\mathrm{B}$ to get an effective eigenvalue problem with an effective Hamilton operator $\mathbf{H}^\mathrm{eff}$.

$$\mathbf{H}^\mathrm{eff} = \mathbf{S}^{-\frac{1}{2}} \mathbf{H} \mathbf{S}^{-\frac{1}{2}} \tag{214}$$

The effective eigenvalue equation reads

$$\mathbf{H}^\mathrm{eff} \mathbf{C}^\mathrm{eff} = E\mathbf{C}^\mathrm{eff} \tag{215}$$

and the components of the effective Hamilton matrix in the orthogonal basis are now identified with the site-energy $\varepsilon_{A(B)}$ and the transfer integral J_AB.

$$\mathbf{H}^\mathrm{eff} = \begin{pmatrix} e_\mathrm{A}^\mathrm{eff} & H_\mathrm{AB}^\mathrm{eff} \\ H_\mathrm{AB}^{*\mathrm{eff}} & e_\mathrm{B}^\mathrm{eff} \end{pmatrix} = \begin{pmatrix} \varepsilon_\mathrm{A} & J_\mathrm{AB} \\ J_\mathrm{AB}^* & \varepsilon_\mathrm{B} \end{pmatrix} \tag{216}$$

In conclusion, the DIPRO approach uses the projection of the monomer orbitals on the dimer orbitals to calculate the transition matrix element $|J_\mathrm{AB}| = |H_\mathrm{AB}^\mathrm{eff}|$ for intermolecular charge transfer, which requires the overlap matrix for the atomic orbitals $\mathbf{O}$, the development coefficients for the monomer and dimer orbitals and the dimer orbital energies as an input to solve equation 215 for (Eq. 209) by means of (Eq. 210).

Therefore, one needs to perform two calculations on individual monomers A and B in the dimer configuration and one calculation for the dimer. This can employ different levels of theory using DFT (Sec. 1.2.2), DFTB (Sec. 1.2.3), or semiempirical approaches (Sec. 1.2.4).

1.4.3.2 ZINDO-based Molecular Orbital Overlap Method

A fast evaluation of the charge transfer integral can be carried out using the molecular orbital overlap (MOO) based on the ZINDO Hamiltonian [157,214].

This method does not require a self-consistent evaluation for each configuration of monomers and dimers. For each dimer configuration, the method constitutes the matrix elements of the ZINDO-based Hamiltonian on the basis of the weighted overlap of molecular orbitals from a pair of involved monomers. If homo-molecular transitions between rigid segments are present, then only one self-consistent reference calculation of a single, isolated, optimised molecule is required. With the coordinates of optimised geometries of all conjugated segments and the corresponding MO coefficients at hand, the MOO method makes the dimer Fock operators $\hat{\mathbf{F}}$ up of the MOs of monomers by rotating and translating the orbitals of rigid fragments.

For simplicity, one assumes in the following the case of evaluating the electronic coupling elements for hole transfer between a pair of identical molecules with two Slater determinants, which differ in only one MO. The schema can be extended to the general case. Using the approximation again that the multielectron wavefunctions are described by single Slater determinants and restricting the excess charge to the frontier orbitals with the frozen orbital approximation then the charge transfer integral can be written as

$$|J_{\mathrm{AB}}| \approx \langle \phi_{\mathrm{A}}^{\mathrm{HOMO}} | \hat{\mathbf{F}} | \phi_{\mathrm{B}}^{\mathrm{HOMO}} \rangle \tag{217}$$

with the Fock matrix $\mathbf{F}$, e.g. for hole transfer from $\phi_{\mathrm{A}}^{\mathrm{HOMO}}$ to $\phi_{\mathrm{B}}^{\mathrm{HOMO}}$.

The basis set of the constituent single molecules $\mathbf{C}_{\mathrm{loc}}$ is given by the MOs, where ϕ_j^i denotes the component of the AO j in the MO i, reads

$$\mathbf{C}_{\mathrm{loc}} = \begin{pmatrix} \phi_1^1 & \phi_1^2 & \dots & \phi_1^{\frac{N}{2}} & 0 & 0 & 0 & 0 \\ \phi_2^1 & \phi_2^2 & \dots & \phi_2^{\frac{N}{2}} & 0 & 0 & 0 & 0 \\ \vdots & \vdots & \dots & \vdots & 0 & 0 & 0 & 0 \\ \phi_{\frac{N}{2}}^1 & \phi_2^2 & \dots & \phi_{\frac{N}{2}}^{\frac{N}{2}} & 0 & 0 & 0 & 0 \\ 0 & 0 & 0 & 0 & \phi_{\frac{N}{2}+1}^{\frac{N}{2}+1} & \phi_{\frac{N}{2}+1}^{\frac{N}{2}+2} & \dots & \phi_{\frac{N}{2}+1}^{N} \\ 0 & 0 & 0 & 0 & \phi_{\frac{N}{2}+2}^{\frac{N}{2}+1} & \phi_{\frac{N}{2}+2}^{\frac{N}{2}+2} & \dots & \phi_{\frac{N}{2}+2}^{N} \\ 0 & 0 & 0 & 0 & \vdots & \vdots & \dots & \vdots \\ 0 & 0 & 0 & 0 & \phi_N^{\frac{N}{2}+1} & \phi_N^{\frac{N}{2}+2} & \dots & \phi_N^N \end{pmatrix} \tag{218}$$

Here, the AOs are labelled to localise the first $\frac{N}{2}$ AOs on A and the second $\frac{N}{2}$ AOs on molecule B, respectively. In the same manner j numbers the first $\frac{N}{2}$ MOs on A and the second $\frac{N}{2}$ MOs on molecule B. The localised orbitals are extracted from reference SCF calculations on isolated molecules.

The spectral theorem is applied to execute the projection of the MOs of the pair $\mathbf{C}_{\mathrm{pair}}$ on the MOs of the individual molecules $\mathbf{C}_{\mathrm{loc}}$

$$\mathbf{C}_{\mathrm{pair}}^{\mathrm{loc}} = [\mathbf{C}_{\mathrm{loc}}]^T \, \mathbf{C}_{\mathrm{pair}}, \tag{219}$$

where the superscript T indicates the transposition of the matrix and $\mathbf{C}_{\mathrm{pair}}^{\mathrm{loc}}$ entitles the orbitals of the pair in the localised basis set. This equation presumes the orthogonality of

the basis set in C_{loc} and $\mathbf{C}^{\mathrm{loc}}_{\mathrm{pair}}$. Finally, one can set up the Fock matrix $\mathbf{F}$ in the novel basis set to get the localised Fock matrix $\mathbf{F}^{\mathrm{loc}}$.

$$\mathbf{F}^{\mathrm{loc}} = \left[\mathbf{C}^{\mathrm{loc}}_{\mathrm{pair}}\right]^{T} \boldsymbol{\varepsilon}_{\mathrm{pair}} \mathbf{C}^{\mathrm{loc}}_{\mathrm{pair}} \tag{220}$$

Here, the diagonal matrix of eigenvalues of the pair is $\boldsymbol{\varepsilon}_{\mathrm{pair}}$. The charge transfer integrals are found at the off-diagonal elements of matrix $\mathbf{F}^{\mathrm{loc}}$. As an example the transfer integral between two similar molecules A and B for a hole transition between the HOMO on A and to the HOMO on B is found at the element $\mathbf{F}^{\mathrm{loc}}_{h,h+\frac{N}{2}}$, where h is the index of the HOMO in A.

The evaluation of the charge transfer integral based on an approximation to ZINDO is detailed in the next section. If one expresses the AOs, that determine the HOMOs on the monomers A and B, in the same way as it is done for the MOs in the expression for $\mathbf{C}_{\mathrm{loc}}$ above (Eq. 218), then one finds that the off-diagonal blocks of the Fock matrix liking the AOs on A with those on B are sufficient to determine the charge transfer integral. So, the desired Fock matrix elements include AOs on distinct atomic centres and that can be written in the form

$$\mathbf{F}_{\mu\nu} = \overline{\mathbf{S}}_{\mu\nu} \frac{\beta_a + \beta_b}{2} + \mathbf{P}_{\mu\nu} \frac{\gamma_{ab}}{2}. \tag{221}$$

This expression contains the overlap matrix $\overline{\mathbf{S}}$ for the overlap between atomic orbitals and the density matrix $\mathbf{P}_{\mu\nu}$. Especially overlaps with σ- and π-character from p-type orbitals are weighted differently in $\overline{\mathbf{S}}$. The atom centre a for the AO μ is associated with a bonding parameter β_a, and in the same way, the atom centre b for the AO ν and β_b is labelled. The Mataga-Nishimoto potential is denoted by γ_{ab} [220]. One can assume that the density matrix $\mathbf{P}_{\mu\nu}$ is block-diagonal, if (1) the MOs of the isolated monomer are of the same kind as the ones of the dimer or if (2) the MOs of each pair can be expressed as a linear combination of bonding and antibonding pairs of MOs of the isolated monomer (see [214]). Hence, $\mathbf{P}_{\mu\nu}$ does not influence sought-after off-diagonal elements in $\mathbf{F}$ and the task is reduced to evaluate the weighed atomic orbital overlap.

With the help of analytic expressions, as in reference [221], one can determine the atomic overlaps, e.g. for $1s, 2s, 2p$ orbitals. Furthermore, especially overlaps of $\langle p|p\rangle$-type are weighted by scaling factor from Zerner's schema to distinguish the appropriately π-type and σ-type overlaps.

In conclusion, ZINDO/MOO allows to approximately determine $|J_{\mathrm{AB}}|$ without an explicit SCF-calculation of the dimer.

1.4.3.3 Fragment Orbital DFT

Fragment orbital density functional theory (FODFT) is another method, which can be applied to compute the charge transfer integral $|J_{\mathrm{AB}}|$, it is conceptually similar to CDFT but computationally less demanding (Sec. 1.2.2.5) [113,222]. In FODFT, the orbitals to construct the wavefunctions ϕ_a and ϕ_b are calculated based on isolated molecule fragments of donor and acceptor in the dimer configuration and recomposed to construct the wavefunctions of diabatic states for the evaluation of the charge transfer integral. As a simplification, the interaction between donor and acceptor contributions is disregarded in FODFT.

In the following, a cationic or hole transfer reaction $A^+ + B \rightarrow A + B^+$ from a donor molecule A to an acceptor B is discussed. In a simplified initial situation, the compounds A and B are neutral, and A possesses n_A electrons, and B possesses n_B. Nevertheless, the

presented scheme can be extended for anionic charge transfer, including one virtual orbital per fragment or using charged instead of neutral states [222]. In the initial state, the donor A has $n_A - 1$ electrons and the acceptor n_B. In contrast, the situation is reversed in the final state. The initial ϕ_a and final state ϕ_b are represented as a single determinate, which is made up of $n_A + n_B - 1$ orbitals ϕ.

$$\phi_a = \frac{1}{\sqrt{(n_A + n_B - 1)!}} \det\left(\phi_a^1, \ldots, \phi_a^{n_A+n_B-1}\right) \tag{222}$$

$$\phi_b = \frac{1}{\sqrt{(n_A + n_B - 1)!}} \det\left(\phi_b^1, \ldots, \phi_b^{n_A+n_B-1}\right) \tag{223}$$

In the following non-interacting orbitals of isolated, neutral molecules are used in FODFT in order to construct the determinants ϕ_a and ϕ_b.

$$\phi_a \approx \phi_a^{\mathrm{FO}} = \frac{1}{\sqrt{(n_A + n_B - 1)!}} \det\left(\phi_A^1, \ldots, \phi_B^{n_A-1}, \phi_A^1, \ldots, \phi_B^{n_B}\right) \tag{224}$$

$$\phi_b \approx \phi_b^{\mathrm{FO}} = \frac{1}{\sqrt{(n_A + n_B - 1)!}} \det\left(\phi_A^1, \ldots, \phi_B^{n_A}, \phi_A^1 \ldots \phi_B^{n_B-1}\right) \tag{225}$$

Two KS-DFT calculations are carried out at the isolated fragments of A and B in the dimer arrangement, which result in two sets of KS-orbitals $(\phi_A^{1'} \cdots \phi_A^{n'})$ and $(\phi_B^{1'} \cdots \phi_B^{n'})$. Thereupon, these orbitals are orthogonalised with Löwdin's method [219] to obtain two sets of orbitals $(\phi_A^1 \cdots \phi_A^n)$ and $(\phi_B^1 \cdots \phi_B^n)$, which are combined to construct the wavefunctions ϕ_A and ϕ_B in (Eq. 224) and (Eq. 225), respectively. With these wavefunctions at hand, one can generate the dimer Kohn-Sham Hamiltonian with the help of the single-particle KS-Hamiltonians $h_{a,i}^{\mathrm{KS}}$ and $h_{b,i}^{\mathrm{KS}}$

$$\mathcal{H}_a^{\mathrm{KS}} = \sum_{i=1}^{n_A+n_B-1} h_{a,i}^{\mathrm{KS}} \quad \text{and} \quad \mathcal{H}_b^{\mathrm{KS}} = \sum_{i=1}^{n_A+n_B-1} h_{b,i}^{\mathrm{KS}} \tag{226}$$

The one-particle KS-Hamiltonians $h_{a,i}^{\mathrm{KS}}$ and $h_{b,i}^{\mathrm{KS}}$ are built from the $(n_A + n_B - 1)$ orbitals that produce ϕ_a^{FO} and ϕ_b^{FO}. The transition matrix elements are now approximated

$$H_{ab} = \langle\phi_a|\mathcal{H}|\phi_b\rangle \overset{(1)}{\approx} \langle\phi_a|\mathcal{H}_b^{\mathrm{KS}}|\phi_b\rangle \overset{(2)}{\approx} \langle\phi_a^{\mathrm{FO}}|\mathcal{H}_b^{\mathrm{KS}}|\phi_b^{\mathrm{FO}}\rangle \overset{(3)}{=} \begin{cases} \langle\phi_B^{n_B}|h_b^{\mathrm{KS}}|\phi_A^{n_A}\rangle & \text{for holes} \\ \langle\phi_B^{n_B+1}|h_b^{\mathrm{KS}}|\phi_A^{n_A+1}\rangle & \text{for electrons} \end{cases} \tag{227}$$

All in all FODFT is based on two assumptions. On the one hand, the exact Hamiltonian is substituted by a KS-Hamiltonian depending on $n_A + n_B - 1$ orbitals (Eq. 227,1) and on the other hand the wavefunctions ϕ_a and ϕ_b are exchanged by their fragment orbital counterparts $\phi_a^{\mathrm{FO}}, \phi_b^{\mathrm{FO}}$ (Eq. 227,2). The only difference in ϕ_a^{FO} and ϕ_b^{FO} is the occupation of the HOMO on each fragment site, as the sites and orbitals are not allowed to relax after a charge is transferred. Therefore, the equality in (Eq. 227,3) holds exactly. So, the electronic coupling matrix element is reduced from a description concerning determinants to one with respect to orbitals under these conditions. The presented method is also called FO-DFT$(2n-1)$ method, with $n_A = n_B$, where the HOMO occupation number for A and B is zero. In contrast, in FO-DFT$(2n)$ the occupation numbers are maintained, and both h_a^{KS} and h_b^{KS} are constructed from $2n$ orbitals. The transfer integral H_{ba} is also constructed as $H_{ba} = \langle\phi_A^{n_A}|h_a^{\mathrm{KS}}|\phi_B^{n_B}\rangle$ likewise. As H_{ab} and H_{ba} should be similar in general, but they can vary for asymmetric donor-acceptor pairs, the average is applied $|J_{\mathrm{AB}}| = \frac{H_{ab}+H_{ba}}{2}$ for the charge transfer integral.

1.4.4 Outer-sphere Contributions in Charge Transfer Reactions

The accurate description of the electrostatic and the polarisation effects of a localised charge, excited molecules or charge transfer states inside a neutral environment is challenging since long-range interactions need to be considered. In this section, we present different approaches to determine outer-sphere contributions in charge transfer reactions. We determine the outer-sphere reorganization energy from the dielectric displacement fields with an expression as a sum over atom-centred partial charges (Sec. 1.4.4.1). An analogous expression is set up for the electrostatic energy, in which polarisation effects can be incorporated via a screening function (Sec. 1.4.4.2). In an alternative approach, the electrostatic contributions are determined using distributed multipoles (Sec. 1.4.4.3) and additional induction effects can be included using the Thole model (Sec. 1.4.4.4).

These expressions with sums over partial charges suffer from convergence problems. For instance, charge quadrupole interactions converge only on certain conditions in periodic systems in 3D [223,224] and slowly in 2D systems [225]. Ewald summation techniques [176] are usually applied, which remedies this problem as the sum is split into a short-range term, which is summed in real space, and a long-range term, which is evaluated in reciprocal Fourier space [226]. Poelking and Andrienko amplified this scheme to treat long-range interactions of individual charged molecules and a polarised cloud on a neutral periodic background [227].

1.4.4.1 Reorganization Energy from Partial Charges

In the course of the charge transfer process also molecules in the vicinity of a charge-transfer complex undergo a reorientation due to alternations in the electric field and changes in the charge distribution as they get polarised [57]. These effects are taken into account by the outer-sphere contributions to the reorganization energy $\lambda_{\mathrm{AB}}^{\mathrm{out}}$ and become essential in highly polarisable environments. The term $\lambda_{\mathrm{AB}}^{\mathrm{out}}$ can be assessed based on the electric displacement, assuming that the charge transfer reaction is slower than the polarisation of the environment and faster than the reorientation of the nuclei. The outer-sphere contributions to the reorganization energy is given by

$$\lambda_{\mathrm{AB}}^{\mathrm{out}} = \frac{c_p}{2\varepsilon_0} \int_{V^{\mathrm{out}}} \left[\mathbf{D}_{\mathrm{A}}(\mathbf{R}_c) - \mathbf{D}_{\mathrm{B}}(\mathbf{R}_c)\right]^2 \, \mathrm{d}\mathbf{R}_c \ , \tag{228}$$

where ε_0 is the vacuum permittivity, and V^{out} is the polarisable volume generated by the charge-transfer complex. The Pekar-factor [228,229]

$$c_p = \frac{1}{\varepsilon_{\mathrm{opt}}} - \frac{1}{\varepsilon_{\mathrm{s}}} \tag{229}$$

includes the dielectric constant at the high, $\varepsilon_{\mathrm{opt}}$, and low, ε_{s}, optical frequency limits, respectively. The electric displacement fields $\mathbf{D}_{\mathrm{A,B}}(\mathbf{R}_c)$ in the integrand are evaluated using atomic partial charges in the neutral q^{n}, and charged state q^{c}:

$$\mathbf{D}_{\mathrm{A}}(\mathbf{R}_c) - \mathbf{D}_{\mathrm{B}}(\mathbf{R}_c) = \sum_a \frac{q_a^{\mathrm{c}} - q_a^{\mathrm{n}}}{4\pi} \frac{(\mathbf{R}_c - \mathbf{R}_a)}{|\mathbf{R}_c - \mathbf{R}_a|^3} + \sum_b \frac{q_b^{\mathrm{n}} - q_b^{\mathrm{c}}}{4\pi} \frac{(\mathbf{R}_c - \mathbf{R}_b)}{|\mathbf{R}_c - \mathbf{R}_b|^3} \tag{230}$$

where the index a refers to atoms in molecule A, b to atoms in molecule B and c to atoms in the environment.

The integral in equation (Eq. 228) is evaluated including all neighbouring molecules with a centre of mass inside a sphere of a cutoff radius r_{cut} around the charge-transfer complex:

$$\lambda_{\mathrm{AB}}^{\mathrm{out}} = \frac{c_p}{2\varepsilon_0} \frac{4\pi r_{\mathrm{cut}}^3}{3} \frac{1}{N_c} \sum_c [\mathbf{D}_{\mathrm{A}}(\mathbf{R}_c) - \mathbf{D}_{\mathrm{B}}(\mathbf{R}_c)]^2 \ . \tag{231}$$

Here, N_c is the total number of neighbouring atoms c and this double sum is evaluated individually for each charge transfer pair AB embedded in an amorphous environment using the minimum image convention.

1.4.4.2 Electrostatic Energy from Partial Charges

Alternations in the local electric field can lead to high electrostatic contributions to the site-energy inside an organic material [57]. One can compute the electrostatic contribution to the energetic disorder as a sum over the atomic partial charges at the atomic positions in the environment of the charge-transfer complex for both molecules A and B.

$$\Delta E_{\mathrm{AB}}^{\mathrm{out}} = E_{\mathrm{B}}^{\mathrm{out}} - E_{\mathrm{A}}^{\mathrm{out}} \tag{232}$$

The expression

$$E_{\mathrm{A}}^{\mathrm{out}} = \frac{1}{4\pi\varepsilon_0} \sum_a \sum_c \frac{(q_a^{\mathrm{c}} - q_a^{\mathrm{n}}) q_c^{\mathrm{n}}}{\varepsilon_s |\mathbf{R}_a - \mathbf{R}_c|} \tag{233}$$

for the electrostatic Coulomb energy involves the difference of the partial atomic charges in the charged, q^{c}, and neutral state, q^{n} in molecule A and the partial charges q_c^{n} for the neutral neighbours c [57,230].

The sum includes all atoms a in molecule A and all neighbours c, within a certain cutoff radius $r_{\mathrm{cut}}^{\mathrm{out}}$ or we exploit the nearest image convention by shifting the molecule A in the centre of the simulation box and computing the sum for all pairs of atoms. Analogously the sum is carried out for all atoms b in molecule B to determine $E_{\mathrm{B}}^{\mathrm{out}}$. This approach assumes only minor changes in the molecular geometry while charging and discharging. Furthermore, this approach can be extended using the Ewald summation technique [176].

Polarisation Effects A relative dielectric constant ε can include polarisation effects in the environment of a charge-transfer complex (Eq. 233). The phenomenological screening of a charge can be addressed by a distance-depended screening function

$$\varepsilon(R_{ac}) = \varepsilon_s - (\varepsilon_s - 1) \left(1 + \kappa R_{ac} + \frac{1}{2}\kappa^2 R_{ac}^2\right) e^{-\kappa R_{ac}} \ . \tag{234}$$

Here, the parameter κ is the inverse screening length, the distance between two atoms a and c is abbreviated as $R_{ac} = |\mathbf{R}_a - \mathbf{R}_c|$. The screening function ensures that atoms in the proximity interact without a screening of the Coulomb potential ($\varepsilon \approx 1$) and for longer distances the screening ε proceeds with ε_s. In general, the parameters ε_s and κ are unknown for novel synthesised compounds. As the dielectric function is relatively small in organic semiconductors $\varepsilon \approx 3 - 4$, also the screening length exhibits small values, e.g. $\kappa = 3$ nm^{-1} in H_2O and $\kappa = 1.3$ nm^{-1} in Alq_3 [57]. An alternative approach to take polarisation effects into account is the use of polarisable force fields and the Thole model [231] (see Sec. 1.4.4.4).

1.4.4.3 Electrostatic Interaction Energy from Distributed Multipoles

We can determine the electrostatic interaction energy from a set of permanent multipole moments, that reproduce the molecular electrostatic potential (ESP). The charge density of a given molecule is therefore expressed by the multiple moments $\{Q^a_{kl}\}$ (spherical-tensor notation), which are located on sites a of the molecule A. So the interaction between molecule A and B with (polarisable) sites a and b leads to electrostatic interaction contributions, which are given in a sum over sites expression

$$U^{\mathrm{el}}_{\mathrm{AB}} = \sum_a \sum_b Q^a_{l_1k_1} \mathbf{T}^{a,b}_{l_1k_1l_2k_2} Q^b_{l_2k_2} \ . \tag{235}$$

The interaction between a component l_1k_1 of the multipole expansion at a site a and the component l_2k_2 at site b is determined by the tensor $\mathbf{T}^{a,b}_{l_1k_1l_2k_2}$, which mediates the distance and orientation dependence (see a list up to $l_1 + l_2 = 5$ in [232]). If we consider the single-molecule Hamiltonian and summarise the influence of the surrounding molecules in a perturbation term W, then the above expression is precisely the first-order correction for the energy in which the quantum mechanical details are incorporated into the classical multipole moments.

There are different ways how to obtain the set of distributed multipoles of a molecule, e.g. they are determined from the electrostatic potential by means of SCF calculations for the charge density (e.g. using the CHELPG approach [233]) or they are determined with a Distributed-Multipole-Analysis (DMA) approach based on the wavefunction [234–236].

In the framework of the CHELPG (CHarges from ELectrostatic Potentials, Grid-based) method, one can determine a set of atomic partial charges $\{q_a\}$ for a molecule with total molecular charge q_{mol} by minimising the following expression Z using a Lagrange multiplier technique with Lagrange multiplier Λ:

$$Z(\{q_a\}) = \sum_{k=1}^{M} \left(\phi(\mathbf{R}_k) - \sum_{a=1}^{N_a} \frac{1}{4\pi\epsilon_0} \frac{q_a}{|\mathbf{R}_a - \mathbf{R}_k|} \right) + \left(q_{\mathrm{mol}} - \sum_{a=1}^{N_a} q_a \right) \Lambda \ . \tag{236}$$

Here, we exploit that the SCF potential ϕ is evaluated on a cubic spatial grid with M points and the fitted partial charges $\{q_a\}$ are located at the N_a atomic centres.

Alternatively, we can employ the density matrix $\boldsymbol{\rho}$ and develop it in a basis of atom-centred and bond-centred Gaussians χ in order to evaluate the multipole moments by means of the DMA approach [235, 236].

$$\boldsymbol{\rho}(\mathbf{r}) = \sum_{\alpha,\beta} \boldsymbol{\rho}_{\alpha,\beta} \chi_\alpha(\mathbf{r} - \mathbf{s}_\alpha) \chi_\beta(\mathbf{r} - \mathbf{s}_\beta) \tag{237}$$

Here, $\chi_\alpha = f_\alpha(\mathbf{r} - \mathbf{s}_\alpha) e^{\zeta_\alpha(\mathbf{r}-\mathbf{s}_\alpha)^2}$ is a Gaussian primitive function centred at $\mathbf{s}_\alpha$, and f_α is a homogeneous polynomial of degree l according to the angular momentum l of the basis function χ_α.

This treatment allows us to exploit the feature that the overlap product $\chi_\alpha\chi_\beta$ of two Gaussians can be written as a new Gaussian function centred at

$$\mathbf{P} = \frac{\zeta_\alpha \mathbf{s}_\alpha + \zeta_\beta \mathbf{s}_\beta}{\zeta_\alpha + \zeta_\beta} \ . \tag{238}$$

Hence, each product yields an overlap charge density centred at its $\mathbf{P}$. The L component of the rank K multipole moment of this overlap density with respect to $\mathbf{P}$ reads

$$Q_{LK}[\mathbf{P}] = -\int R_{LK}(\mathbf{r} - \mathbf{P}) \boldsymbol{\rho}_{\alpha\beta} \chi_\alpha \chi_\beta \, \mathrm{d}\mathbf{r} \ , \tag{239}$$

and is expressed using the regular solid harmonics R_{LK}. In a subsequent step, we can get the multipole moments $Q_{nm}[\mathbf{S}]$ located at the polar site $\mathbf{S}$ on the basis of the resulting $Q_{lk}[\mathbf{P}]$, if one exploits the transformation rules [235]

$$Q_{nm}[\mathbf{S}] = \sum_{l=0}^{L} \sum_{k=-l}^{l} \left[\binom{n+m}{l+k} \binom{n-m}{l-k} \right]^{1/2} Q_{lk}[\mathbf{P}] \; R_{n-l,m-k}(\mathbf{S}-\mathbf{P}) \; . \tag{240}$$

This method needs an instruction on how to choose the target sites for the multipole expansion. For example, the nearest-site algorithm attributes the multipole moments to the closest polar site $\mathbf{S}$ in the vicinity of an overlapping site $\mathbf{P}$. The introduction of weighting functions and a grid-based integration methods yields a reduced basis set dependence of the derived multipoles, especially for diffuse basis functions [236].

1.4.4.4 Evaluating the Induction Energy within the Thole Model

With a set of permanent multipole moments $\{Q_{kl}^a\}$ for each molecular species at hand, one can also include induction effects if one introduces induced multipole moments $\{\Delta Q_{kl}^a\}$. Their generation is penalized by a bilinear form, which hinders the formation of induced multipole moments,

$$U^{\mathrm{pol}} = \frac{1}{2} \sum_{A} \Delta Q_t^a \boldsymbol{\eta}_{tt'}^{tt'} \Delta Q_{t'}^{a'} \; , \tag{241}$$

where the tensor $\boldsymbol{\eta}$ is the inverse of the polarisability tensor $\boldsymbol{\alpha}$. We denote a component of the multipole expansion at site a as $t \equiv l_1 k_1$ and at site b as $u \equiv l_2 k_2$.

The induction correction to the site-energy can be regarded as a second-order correction to the molecular interaction energy [234]. The interactions between permanent and induced moments read

$$U_{pu} = \frac{1}{2} \sum_{A} \sum_{B \geq A} \left[\Delta Q_t^a \mathbf{T}_{tu}^{ab} Q_u^b + \Delta Q_t^b \mathbf{T}_{tu}^{ab} Q_u^a \right] \; . \tag{242}$$

Solving the equations 242 and 243 in self-consistent cycles yields induction energy contributions to site energies. This requires the evaluation of expression

$$\Delta Q_t^a = - \sum_{B \neq A} \boldsymbol{\alpha}_{tt'}^{aa'} \mathbf{T}_{t'u}^{a'b} (Q_u^b + \Delta Q_u^b) \tag{243}$$

to obtain the induced polarisabilites ΔQ_t^a for a set of distributed multipoles $\{Q_t^a\}$ and a set of polarisabilities $\left\{ \boldsymbol{\alpha}_{tt'}^{aa'} \right\}$.

The polarisabilities are evaluated in the framework of the Thole model using the local dipole approximation $[\boldsymbol{\alpha}_{tt'}^{aa'}] = \boldsymbol{\alpha}_{tt'}^{aa'} \delta_{ti} \delta_{t'i} \delta_{aa'}$ with $i \in \{x, y, z\}$, which refers to the component of the dipole moment [231, 237].

The Thole model applies an adapted dipole-dipole interaction, which models the interaction of smeared charge distributions in order to imitate the QM wavefunction behaviour. Following this route one can overcome the difficulties that arise due to the divergence in the head-to-tail dipole-dipole interaction at small distances, which results in an unphysical performance [238]. In this dipole approximation, the correlation effects are disregard, as every local point dipole interacts individually with the external field and only correlations owing to pure classical field interaction remain present.

The introduction of a fractional charge density $\rho_f(\mathbf{u})$ allows us to smear the multipole moments, which are located at the nuclei. It is normalised to unity and decays quickly within a radius $\mathbf{u} = \mathbf{u}(\mathbf{R})$. The Thole model in VOTCA [57,213,239] applies a fractional charge density

$$\rho_f(\mathbf{u}) = \frac{3\zeta}{4\pi} e^{-\zeta|\mathbf{u}|^3} \ , \tag{244}$$

which exhibits an exponential decay with a smearing parameter $\zeta = 0.39$ and a scaled distance vector $\mathbf{u}(\mathbf{R}, \alpha^a, \alpha^b) = (\alpha^a \alpha^b)^{-6}\mathbf{R}$, where $\alpha^{a,b}$ are isotropic site polarisabilities for the sites a and b. Furthermore, the adapted interaction tensor is evaluated using damping functions $\Xi_n(\mathbf{u}(\mathbf{R}))$, which depend on the power n of the distance $|\mathbf{R}|$ [223]. As the fractional charge density is associated with an adapted potential

$$\phi(u) = -\frac{1}{4\pi\epsilon_0} \int_0^u 4\pi u' \rho(u') \, \mathrm{d}u' \tag{245}$$

one can also adapt the tensor $\mathbf{T}_{ij}$, which incorporates the distance and orientation dependence. Therefore, one needs to express the multipole interaction tensor

$$\mathbf{T}_{ij\ldots}(\mathbf{R}) = f(\alpha^a \alpha^b) t_{ij\ldots}(\mathbf{u}(\mathbf{R}, \alpha^a \alpha^b)) \tag{246}$$

by means of $\mathbf{u}(\mathbf{R}, \alpha^a \alpha^b)$ using an adaptive function $f(\alpha^a \alpha^b)$ [223]. The interaction tensor $t_{ij\ldots}$ including the smearing, is then obtained as a partial derivative of the potential (Eq. 245).

$$t_{ij\ldots}(\mathbf{u}) = -\partial_{u_i} \partial_{u_j} \ldots \phi(\mathbf{u}) \tag{247}$$

The Thole Model provides reasonable results for a set of atomic polarisabilities ($\alpha_\mathrm{H} = 0.496$ Å^3, $\alpha_\mathrm{C} = 1.334$ Å^3, $\alpha_\mathrm{N} = 1.073$ Å^3, $\alpha_\mathrm{O} = 0.873$ Å^3, $\alpha_\mathrm{S} = 2.926$ Å^3), which are common elements in organic semiconductors [237].

1.5 Kinetic Monte Carlo Simulations for Charge Transport

1.5.1 Master equation

If all the charge transfer rates between the different hopping sides are determined, the next step is to obtain the time-evolution of the system by solving the master equation

$$\frac{\partial P_a}{\partial t} = \sum_b P_b \Omega_{ba} - \sum_b P_a \Omega_{ab}. \tag{248}$$

Here, P_a is the probability to find the system in state a at the time t, and Ω_{ab} abbreviates the transition rate from state a to b. The matrix $\mathbf{\Omega}$ consists of individual rates k_{ij}, and a state of the system a is given by a set of occupations $\{a_i\}$, where $a_i = 1$ stands for an occupied site and $a_i = 0$ for an unoccupied site. If only a single excess charge is present in the system (simulation box) a state can be identified by $i = \begin{cases} 1 & \text{for } a_i = 1 \\ 0 & \text{else} \end{cases}$ and the associated probabilities P_i are the same as the site occupation probabilities p_i and also the transfer rates Ω_{ab} and k_{ij} are alike. In this case, the equation 248 reduces to

$$\frac{\partial p_i}{\partial t} = \sum_j p_j k_{ji} - \sum_j p_i k_{ij}. \tag{249}$$

Applying linear algebra this equation can be solved for small charge carrier densities, but it gets instable if a high degree of energetic disorder is present in the system or the emerging rates differ several orders of magnitude.

If several charge carriers are present in the simulation box, the master equation can be expressed in terms of occupation probabilities [57] by limiting oneself to the site-blocking charge-charge interactions in a mean-field approach [240]. If multiple different charges like holes, electrons and excitons as well as processes like charge injection/creation and charge drain/recombination appear in a simulation, it is unfeasible to solve the nonlinear equation (Eq. 248) analytically. Thus, one can solve the master equation employing a kinetic Monte Carlo algorithm to obtain the charge carrier trajectories. Hence, stationary and transient solutions to the master equation can emerge. The construction of a Markov chain of processes in state-space allows us to determine a series of possible events, where the probability of each event is only affected by the state of the previous event [241,242]. Therefore, only states with a consecutive connection to the actual state need to be incorporated. As exclusively the current occupation state of the sites is the decisive factor, the inclusion of additional features that require a direct treatment of the Coulomb interactions becomes feasible. For example, an extension to consider multiple charge carriers, competing interactions of particles and processes, and rates that depend on space occupation are conceivable.

1.5.2 Kinetic Monte Carlo Algorithm

We employ kinetic Monte Carlo simulations (kMC) to simulate the trajectories of individual charge carriers using a combination of the first reaction method (FRM) and the variable step-size method (VSSM) [243]. The procedure to solve the master equation for a Markov chain (Eq. 248) works as follows (see SI in [57]).

At the beginning of every kMC run, N_c charge carries are distributed randomly on the hopping sites inside the simulation box, favourably at the donor-acceptor interface in case of a bled morphology. Then the charge transfer rates k_{ij} are calculated for every occupied hopping site i to a neighbour j in the set of nearest neighbours N^{NN}. In a subsequent step, the total escape rate k_i^{esc} for a charge to leave a certain hopping site i is evaluated. It is given as the sum of all rates to the nearest neighbours N^{NN} according to

$$k_i^{\mathrm{esc}} = \sum_j k_{ij} \ . \tag{250}$$

Thereupon, the FRM selects a certain charge carrier that is supposed to jump to an adjacent hopping site. Therefore, one needs to calculate the waiting time

$$\tau_i = t - \frac{\ln(r_1)}{k_i^{\mathrm{esc}}} \tag{251}$$

for every charge carrier i using a random number $r_1 \in (0, 1]$. Here, t is the total simulation time. Taking the negative logarithm of a random number in the interval (0,1] provides a mapping of the random number to the interval 0 to ∞. In this way, the charge does not always jump with the exact waiting time, but the charge waits a random portion of the time. In other words, the charge waits the inverse of the rate, multiplied by a random number. Then the charge l with the smallest waiting time $\tau_l = \min\{\tau_i\}$ is selected, and the simulation time t is updated to $t = \tau_l$.

The second VSSM approach chooses the target hopping site m from the nearest neighbours where the charge is transferred.

$$\min\left\{m\left|\sum_m \frac{k_{lm}}{k_l^{\mathrm{esc}}} > r_2\right.\right\} \tag{252}$$

A particular process has got the probability $\frac{k_{lm}}{k_l}$, which is given as the fraction of an individual transfer rate over the total escape rate. Now one generates a second random number $r_2 \in (0,1]$ and sums up all probabilities $\frac{k_{lm}}{k_l^{\mathrm{esc}}}$ until one gets the index m, where the sum exceeds the value r_2. The charge is transferred to the site with index m and its waiting time is updated to $\tau_m = t - \frac{\ln(r_1)}{k_m^{\mathrm{esc}}}$. If no explicit interaction between the charges is present, then the rates and the waiting times of all other charges remain unchanged. The process starts again by selecting the charge l with the smallest waiting time τ_l and is repeated till a maximum number of kMC steps N_{steps} are evaluated.

The main advantage of the FRM is that the stand-alone event groups belonging to a particular charge do not change, if the kMC rates do not vary. Therefore, just the group of events of a transferred charge has to be modified.

All in all, with the charge transfer rates k_{ij} at hand, we can obtain charge carrier trajectories of holes, electrons and excitons inside the solar cell with the kMC algorithm.

1.5.3 Macroscopic Observables

The goal of the kMC simulations in the present work is to get access to macroscopic observables based on a microscopic description [57]. Accessible observable are for instance the charge carrier mobility $\boldsymbol{\mu}$, the current density ϱ or the electronic current $\mathbf{I}$ [244].

The ensemble average $\langle O\rangle$ for a macroscopic observables O at a certain time t is given as the sum over all states a

$$\langle O\rangle = \sum_a P_a O_a \ . \tag{253}$$

The value of the observable O_a in state a is weighted in this expression with the probability P_a being found in this state.

The time evolution for $\langle O\rangle$ can be computed using Heisenberg's equation of motion if the observable O does not exhibit an explicit time-dependence

$$\frac{d\langle O\rangle}{dt} = \sum_{a,b} O_a(P_b\Omega_{ba} - P_a\Omega_{ab}) = \sum_{a,b} P_b\Omega_{ba}(O_a - O_b) \ . \tag{254}$$

On the one hand, the average can be taken for multiple kMC trajectories N_a that terminate at a certain site a after a simulation time t_{tot}, which gives rise to a probability $P_a = N_a/N_{\mathrm{tot}}$, where N_{tot} gives the total number of Markov chains. On the other hand, a time average along a single trajectory is achieved by

$$\overline{O} = \frac{1}{\tau}\sum_a O_a\tau_a \tag{255}$$

if the total occupation time of a state a is given by τ_a and the total averaging time is $\tau = \sum_a \tau_a$. In general, the time and ensemble average should lead to the same result in ergodic systems. An ensemble average for multiple trajectories with distinct initial occupation configurations mimics the experimental setup in time-of-flight experiments best.

Charge Carrier Mobility and Diffusion Tensor The charge carrier mobility can be extracted in two ways from the kMC simulations. On the one hand, Einstein's relation [245] gives access to the zero-field mobility tensor $\boldsymbol{\mu}$ via the diffusion tensor $\mathbf{D}$ with

$$D_{lm} = \frac{k_\mathrm{B}T}{e}\mu_{lm} \tag{256}$$

in a Cartesian representation $l, m \in \{x, y, z\}$. In this expression, T is the absolute temperature, k_B is the Boltzmann constant and e is the elementary charge. The diffusion tensor $\mathbf{D}$ can be approximated by means of a linear fit of the mean squared displacement $\langle \mathbf{r}^2 \rangle$ in a kMC simulation with a total simulation time t_tot

$$\langle \mathbf{r}^2(t_\mathrm{tot}) \rangle = 2d\mathbf{D}t_\mathrm{tot} \ . \tag{257}$$

Here, $d = 3$ is applied for a three-dimensional system, and one obtains the mobility μ

$$\boldsymbol{\mu} = \frac{q_e}{6t_\mathrm{tot}k_\mathrm{B}T}\langle \mathbf{r}^2 \rangle \tag{258}$$

One needs to bear in mind the corrections due to the periodic boundary conditions of the simulation box when taking the average of the mean square displacement.

On the other hand, the charge carrier mobility is computed directly from the kMC trajectory, using the charge carrier mobility tensor $\boldsymbol{\mu}$ to calculate the field-effect mobility μ^FEM with respect to the orientation of the external field $\mathbf{F}^\mathrm{ext}$.

$$\langle \mathbf{v} \rangle = \sum_{i,j} p_j k_{ji} (\mathbf{r}_i - \mathbf{r}_j) = \boldsymbol{\mu}\mathbf{F}^\mathrm{ext} \tag{259}$$

The expression for the field-effect mobility μ^FEM [230,246,247] reads

$$\mu^\mathrm{FEM} = \frac{\langle \mathbf{v} \rangle \mathbf{F}^\mathrm{ext}}{|\mathbf{F}^\mathrm{ext}| \cdot |\mathbf{F}^\mathrm{ext}|} = \frac{\langle \mathbf{v} \rangle \mathbf{e}_{\mathrm{F}^\mathrm{ext}}}{|\mathbf{F}^\mathrm{ext}|} \tag{260}$$

Here, one evaluates the projection of the average charge velocity $\langle \mathbf{v} \rangle$ on the axis with a unit vector $\mathbf{e}_{\mathrm{F}^\mathrm{ext}}$ of the external field $\mathbf{F}^\mathrm{ext}$. The average velocity $\langle \mathbf{v} \rangle$ is given as the charge displacement vector divided by the simulation time t_tot.

The charge carrier mobilities are averaged for multiple kMC trajectories with varying initial charge positions in the simulation box to improve statistics. Furthermore, one can average different orientations and magnitudes of the external field, the number of different frames in the underlying atomistic morphology.

As the calculation is computational demanding for the hopping rates to all nearest neighbours in the kMC simulation, the system size of the simulation boxes is usually restricted to the nanometer regime. Charge transport exhibits dispersive behaviour for systems with an energetic disorder at room temperature T and therefore the charge carrier mobility μ reveals a system size dependence [248]. This arises as an injected charge, which is inserted in the system does not visit sufficient distinct hopping sites before relaxation to an equilibrium transport energy E^eq [193].

$$E^\mathrm{eq} = \frac{\int_{-\infty}^{\infty} p(E) E e^{-\beta E} \, \mathrm{d}E}{\int_{-\infty}^{\infty} p(E) e^{-\beta E} \, \mathrm{d}E} \tag{261}$$

In this equation enter $\beta = (k_\mathrm{B}T)^{-1}$, and the distribution $p(E)$ of site energies E. The integral in Eq. 261 can be expressed as an average of all realised site energies N (Eq. 263) assuming a Gaussian-shaped distribution function of the density of states (GDOS, Gaussian density of states) (Eq. 262), where N is the total number of hopping sites.

$$p(E) = \frac{1}{\sqrt{2\pi\sigma^2}} e^{-\frac{E^2}{2\sigma^2}} \tag{262}$$

The characteristic width of this distribution σ is called energetic disorder [194].

$$E_N = \left\langle \frac{\sum_{n=1}^{N} E_n e^{-\beta E_n}}{\sum_{n=1}^{N} e^{-\beta E_n}} \right\rangle \tag{263}$$

The temperature dependence of non-dispersive charge carrier mobility $\mu(T)$ can be extrapolated using

$$\mu(T) = \frac{\mu^0}{T^{\frac{3}{2}}} e^{-\left(\frac{\chi}{T}\right)^2 - \left(\frac{\zeta}{T}\right)} \tag{264}$$

with material constants μ^0, χ, ζ [248,249].

Current Density For holes and electrons in a kMC simulation, we can obtain the microscopic charge density from the occupation probability p_i^{occ} of a given site with index i and the associated effective volume V_i [244].

$$\varrho_i = \frac{e p_i^{\mathrm{occ}}}{V_i} \tag{265}$$

A Voronoi tesselation of spaces gives access to the effective volume V_i in the case of an aperiodic distribution of hopping sites.

Current The time evolution of the position of a charge $\mathbf{r}(t)$ in the course of a kMC simulation can be used to calculate the total current in a system $\mathbf{I}$ by taking the average $\langle \mathbf{r} \rangle$. Here, the charge position $\mathbf{r}$ is regarded as an observable. The current reads

$$\mathbf{I} = e\langle \mathbf{v} \rangle = e\frac{\mathrm{d}\langle \mathbf{r} \rangle}{\mathrm{d}t} = e\sum_{i,j} p_j^{\mathrm{occ}} k_{ji} (\mathbf{r}_i - \mathbf{r}_j) = \frac{e}{2}\sum_{i,j} (p_j^{\mathrm{occ}} k_{ji} - p_i^{\mathrm{occ}} k_{ij}) \mathbf{r}_{ij} \ . \tag{266}$$

The introduction of the distance vector $\mathbf{r}_{ij} = \mathbf{r}_i - \mathbf{r}_j$ and the associated unit vector in this direction $\mathbf{e}_{ij}$ help with the symmetrisation of the equation guarantees an equal flux splitting between adjacent sites and mitigates the appearance of local average fluxes in equilibrium [250].

In this manner the local current passing through a single site i is

$$\mathbf{I}_i = \frac{e}{2}\sum_{j} (p_j^{\mathrm{occ}} k_{ji} - p_i^{\mathrm{occ}} k_{ij}) \mathbf{e}_{ij} \tag{267}$$

and it is a measure of the contribution of the local electronic current to the global current inside the morphology. The principal charge carrier pathways can now be identified, where a couple of closely located sites with high values of $\mathbf{I}_i$ span a connected network.